University of Southern Queensland

Faculty of Health, Engineering and Sciences

Investigation Of The Critical Zone Of CFRP Type-V Pressure Vessels For H^2 Storage In The Transportation Sector

A dissertation submitted by

Ryan Richards

In fulfilment of the requirements of

ENP4111 Professional Engineering Research Project

towards the degree of

Bachelor of Engineering (Honours) (Mechanical)

Submitted December 2024

ABSTRACT

This paper aims to investigate and optimize the critical zone of carbon-fibre reinforced polymer type V pressure vessels used for hydrogen storage in the transportation sector. The critical zone is identified as one of two possible locations for failure and therefore is crucial for maintaining safety under high internal pressures. Despite its promise, the use of hydrogen as a sustainable energy source is limited by existing storage technologies.

The study begins with an extensive literature review to establish the current state of knowledge on CFRP type V pressure vessels. Key publications are used to define design parameters and develop a theoretical model. Finite element simulations were conducted utilizing ANSYS software to analyze the effects of varying polar boss width, flange length, and angle on stress and strain distributions.

Reducing polar boss width showed variable effects on the stress concentration factor whilst the introduction of a flange was found to decrease localized stress and strain concentrations. Increasing the angle of the flange significantly reduced localized stress and strain concentrations in the critical zone and improved stress distribution across the entire vessel. The optimal design parameters were found to be a reduced boss width of 63 mm coupled with an 8 mm flange orientated at 7.5°.

The findings from this research contribute to the design and development of safer and more reliable type V pressure vessels and will aid in the widespread adoption into the transportation sector.

University of Southern Queensland

School of Engineering

ENP4111 Professional Engineering Research Project

Limitations of Use

The Council of the University of Southern Queensland, its School of Engineering, and the staff of the University of Southern Queensland, do not accept any responsibility for the truth, accuracy or completeness of material contained within or associated with this dissertation.

Persons using all or any part of this material do so at their own risk, and not at the risk of the Council of the University of Southern Queensland, its School of Engineering or the staff of the University of Southern Queensland.

This dissertation reports an educational exercise and has no purpose or validity beyond this exercise. The sole purpose of the course pair entitles "Research Project" is to contribute to the overall education within the student's chosen degree program. This document, the associated hardware, software, drawings, and any other material set out in the associated appendices should not be used for any other purpose: if they are so used, it is entirely at the risk of the user.

Certification

I certify that the ideas, designs and experimental work, results, analyses and conclusions set out in this dissertation are entirely my own effort, except where otherwise indicated and acknowledged.

I further certify that the work is original and has not been previously submitted for assessment in any other course or institution, except where specifically stated.

Ryan Richards

Student Number: [redacted]

ACKNOWLEDGEMENTS

First, I would like to express my gratitude to my partner and parents, whose unwavering support, patience, and encouragement has been my anchor throughout this journey. Your support has been my source of strength during the most challenging moments.

I would like to thank Assoc. Prof. Dr Belal Yousif for his supervision and assistance throughout this project.

Table of Contents

TABLE OF FIGURES

TABLE OF TABLES

TABLE OF NOMENCLATURE

The following abbreviations have been used throughout the dissertation:

H^2	Hydrogen
CFRP	Carbon-Fibre Reinforced Polymer
PV	Pressure Vessel
AFP	Automated Fibre Placement
CZM	Cohesive Zone Model

CHAPTER 1

INTRODUCTION

1.1 Aim

The aim of this dissertation is to investigate the critical zone of carbon-fibre reinforced polymer (CFRP) type-V pressure vessels (PV) under the specific application of hydrogen (H^2) storage in the transportational sector. The region of contact where the internal polar bosses adhere to the composite material of the vessel body is referred to as the 'critical zone'. Generally constructed from a variety of alloys, the polar bosses allow for external components to interact with the contents of the pressure vessel. For the purpose of this dissertation, the key considerations, mechanical performance, and potential failure mechanisms of the critical zone will be evaluated through software modelling. To maintain structural integrity of the vessel, a secure and dependable connection is essential in recognition of the high internal forces involved. Optimizing the critical zone, whilst enhancing the overall vessel performance, durability and safety, is the foundation of this research.

1.2 Background

Hydrogen has reemerged as a viable alternative to traditional fossil fuels as the global demand for cleaner, more sustainable energy solutions increases. The utilization of H^2 as a fuel source for transportation is not a new concept, with the first recorded case over 200 years ago (IEA 2019). However, hydrogen use remains limited in the transportation, construction and power generation sectors where its use could play a pivotal role in the transition to clean energy.

Limitations surrounding contemporary storage technology pose the main challenge to adopting hydrogen as a sustainable energy source, despite its potential. Hydrogen has limited energy per unit volume when at its lowest density in ambient temperature, however it offers the highest energy density by mass (EERE 2015). Practical and efficient use of hydrogen therefore requires advanced storage methods. For gaseous hydrogen, high-pressure vessels capable of withstanding pressures of

approximately 35 to 70 MPa (5,000 to 10,000 psi) are required. For liquid hydrogen, storage requires cryogenic conditions due to its boiling point of -252.8°C at atmospheric pressure (EERE 2015). Both storage methods currently present distinct and unique technical challenges and limitations.

Primarily utilized in aerospace and automotive engineering, Carbon-fibre reinforced polymer (CFRP) is an engineered epoxy polymer matrix reinforced with carbon fibres. Its popularity and application to various engineering fields arises from its exceptional mechanical properties, primarily pertaining to its strength. Specifically, in comparison to steel and aluminum, CFRP offers up to ten times the specific strength. This makes it ideal for applications that require a significant reduction in weight without compromising durability, strength and fatigue resistance under high cyclic loads (Zhang, Jin et al. 2023). Additionally, CFRP has excellent chemical resistance, reduced weight and thermal expansion (Deeraj et al. 2020).

Constructing pressure vessels with CFRP presents a unique and complex set of challenges to ensure they can withstand the pressures required for hydrogen storage. Despite the numerous advantages and useful mechanical properties of CFRP, its structural characteristics may cause significant barriers to its application in a practical setting. In addition, the nonhomogeneous nature of CFRP's results in variations in the density distribution of fibre strands within the polymer matrix, which can reduce the material's ultimate strength. The fibres must be aligned parallel to the load direction to optimize performance as carbon fibre exhibits its greatest strength along its length (Fibreglast 2023). Figure 1 (i) shows the effect of fibre orientation to the tensile strength of the composite while (ii) exemplifies common laminate stacking sequences.

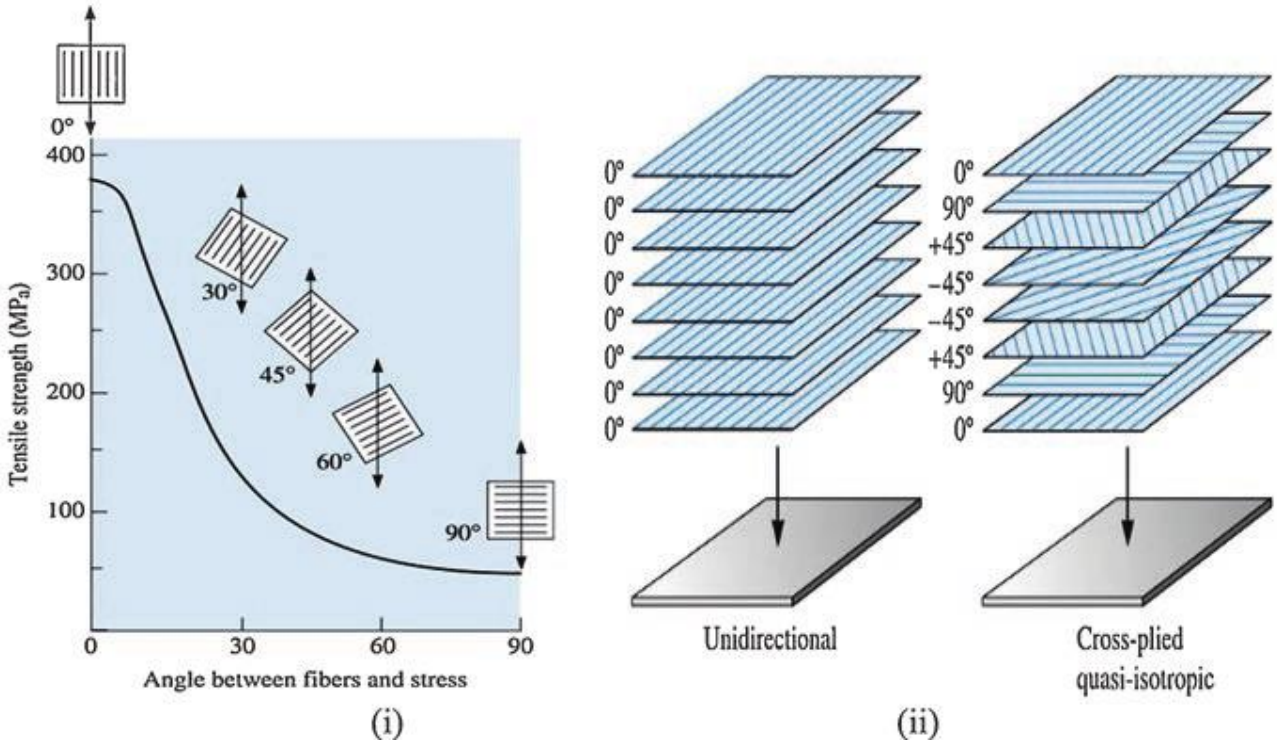

Figure 1 - (i) Composite Tensile Strength as a Function of Fibre Orientation Angle (ii) Common Laminate Stacking Sequences (Ahmad Sobri et al. 2020)

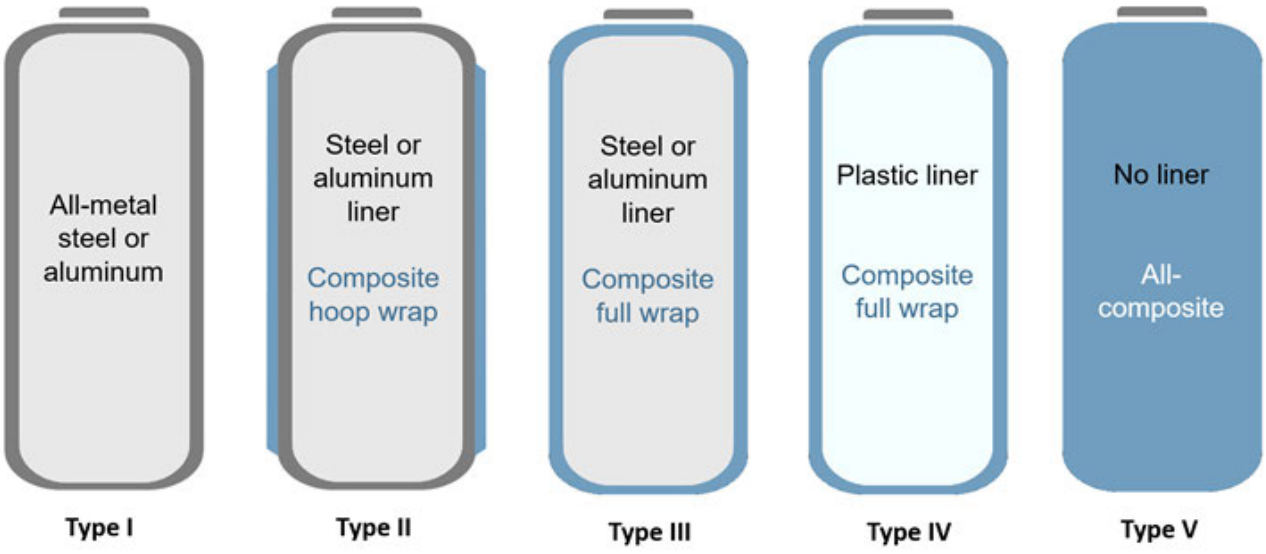

Figure 2 - ASME Pressure Vessel Classifications (Sloan 2023)

Although, due to the isotropic internal pressures, the pressure vessels experience equal force exertion in all directions. In consideration of the multidirectional forces, the CFRP must therefore be used in multiple layers with varied fibre orientations. Consequently, advanced manufacturing processes and strict quality control are necessitated to ensure adequate alignment and adhesive bonding across these layers, adding to the complexity of CFRP-based pressure vessel design.

The American Society of Mechanical Engineers (ASME) classifies pressure vessels into five categories, as shown in Figure 2. This dissertation will focus exclusively on Type V pressure vessels.

Type V pressure vessels represent the latest innovation in pressure vessel storage technology, eliminating the need for an internal gas barrier and enabling construction from a single material. Both the overall gas containment and structural integrity of these vessels are entirely reliant on the CFRP, simplifying the design whilst also reducing weight (Air, Shamsuddoha, et al. 2023). Varying from traditional pressure vessels, Type V vessels do not have an integrated liner, and instead, a polar boss acts as the interface for external components. Sensors, monitoring equipment and the attachment of fittings required for filling or emptying the vessel, can be accommodated by the polar boss, making it a critical feature (Composites 2019; Air, Shamsuddoha, et al. 2023).

The use of a single material construction has both advantages and disadvantages. The design presents two primary areas of potential failure: the CFRP body and the critical zone. Failures in either of these areas are certain to compromise the vessel's structural integrity or its ability to safely contain hydrogen. This could have significant consequences such as leakage or burst failure (Harada et al. 2018). Furthermore, two potential failure mechanisms include delamination or permeation. Permeation involves the loss of hydrogen molecules through the vessel material and delamination occurs when layers of CFRP separate under stress (Zhang, Jiaqiao et al. 2023). These challenges can be addressed through comprehensive analysis to optimize the critical zone, as well as the CFRP material, to ensure reliable performance under high-pressure conditions. Overall, ongoing advances

in material design, bonding techniques, and quality control are essential to mitigate risks and improve the safety and efficiency of Type V pressure vessels.

1.3 Problem Definition

Requiring comparatively newer technology, the development processes for type V pressure vessels are not well defined, with limited adoption and application compared to other more traditional types. A notable lack of published research and comprehensive data on the long-term performance, failure mechanisms and design optimization, also poses a significant challenge to widespread implementation of these vessels. Industries reliant on dependable and safe storage solutions are similarly affected by the scarcity of established type V pressure vessel standards and guidelines, further complicating the vessels integration into these sectors. Addressing these research gaps is crucial to building knowledge and confidence in type V pressure vessels to unlock their potential as a lightweight, efficient, and sustainable solution for hydrogen storage.

1.4 Project Objectives

To achieve the outlined project aim, this dissertation intends to address six key objectives. The proposed objectives are:

Objective 1: Research

This dissertation aims to provide an up-to-date extensive review of current known literature on the proposed project, focusing specifically on the mechanical behaviour and failure modes of CFRP-based Type V pressure vessels. The design considerations, complexities unique to hydrogen storage and the challenges of creating a reliable bond at the critical zone will also be considered. Aiding in the development of a theoretical model, key studies addressing the critical zone of CFRP type V pressure vessels will be identified.

Objective 2: Critical Zone Identification

From the information presented in the literature review, the critical zone for the CFRP pressure vessel will be identified and analyzed. Specifically, the stresses, load transfer mechanisms, and potential failure modes within this region will be examined. Additional influencing factors such as adhesive joint geometry, surface preparation techniques, material compatibility and stress concentrations will also be evaluated if time permits.

Objective 3: Generate a Finite Element Model

A finite element model of the critical zone utilizing the ANSYS or equivalent software will be developed with the information gained in the previous objectives. The model geometry, material properties, and boundary conditions will be defined and justified based on the findings from the literature review.

Objective 4: Modelled Mechanical Behaviour Analysis

The model will be analyzed under the relevant loading conditions to examine stress distribution, material deformation, and potential failure modes. This enables a deeper understanding of the mechanical behavior of the critical zone, enhancing the accuracy of future predictions.

Objective 5: Modelled Failure Mode Analysis

Potential failure modes in the critical zone will be identified through analysis of the simulation results. Factors such as adhesive debonding, interfacial delamination, and adhesive or cohesive failure will be investigated. The findings will be compared against established failure criteria to assess the reliability of the critical zone under the specified loading conditions.

Objective 6: Optimization & Proposed Design Improvements

This dissertation aims to propose potential design modifications to enhance the performance of the critical zone. Design or manufacturing adjustments may include reducing stress concentrations, improving bonding methods, optimizing joint configurations, or applying protective coatings.

1.5 Conclusions

This dissertation investigates the critical zone of type V pressure vessels manufactured from CFRP when under conditions of a stored hydrogen load within the transportation sector. The research aims to optimize the critical zone to improve the vessel's structural integrity, performance, durability, and safety. Evident in preliminary research, type V vessels lack research on long-term performance and failure modes as well as established guidelines, making this a major barrier to their widespread adoption.

The proposed outcomes of this project include the review of current known literature and thus the identification and quantification of factors contributing to failure modes in the critical zone. Additionally, the project aims to develop a theoretical model of the critical zone supported by the literature review findings. Furthermore, it seeks to utilise simulation results to establish refined metrics that can be used to evaluate and predict the behaviour of new designs.

The benefits of these outcomes include enhanced safety and reliability in the design of type V CFRP pressure vessels. These outcomes are expected to lead to increased use of CFRP pressure vessels across various industries. It can be hypothesised that a reduction in cost and complexity of hydrogen storage through the aforementioned advancements will promote hydrogen as a sustainable energy source, supporting the transition away from fossil fuels.

CHAPTER 2

LITERATURE REVIEW

2.1 Introduction

This chapter reviews recently published literature in order to provide an extensive review of existing knowledge relevant to CFRP type V pressure vessels. There is particular focus on H^2 storage and factors relevant for the widespread adoption into the transportational sector.

The section begins by exploring the feasibility of hydrogen as a sustainable energy source and its current utilization in commercial vehicles. This establishes the key design parameters required for the development of a theoretical model.

Furthermore, the design and functionality of type IV and type V pressure vessels is assessed. Key advancements in composite pressure vessel design such as emerging automated fibre placement (AFP) manufacturing processes, defect management and challenges associated with accurate failure predictions are also reviewed.

This chapter establishes a foundation of understanding the current state of type V pressure vessels and their potential and identifies gaps in knowledge in critical areas for further exploration.

2.2 Utilization of Hydrogen as an Energy Source in the Transportational Sector

A review of current hydrogen storage technology by Hwang and Varma (2014) found that hydrogen's potential as a transportation fuel is dependent on developing efficient and cost-effective storage solutions. Current approaches including compressed and cryogenic tanks are becoming more commercialised whilst alternative storage solutions such as solid-state offer long-term potential.

Whilst hydrogen's high gravimetric energy density (120 MJ/kg compared to gasoline's 44 MJ/kg) is advantageous, its poor volumetric energy density (0.01 MJ/L at standard temperature and pressure

versus 32 MJ/L for gasoline) presents challenges for storing large quantities. Hwang and Varma (2014) propose that a practical driving range is greater than 500 km, and thus advanced hydrogen storage solutions are required. Three storage solutions are presented; compressed gas (35 to 70 MPa), cryogenic liquid (20 K) and cryo-compressed (20 K stored at 27.6 MPa). Although promising, compressed storage systems have limited efficiency due to low volumetric energy densities (18–28 g/L). Alternatively, cryogenic storage increases volumetric density by liquefying hydrogen at 20 K, achieving up to 70 g/L. Cryogenic storage systems however are less practical due to boil-off losses, energy requirements to sustain the low temperatures and safety concerns.

The findings of Hwang and Varma (2014) suggest that compressive storage of H^2 is the only suitable option for the transportational sector. This is supported by the use of 70 MPa type IV pressure vessels in both prototype and production vehicles.

An abridged table of the advantages and disadvantages of the different approaches to hydrogen storage compiled by Hwang and Varma (2014) is shown below (Table 1).

Table 1 - Advantages and Disadvantages of Hydrogen Storage Approaches (Hwang & Varma 2014)

Storage System	Advantages	Disadvantages	Ongoing Efforts
Compressed	Commercially available	Low volumetric capacity. High compression energy. Heat management during charging required.	Develop and design cost-effective vessel.
Liquid (Cryogenic)	Commercially available	H^2 loss. Safety issues. High liquefaction energy. Heat management to reduce boil-off.	
Cryo-Compressed	High volumetric capacity	High combined compression and liquefaction energy.	

2.2.1 Current Use in Commercial Vehicles

Hydrogen has been utilized as a fuel source for protype vehicles for decades however it has only been recently that the technology has been transferred to production vehicles and thus available to the majority of the public. There are currently three prominent examples of current generation vehicles on the market, all of which utilise type IV pressure vessel technology. Since the oldest of these vehicles was released in 2021, there are very little scientific publications on these vehicles and even less on the specifics of the hydrogen storage solutions due to IP.

The key parameters of the Toyota Mirai, Hyundai Nexo and Honda CRVe are listed below in table 2. These metrics form a baseline for comparison against. It can be seen that all manufacturers employ multiple tanks operating at a pressure of 70 MPa to store sufficient hydrogen to achieve a practical range. To meet packaging constraints, several smaller pressure vessels are combined to fulfill the required capacity. This approach also enhances vehicle performance and passenger comfort as the smaller tanks can be distributed throughout the vehicle chassis. These factors establish the key design criteria for the theoretical model.

Table 2 - Principal Attributes of Current H2 Production Vehicles

	Toyota Mirai	Hyundai Nexo	Honda CRV e
Date of release	2024	2021	2025
Pressure (MPa)	70	70	70
Capacity (kg)	5.60	6.33	4.30
Volume (m^3)	0.1414	0.1560	0.1086
Range (km)	575-647	666	435
No. Tanks	3	3	2
	(Toyota 2024)	(Hyundai 2021)	(Car Expert 2023; Gardiner 2024)

2.3 Carbon-Fibre Reinforced Polymer Pressure Vessels

Zhang, Jin et al. (2023) proposes that pressure vessels represent one of the fastest-expanding markets for advanced composite materials with the 2021 global demand estimated at 11 kilotonne. Carbon fibre reinforced polymers offer numerous advantages over traditional materials. This is supported by the work of Mawaire (2019), who takes note of CFRPs superior strength-to-weight ratio. This is ideal for applications that demand high strength and stiffness whilst minimizing weight. Furthermore, the corrosion resistance of CFRPs increases the durability of pressure vessels whilst reducing maintenance expenses and improving safety in harsh environments.

Liu et al. (2012) suggests that one of the primary advantages of composites lies in their ability to be tailored to the specific requirements of the chosen application. This can be achieved through varying fibre orientations and layer thicknesses.

Conversely, Liu et al.'s (2012) paper acknowledges that composite pressure vessels are prone to multiple failure modes. These are unique to composite materials and include matrix cracking, fibre-matrix debonding, and fibre breakage. It is also noted that accurate prediction of burst pressure and reliability over the entirety of the vessel's lifecycle pose significant challenges.

A review of manufacturing techniques specific to CFRP pressure vessels by Azeem et al. (2022) produced a tabulated comparison (Table 3) of the various pressure vessel classifications, with specific emphasis on parameters such as pressure limits, weight, cost, material selection and load sharing.

Table 3 - Pressure Vessel Classification Comparison (Azeem et al. 2022)

Vessel Type	Built features and; Pressure limits	Weight (Kg/Litre) Comparison	Cost/Litre and; Comparison	Liner material; Load bearing	Composite layers load sharing
Type I	Full metal; Limited to 500 bars	0.80 - 1.4 (Heaviest)	$3 - $5 /litre	Aluminium or steel (or their alloys) 100% load bearing	-
Type II	Composite hoop wrapped on metallic liner; No pressure limit	0.50 - 0.68 (15 to 35% lighter than type 1)	$5 - $7/ liter (50% costly than type 1)	Aluminium or steel (or their alloys) 55% load bearing	45% load bearing
Type III	Composite hoop and helically wrapped on metallic liner; Pressure up to 450 bar (cyclic) and up to 700 bar (static)	0.41 - 0.45 (44% - 48% lighter than type 1)	$9 - $14/ liter (twice of type 2)	Aluminium or steel (or their alloys) 20% load bearing	80% load bearing
Type IV	Composite hoop and helically wrapped on polymeric liner; Up to 1000 bar	0.25 - 0.39 (70% - 75% lighter than type 1)	$11 - $18/ liter (3.5 times of type 1)	HDPE, Polyamide; 0% load bearing	100% load bearing
Type V	Composite hoop and helical composite layers	10 - 20% lighter than type 4	-	Linerless	100% load bearing

Liu et al. (2012) concludes that the feasibility of using composite materials for pressure vessel design is supported by its superior strength, weight and ability for localised reinforcement. However, to fully utilise its potential, ongoing research is needed to address challenges related to the accurate prediction of failure mechanisms under complex operating conditions.

2.3.1 Existing Research and Application of Type-IV PV

An abridged table of the previous work published on Type-IV pressure vessels, organized by key content covered, compiled by Air et al. (2023) is shown below (Table 4).

It can be seen that of the publications reviewed by Air et al. (2023), the majority cover topics such as mathematical theory, simulation and experimental data. This provides a clear basis for the development of a type V theoretical model. Whilst type IV and V share many similarities, the lack of an internal liner and the implications this has on the design of the polar bosses and the critical zone will need to be explored in the methodology.

There is a clear reduction in the number of journal articles that cover the design of the boss and liner and even less that cover failure modes. This was addressed as early as a decade prior by the work of Liu et al. (2012).

Table 4 - Breakdown of existing Type-IV pressure vessels based on content type. (Air, Shamsuddoha, et al. 2023)

Author	Year	Mathematical Theory	Simulation	Experimental Data	Materials	Boss Design	Liner Design	Health Monitoring
Alves et al.	2022	X	X		X			
Wang et al.	2022				X		X	
Rafiee & Salehi	2022	X	X	X				
Nebe et al.	2022	X	X	X				
Su et al.	2021				X		X	
Schakel et al.	2021			X				
Park et al.	2021	X	X			X		
Munzke et al.	2021			X				X
Jois et al.	2021	X	X	X				
Zhang et al.	2020	X	X				X	
Souza & Tarpani	2020			X				X
Sapre et al.	2020	X	X				X	
Alam et al.	2020		X	X				
Nebe et al.	2019		X	X				
Raifee & Torabi	2018	X	X				X	
Cho et al.	2018	X	X	X				
Johnson et al.	2017	X	X	X	X	X		
Hua et al.	2017	X	X			X	X	
O' Bradaigh et al.	2016		X	X	X		X	
Shao et al.	2016			X	X			X
Yamashita et al.	2015					X	X	

Magneville et al.	2015	X	X					
Leh et al.	2015	X	X	X				
Leh et al.	2015	X	X					
Berro Ramirez et al.	2015	X	X	X				X
Leavitt & Lam	2014	X	X	X	X		X	
Gentilleau et al.	2014	X	X		X			
Roh et al.	2013	X	X					
Liu et al.	2012	X	X					
Bertin et al.	2012		X	X				
Villalonga et al.	2011			X				
Villalonga et al.	2009		X	X	X		X	X
Funck & Fuchs	2001			X				

Additional publications not covered by the work of Air et al. (2023) are collated in table 5, below. These papers have particular interest in failure criteria (titled health monitoring below) and are explored in the later sections.

Table 5 - Breakdown of existing Type-IV pressure vessels based on content type. Continued.

Author	Year	Mathematical Theory	Simulation	Experimental Data	Materials	Boss Design	Liner Design	Health Monitoring
Zhang et al.	2019	X	X	X	X		X	X
Zhou et al.	2022	X	X	X	X		X	X
Bouhala et al.	2024	X	X		X		X	X
Zu et al.	2014	X	X		X		X	
Azeem et al.	2022	X	X		X	X	X	X
Wu et al.	2015	X	X	X	X		X	X

2.3.2 Existing Research and Application of Type-V PV

The scarcity of published research on Type V composite pressure vessels is considered to be largely due to the relative novelty of the technology, lack of regulatory standards and challenges regarding intellectual property (IP). The lack of established standards for design, manufacturing, and testing

creates additional barriers for further academic research. Critical advancements are further restricted by the limited publication of new information as a result of IP legalities. The combination of regulatory gaps, propriety restrictions and overall novelty of the vessels, has resulted in a significant lack of publications in comparison to type IV and earlier designs.

Publications specific to type V pressure vessels are tabulated below (Table 6) and categorised in accord with the prior depicted data. Compared to the papers covering type IV design, there is a significant increase in material testing and vessel health monitoring (failure modes). However, approximately a third of the publications cover cryogenic or cryo-compressed storage solutions and thus are not applicable.

Table 6 - Breakdown of existing Type-V pressure vessels based on content type

Author	Year	Mathematical Theory	Simulation	Experimental Data	Materials	Boss Design	Literature Review	Health Monitoring
Air et al.	2023				X		X	X
Air et al.	2023	X	X	X	X			X
Jaber et al.	2024		X		X			X
Hubner et al.	2021	X		X	X		X	X
Yan et al.	2024			X	X			X
Zhang et al.	2023			X	X		X	X

Two articles, both published by Air et al. (2023), have been identified as key significant publications that cover the latest development of type V pressure vessel technology. ‘A review of Type V composite pressure vessels and automated fibre placement based manufacturing’ explores hydrogen as a promising energy source, focusing on the advancements in composite overwrapped pressure vessels (COPVs) and manufacturing techniques like automated fibre placement (AFP). Air et al. (2023) reports that type V pressure vessels have the potential to reduce weight by approximately 10-

20 % compared to conventional designs, while enhancing fatigue performance and allowing for higher operating pressures.

Despite these advantages, Air et al. (2023) positions that the hurdles related to the manufacturing processes negatively affect the commercial adoption of Type V vessels. As reviewed by Air et al. (2023), the advancements made in automated fibre placement (AFP) technologies allow their potential utilization in type V pressure vessels. AFP manufacturing processes were found to offer improved flexibility and precision in laying up composite materials, thus producing a stronger vessel. The work presented by Air et al. (2023) highlights critical regulatory gaps concerning guidelines specific to type V construction and the utilisation of advanced manufacturing techniques such as AFP. This is a critical area for future research and presents a legal hurdle that must be overcome to ensure safe widespread adoption.

Air et al. (2023) second publication 'Design and manufacture of a Type V composite pressure vessel using automated fibre placement' presents the design, manufacturing, and testing of an AFP produced composite pressure vessel with a design working pressure of 4.22 MPa. The goal was to explore the feasibility of using AFP for the manufacture of small-scale, liner-less (Type V) composite pressure vessels suitable for automotive and aerospace applications.

The optimal isotensoid shape was used for the dome regions to achieve uniform stress in the fibre direction. Air et al. (2023) developed a thickness control strategy using ply drops to match the desired thickness profile on the domes. Utilising 3D scan technology the masses of the AFP parts were validated to be within 2.23% of the predicted values. Finite element analysis was conducted to evaluate the structural performance of the vessel under internal pressure. The analysis indicated that the maximum stress occurred in the centre of the closed dome, which was designated as the failure location. The polar boss and adhesive lap joint were also assessed and found to have adequate strength. Despite this, Air et al. (2023) found several manufacturing defects including wrinkles, gaps between tows, and a hole in the centre of the closed dome. Hydrostatic pressure testing revealed

leakage starting at 0.13 MPa, well below the 6.33 MPa proof pressure. Air et al. (2023) attributed this leakage to the manufacturing defects, particularly the gaps observed between tows.

To improve the leak-before-burst behaviour, Air et al. (2023) proposes that future work should focus on eliminating or reducing these gaps, as well as incorporating hoop reinforcement on the domes. Additionally, Air et al. (2023) suggests more sophisticated failure criteria should be employed.

2.3.3 Manufacturing Techniques & Limitations

Composite pressure vessels are predominantly manufactured with the filament winding or automated fibre placement (AFP) technique. Filament winding involves winding continuous pre-impregnated fibres under high tension around a rotating mandrel (Addcomposites 2024b). This process often results in excess material and has limited adaptability for complex shapes. In contrast, AFP uses a robotic system to place narrow fibre tows precisely onto a surface. This enables selective reinforcement for more efficient material usage, and has the ability to handle more complex geometries (Addcomposites 2024a). While filament winding is well-established and widely used in the industry, AFP represents a more advanced, flexible method with potential for improved performance and reduced weight.

2.3.3.1 Filament Winding

Azeem et al. (2022) reviews the utility and feasibility of filament winding as a manufacturing technique for pressure vessels, the evolution of the manufacturing process and key parameters. Furthermore, the publication summarizes various optimization methods, numerical analysis approaches, associated challenges, and provides relevant recommendations for future applications. Azeem et al. (2022) indicates that the use of filament winding for the production of a type IV pressure vessels can reduce the weight by up to 75 % compared to traditional metallic vessels.

Additionally, Azeem et al. (2022) found that the process supports a variety of fibre orientations and winding patterns, enabling tailored designs that meet specific mechanical and structural requirements. The findings of Azeem et al. (2022) suggest that the use of automation can enhance consistency and productivity, making it a cost-effective solution for large-scale production.

Conversely, Azeem et al. (2022) acknowledges that despite its advantages, there are notable challenges of filament winding, particularly in achieving defect-free production. Fibre misalignment, gaps and resin-rich zones can lead to gas permeation in high-pressure applications as a consequence of reduced mechanical integrity. These findings are consistent with those of Air et al. (2023). Azeem et al. (2022) proposes that to avoid delamination and microcracking, ensuring uniform resin impregnation is critical to managing fibre tension. Furthermore, the literature identifies that the dome regions of pressure vessels pose geometric complexities, often resulting in variable composite thickness and stress concentrations.

Future research, as suggested by Azeem et al. (2022), is necessary to overcome the challenges of defect management, particularly in complex geometries. Future advancements in computer-aided winding techniques, real-time defect monitoring and material innovation is expected, as per Azeem et al. (2022), to enhance the feasibility and performance of filament-wound pressure vessels in critical applications.

2.3.3.2 Automated Fibre Placement

Air et al. (2023) utilized AFP technologies to manufacture a type V pressure vessel and performed destructive testing to validate the design with comparison against the theoretical model. The vessel consisted of two composite halves, an open dome and a closed dome, joined together using an epoxy adhesive. This was required due to the physical constraints of the AFP machine and the need to apply the fibre tows against a mandrel. This required Air et al. (2023) to design and manufacture specific

custom collapsible mandrels. This concurrently increases the complexity of the manufacturing process, as well as the cost of tooling, as mandrels are unique to each pressure vessel design.

The limitations of the work published in 2023 by Air et al. have been addressed by their latest publication (2024) 'Optimisation of a composite pressure vessel dome using non-geodesic tow paths and automated fibre placement manufacturing'. Air et al. (2024) utilised an optimized non-geodesic path and thickness profile. This resulted in a reduction in the thickness variation from a previous average of 2.23 % to a new average of 1.86 %. However, reoccurring defects from their previous study were identified in regions with tight steering radii. This highlights the limitations of current AFP technology.

Air et al. (2024) demonstrates that AFP can be used to overcome the limitations of filament winding in pressure vessel manufacturing. AFP allows for optimization of both thickness and fibre angles, something that could not be achieved previously. The methods developed in this paper provide a framework for improving the design and manufacture of composite pressure vessels.

2.4 Polar Boss Design

There is an absence of publications that comprehensively cover the specific design of a polar boss for use in a type V pressure vessel. The use of a polar boss is covered in the work produced by Air et al. (2023), however the design of the polar boss is limited to just the external surface geometry which is matched to the isotensoid dome profile.

The theoretical model developed in this project will follow the same assumptions and utilise the same material and adhesion properties in the simulation to allow for comparison.

The design of a polar boss for a type IV pressure vessel is presented in the work by Park et al. (2021). Park et al. (2021) utilised the response surface method to adjust the polar boss parameters; length, thickness, height, and angle to optimise the boss design.

Park et al. (2021) developed a flow chart of optimal pressure vessel design shown below as figure 3.

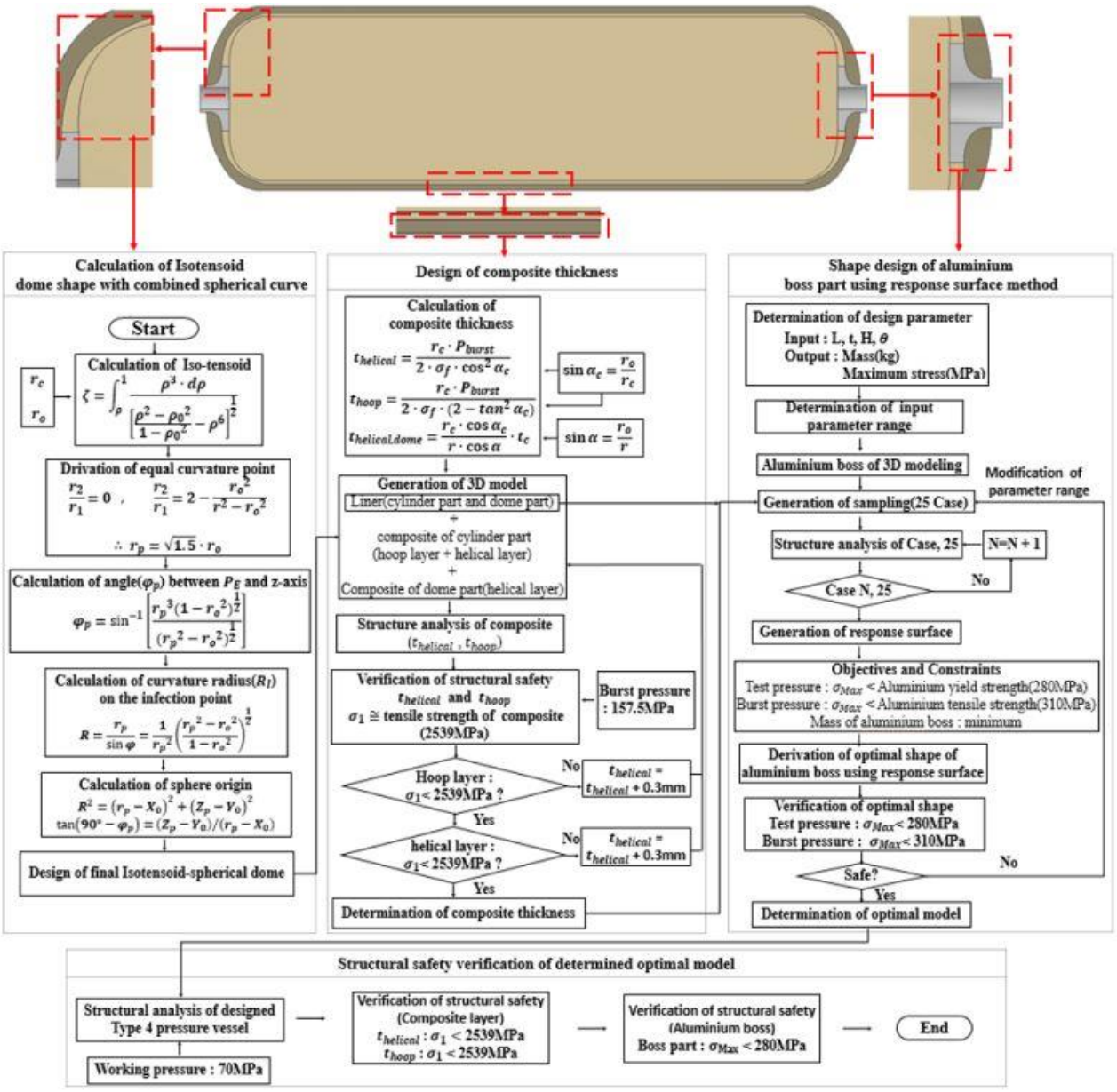

Figure 3 - Flowchart of Optimised Pressure Vessel Design (Park et al. 2021)

2.5 Failure Modes

Zhang et al. (2019) provides a comprehensive overview of the current failure prediction models. Their work focuses specifically on Type III and Type IV designs. The findings of Zhang et al. (2019) suggest that the primary failure modes include burst, fibre damage, and fatigue failure. It was reported by Zhang et al. (2019) that burst pressures were observed around 94 to 96 MPa for type III vessels and 162 to 175 MPa for type IV vessels.

Zhang et al. (2019) synthesises that the progressive failure analysis of composite tanks generally consists of stress analysis, failure evaluation, material degradation, and burst pressure detection. The utilization of a progressive failure analysis allows for the transition from initial damage to final failure. This approach allows for the consideration of stress redistribution within the composite.

Furthermore Zhang et al. (2019) compiled a table of applicable failure modes and their criteria shown below in figure 4. All failure modes, other than ‘Sun’ and ‘Micromechanics of Failure’, are available within the ANSYS simulation software. Future research is needed, as suggested by Zhang et al. (2019), to explore predictive models that integrate multiscale failure analysis, real-time monitoring, and thermal stresses.

Zhang et al.’s (2019) findings are consistent with those of Zhou et al. (2022). Both studies highlighted three primary forms of failure; burst, fatigue and impact. Burst failure occurs when the vessel reaches its maximum pressure capacity, fatigue failure arises from cyclic loading over time, and impact failure is caused by external forces during transport or operation. In the transportational sector, the chances of an impact of significant size to produce failure is limited due to the shielding provided by the vehicle chassis. Zhou et al. (2022) proposes that non-destructive testing (NDT) techniques may play a pivotal role in meeting the increasing demand for safety regulations.

Table 2 – Comparison of failure criteria for composite materials.

	criterion
Tsai-Wu [14]	$F_i\sigma_i + F_{ij}\sigma_i\sigma_j + F_{ijk}\sigma_i\sigma_j\sigma_k \geq 1,$ $i, j, k = 1, 2, \ldots, 6$
Rotem [37]	$\frac{\sigma_X}{X_T} = 1, \frac{\sigma_X}{X_C} = 1, \left(\frac{E_m(\varepsilon_x)\varepsilon_x}{S_m}\right) + \left(\frac{\sigma_Y}{Y_T}\right)^2 + \left(\frac{\sigma_S}{S}\right)^2 = 1 F_{11}^t(\sigma_{11}, \tau_{12}, \tau_{13}) = \left(\frac{\sigma_{11}}{S_{11}^t}\right)^2 + \left(\frac{\tau_{12}}{S_{12}}\right)^2 + \left(\frac{\tau_{13}}{S_{13}}\right)^2 - 1 \gg 0,$
Hashin [38]	$F_{11}^c(\sigma_{11}) = \left(\frac{\sigma_{11}}{S_{11}^c}\right)^2 - 1 \gg 0, F_{22}^t(\sigma_{22}) = \left(\frac{\sigma_{22}}{S_{22}^t}\right)^2 - 1 \gg 0$
Max. Stress [39]	$\frac{\sigma_Y}{Y_T} = 1, \frac{\sigma_X}{X_T} = 1, \frac{\sigma_Y}{Y_C} = 1, \frac{\sigma_X}{X_C} = 1, \frac{\lvert\sigma_S\rvert}{S} = 1,$
Sun [40]	$\frac{\sigma_X}{X} = 1, \left(\frac{\sigma_Y}{Y}\right)^2 + \left(\frac{\sigma_S}{S}\right)^2 = 1$
Puck [28]	For $\sigma_{n(\theta)} \gg 0 : f_E(\theta) = \sqrt{\left[\left(\frac{1}{R_\perp^{(+)}} - \frac{P_{\perp\Psi}^{(+)}}{R_{\perp\Psi}^A}\right)\right]^2 + \left(\frac{\tau_{nt}(\theta)}{P_{\perp\perp}^A}\right)^2 + \left(\frac{\tau_{n1}(\theta)}{R_{\perp\parallel}^A}\right)^2} + \frac{P_{\perp\Psi}^{(+)}}{R_{\perp\Psi}^A}\sigma_n(\theta)$ For $\sigma_{n(\theta)} \gg 0 : f_E(\theta) =$ $\sqrt{\left[\frac{P_{\perp\Psi}^{(-)}}{R_{\perp\Psi}^A}\sigma_n(\theta)\right]^2 + \left(\frac{\tau_{nt}(\theta)}{P_{\perp\perp}^A}\right)^2 + \left(\frac{\tau_{n1}(\theta)}{R_{\perp\parallel}^A}\right)^2} + \frac{P_{\perp\Psi}^{(-)}}{R_{\perp\Psi}^A}\sigma_n(\theta)$
Tsai-Hill [41]	$\frac{\sigma_X^2}{X^2} - \frac{\sigma_X\sigma_Y}{X^2} + \frac{\sigma_Y^2}{Y^2} + \frac{\sigma_S^2}{S^2} = 1$
Hoffman [41]	$-\frac{\sigma_X^2}{X_C X_T} + \frac{\sigma_X\sigma_Y}{X_C X_T} - \frac{\sigma_Y^2}{Y_C Y_T} + \frac{X_C + X_T}{X_C X_T}\sigma_X + \frac{Y_C + Y_T}{Y_C Y_T}\sigma_Y + \frac{\sigma_S^2}{S^2} = 1$
micromechanics of failure [42]	$-C_f < \sigma_{f1} < T_f, \left(\frac{\sigma_{VM}}{\sigma_{VM}^{cr}}\right)^{n_p} + \left(\frac{I_1}{I_1^{cr}}\right) = 1$

Figure 4 - Comparison of Failure Criteria (Zhang et al. 2019)

2.6 Conclusions

Findings from the literature review demonstrate the practicability of compressed gas storage using type IV and type V pressure vessels in current and prospective applications, particularly in the automotive industry. Essential to vehicle performance and durability, CFRP pressure vessels offer remarkable strength-to-weight ratios and corrosion resistance. Existing extensive research addressing the mechanical properties, failure modes and manufacturing methods of type IV vessels have demonstrated their viability and application. However, type V vessels are an emerging technology, promising enhanced performance and even greater weight reduction. Notably, the development and utility of type V vessels are hindered by limited published research. Automated fibre placement processes have shown potential to optimize manufacturing processes although defects such as fibre misalignment and gaps continue to pose barriers to reliability and safety.

Future research is required on the regulatory standardization for type V vessels, enhanced manufacturing defect management and improved predictive modelling for failure mechanisms. Addressing these knowledge gaps is pivotal to increasing the use of these hydrogen storage technologies.

To conclude, materials science and manufacturing innovations have the potential to allow CFRP pressure vessels to overcome existing limitations. The integration of robust failure analysis, advanced production methods, and comprehensive testing protocols, will ensure these technologies meet the demands of efficiency, safety, and useability in the transportation sector.

CHAPTER 3

METHODOLOGY

3.1 Introduction

Multiple programs were used to generate and simulate a theoretical model of a type V pressure vessel. Figure 5 below shows the methodology workflow chart. Design requirements were defined from the literature reviewed. These preliminary parameters, either referenced or calculated, were imported into a MATLAB script to generate a series of data points that constitute the shape of the pressure vessel. These data points were then imported into Fusion 360 to generate a CAD model. The CAD model was imported into ANSYS workbench and the simulation was developed.

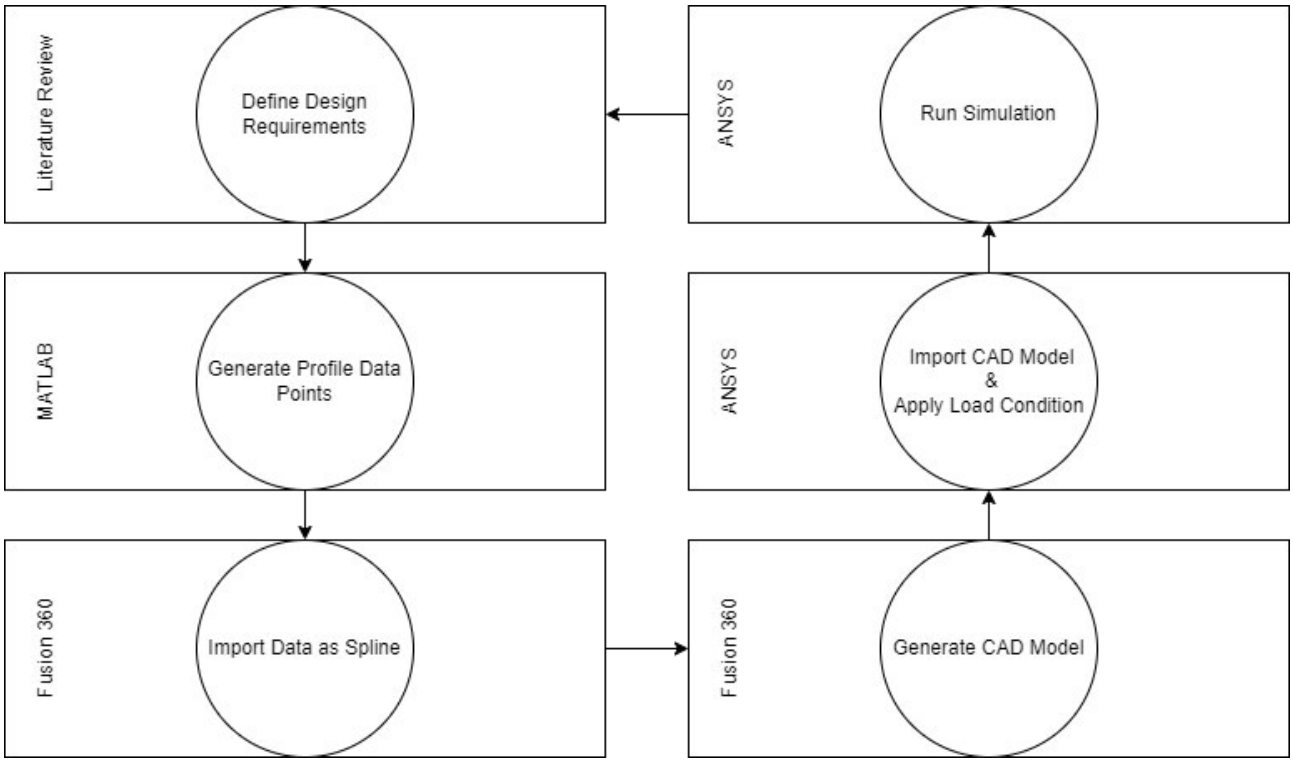

Figure 5 - Methodology Workflow Chart

Table 7 provides an overview of the design parameters and preliminary dimensions calculated in the methodology introduction that were referenced in the generation of the pressure vessel model.

Table 7 - Preliminary Design Parameters and Dimensions

Symbol	Parameter	Value	Units
p_w	Pressure, working	70	MPa
p_b	Pressure, burst	245	MPa
V	Volume, internal	0.1414	m^3
r	Radius	0.2036	m
l	Length, total	1.2216	m
t	Thickness, maximum	0.02035	m

3.1.1 Pressure Vessel Capacity and Working Pressure

The industry standard working pressure (p_w) for H^2 pressure vessels used in the transportational sector, as compiled in section 2.2.1, is 70 MPa. 5.6 kg of hydrogen is required for a targeted driving range of > 500 kg, with an assumed fuel cell efficiency of 50 % (Hwang & Varma 2014). At the given working pressure and standard temperature (20 °C), hydrogen has an approximate density of 39.60 kg / m^3 (GenH2 2022). Therefore, an internal volume (V) of 0.1414 m^3 is required to store a sufficient amount of H^2.

3.1.2 Preliminary Design and Dimensions

The general structure of a Type-V PV takes the form of a cylindrical region capped on either end with a spherical dome of equal radius. The internal volume of a general pressure vessel structure whose cylindrical region length is equal to four times the radius is given by the equation:

$$V\ (m^3) = \frac{16}{3}\pi r^3 \qquad (3.1.2.1)$$

From (3.1.2.1) the radius is given by:

$$r\ (m) = \sqrt[3]{\frac{3\,V}{16\,\pi}} \qquad (3.1.2.2)$$

Given a V of 0.1414 m^3, the pressure vessel has a r of 0.2036 m. The total length of the pressure vessel is equal to six times the radius, equal to 1.2216 m.

In order for the pressure vessel to be considered 'thin-walled' the radius to thickness ratio must be greater than ten as shown :

$$\frac{r}{t} > 10 \qquad \text{(Ibrahim et al. 2015)} \quad (3.1.2.3)$$

Thus, given a r of 0.2036 m, a maximum thickness t of 0.02035 m can be obtained.

3.1.3 Proposed Construction

Given recent advancements in the manufacturing of Type-V PV prototypes such as that published by Air et al. (2023), automated fibre placement (AFP) will be considered the manufacturing technology that is to be used whilst developing the model. The use of AFP will allow a wider range of fibre angles as well as inconsistent ply thickness resulting from variable material deposition. This will allow additional plies to be placed in areas of stress concentrations specifically that surrounding the critical zone.

3.1.4 Material Specification

Epoxy Carbon UD (230 GPa) Prepreg was chosen from the ANSYS composite material library for the pressure vessel body. The material properties are outlined in table 8.

Table 8 - ANSYS Epoxy Carbon UD (230 GPa) Prepreg Material Properties

Symbol	Parameter	Value	Units
$\sigma_{tx,}\ \sigma_{ty,}\ \sigma_{tz}$	Stress, tension	2231, 29, 29	MPa
$\sigma_{tx,}\ \sigma_{ty,}\ \sigma_{tz}$	Stress, compression	-1082, -100, -100	MPa
$\tau_{xy,}\ \tau_{yz,}\ \tau_{xz}$	Shear	60, 32, 60	MPa
E_1, E_2, E_3	Elastic Modulus	121000, 8600, 8600	MPa
G_{12}, G_{23}, G_{13}	Shear Modulus	4700, 3100, 4700	MPa
v_{12}, v_{23}, v_{13}	Poisson's Ratio	0.27, 0.4, 0.27	-

A generic profile for aluminum alloy was selected from the ANSYS material library for the polar boss for preliminary modelling. The material properties are outlined in table 9.

Table 9 - ANSYS General Aluminum Alloy Material Properties

Symbol	Parameter	Value	Units
σ_y	Stress, yield	280	MPa
σ_{ult}	Stress, ultimate	310	MPa
E	Elastic Modulus	71000	MPa

An epoxy adhesive is proposed to bond the polar boss to the CFRP body. To model the adhesion between the two components a fracture-energies based cohesive zone model (CZM) was used within the ANSYS modelling software. The properties for the CZM are listed in table 10, and are taken from results by Katsitopoulos et al. (2012) and referenced in Air et al. (2023).

Table 10 - CZM Epoxy Adhesive Properties

Parameter	Value	Units
Maximum normal contact stress	50	MPa
Critical fracture energy for normal separation	125	J / mm^2
Maximum equivalent tangential contact stress	25	MPa
Critical fracture energy for tangential slip	1500	J / mm^2
Artificial damping coefficient	0.000001	-

3.1.5 Applicable Standards and Criteria

Both Australian Standard AS1210-2010: Pressure Vessels and ASME BPVC calls for a safety factor of 3.5 to be applied to the working pressure (Standards Australia 2010; Red River 2023). Therefore, given a p_w of 70 MPa, the vessel must be designed with a burst pressure of 245 MPa. This exceeds the ISO11119-3:2020 standard that calls for a factor of safety of 3 (Air, Oromiehie, et al. 2023). Thus by compliance with AS1210-2010 the design automatically meets ISO11119-3:2020 and ASME BPVC.

3.2 Theoretical Model Design

The optimal pressure vessel design minimizes weight whilst maximizing capacity. This is especially important for the transportational sector as additional weight directly reduces the fuel efficiency and driving range of the vehicle. Air et al. (2023) and Jois et al. (2021) propose this occurs when the dome shape, known as the isotensoid profile, results in uniform tension across the fibres.

3.2.1 Dome Region

The dome region will be constructed utilizing a theoretical geodesic path to place the prepreg fibres. The geodesic path is unique for each dome geometry and is defined as the shortest path connecting two points on a surface (Jois et al. 2021). It is characterized by the Clairaut equation :

$$\varphi_r = \sin^{-1}\left(\frac{r_o}{r}\right) \quad \text{(Vasiliev \& Jones 2009)} \quad (3.3.1.1)$$

$$\varphi_r = \sin^{-1}\left(\frac{0.075}{0.0200}\right)$$

$$\varphi_r = 22.02°$$

Where φ_r is the winding angle, r_o the radius of polar boss and r the radius of the cylindrical region. Given a polar boss of radius 0.075 m and cylindrical radius of approximately 0.200 m, the winding angle is calculated as φ_r = 22.02°.

Fig 6 (a) shows the general shape of the dome and (b) shows the profile.

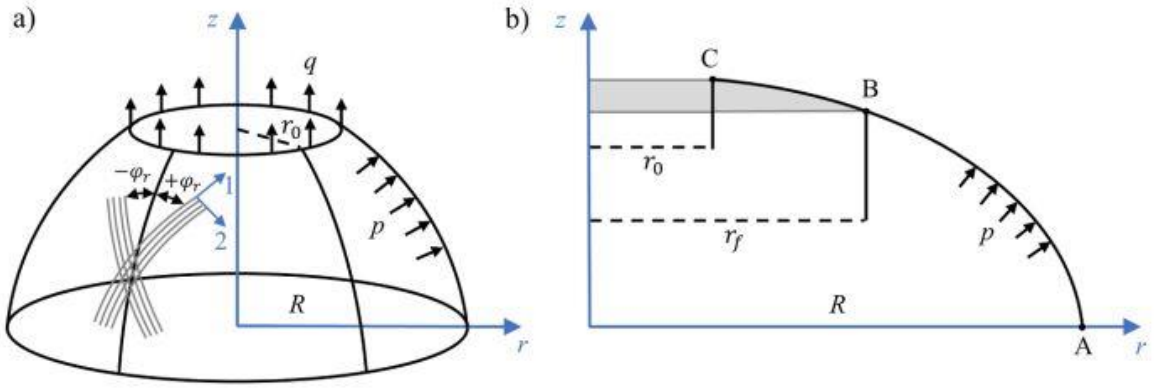

Figure 6 - Isotensoid Dome Profile and Revolution (Air, Oromiehie, et al. 2023)

The profile is split into two sections; AB which ranges from the cylindrical region to the start of the polar boss and BC which covers from the start of the polar boss to the polar boss opening. Section BC is also the adhesion zone between the polar boss and the CFRP body.

These profiles can be numerically solved to produce a table of data points that can be utilized to generate a 3D model of the dome. The values calculated below are normalized to the cylindrical radius *r*. The resultant isotensoid dome profile is shown in figure 7.

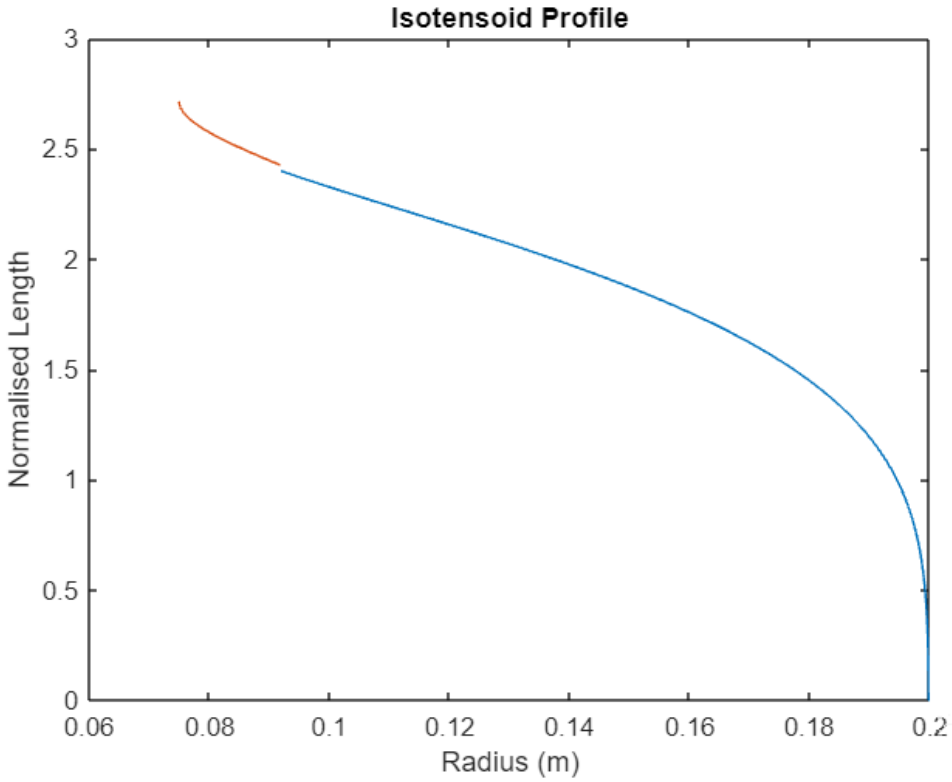

Figure 7 - Isotensoid Dome Profile

3.2.1.1 Section AB Isotensoid Profile

The normalized radius is given by the equation :

$$\bar{r}_{AB} = \sqrt{1 - (1 - \bar{r}_1{}^2) \times \sin(\theta^{(1)})^2} \qquad \text{(Air, Oromiehie, et al. 2023)} \quad (3.2.1.1.01)$$

The normalized height (when viewed vertically as per figure 7) or length (when viewed horizontally as per previous pressure vessel figures) is given by the equation :

$$\bar{z}_{AB} = \sqrt{1 + \bar{r}_2{}^2} \times E\left(k, \theta^{(1)}\right) - \frac{\bar{r}_2{}^2}{\sqrt{1+\bar{r}_2{}^2}} \times F(k, \theta^{(1)})$$

(Air, Oromiehie, et al. 2023) (3.3.1.1.02)

Where ;

$$0 \leq \theta^{(1)} \leq \theta_f{}^{(1)}$$ (Air, Oromiehie, et al. 2023) (3.3.1.1.03)

$$\theta_f{}^{(1)} = \sin^{-1}\sqrt{\frac{1-\bar{r}_f{}^2}{1-\bar{r}_1{}^2}}$$ (Air, Oromiehie, et al. 2023) (3.3.1.1.04)

$\bar{r_0} = \frac{r_0}{R}$ (where R is cylindrical radius r)

(Air, Oromiehie, et al. 2023) (3.3.1.1.05)

$$\bar{r_f} = \sqrt{\frac{3}{2}} \times \bar{r_0}$$ (Air, Oromiehie, et al. 2023) (3.3.1.1.06)

$$k = \sqrt{\frac{1-\bar{r}_1{}^2}{1+\bar{r}_2{}^2}}$$ (Air, Oromiehie, et al. 2023) (3.3.1.1.07)

$$\bar{r}_1{}^2 = \frac{1}{2}\left(\sqrt{\frac{1+3\bar{r}_0{}^2}{1-\bar{r}_0{}^2}} - 1\right)$$ (Air, Oromiehie, et al. 2023) (3.3.1.1.08)

$$\bar{r}_2{}^2 = \frac{1}{2}\left(\sqrt{\frac{1+3\bar{r}_0{}^2}{1-\bar{r}_0{}^2}} + 1\right)$$ (Air, Oromiehie, et al. 2023) (3.3.1.1.09)

And functions $F(k,\theta^1)$ and $E(k,\theta^1)$ are the first and second incomplete elliptic integrals, respectively (Air, Oromiehie, et al. 2023). The normalized profile for section AB was calculated in MATLAB and is shown in figure 8. The MATLAB code can be found in Appendix C.

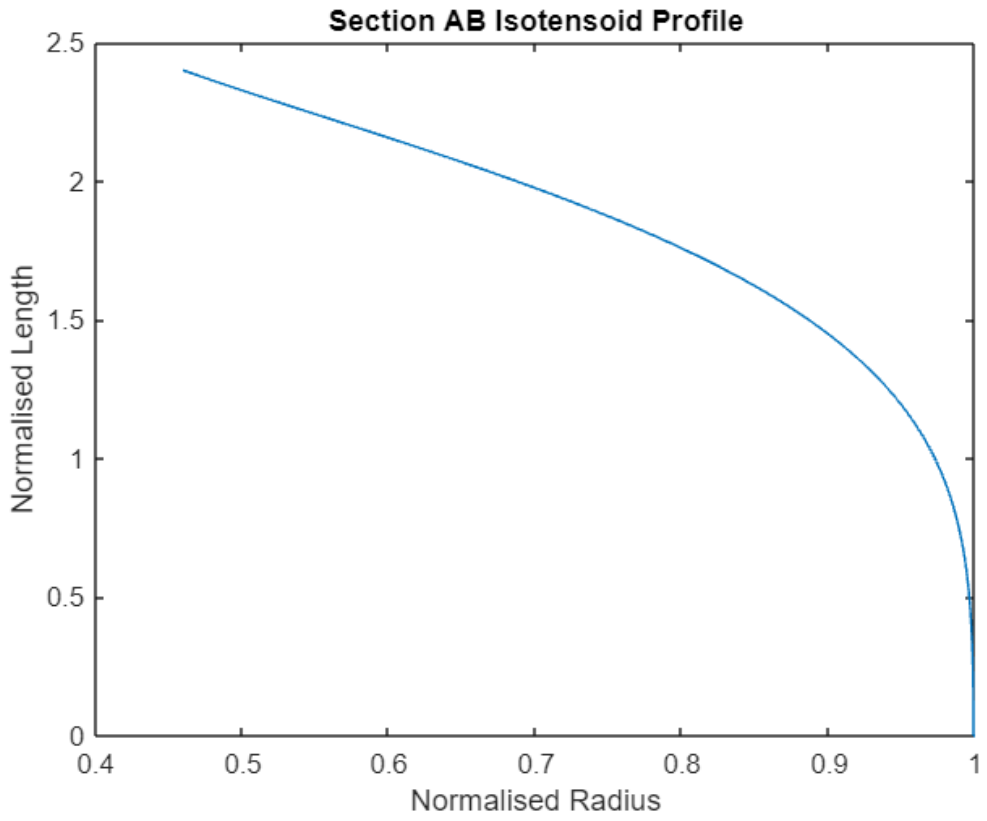

Figure 8 - Section AB Isotensoid Normalised Profile

3.2.1.2 Section BC Isotensoid Profile

Similarly the BC section profile is given by :

$$\bar{r}_{BC} = \sqrt{\bar{r}_0{}^2 + n_1 \times \cos(\theta^{(2)})^2}$$ (Air, Oromiehie, et al. 2023) (3.3.1.1.10)

$$\bar{z}_{BC} = \sqrt{n_1 + n_2} \times \left[E\left(n, \theta^{(2)}\right) - (1 - n^2)F\left(n, \theta^{(2)}\right)\right] + c_2$$

(Air, Oromiehie, et al. 2023) (3.3.1.1.11)

Where ;

$$\theta_f{}^{(2)} \leq \theta^{(2)} \leq \frac{\pi}{2}$$ (Air, Oromiehie, et al. 2023) (3.3.1.1.12)

$$\theta_f{}^{(2)} = \cos^{-1}\sqrt{\frac{\bar{r}_f{}^2 - \bar{r}_0{}^2}{n_1}}$$ (Air, Oromiehie, et al. 2023) (3.3.1.1.13)

$$n_1 = \frac{1}{2}\sqrt{\bar{r}_0{}^4 + \frac{4\left(\bar{r}_f{}^2 - \bar{r}_0{}^2\right)^2}{\bar{r}_f{}^4\left(1 - \bar{r}_0{}^2\right)} - \bar{r}_0{}^2}$$ (Air, Oromiehie, et al. 2023) (3.3.1.1.14)

$$n_2 = \frac{1}{2}\sqrt{\bar{r}_0{}^4 + \frac{4\left(\bar{r}_f{}^2 - \bar{r}_0{}^2\right)^2}{\bar{r}_f{}^4\left(1 - \bar{r}_0{}^2\right)} + \bar{r}_0{}^2}$$ (Air, Oromiehie, et al. 2023) (3.3.1.1.15)

$$n = \sqrt{\frac{n_1}{n_1 + n_2}}$$ (Air, Oromiehie, et al. 2023) (3.3.1.1.16)

$$c_2 = \sqrt{1 + \bar{r}_2{}^2} \times E\left(k, \theta_f{}^{(1)}\right) - \frac{\bar{r}_2{}^2}{\sqrt{1 + \bar{r}_2{}^2}} \times F\left(k, \theta_f{}^{(1)}\right) - \sqrt{n_1 + n_2} \times \left[E\left(n, \theta_f{}^{(2)}\right) - (1 - n^2)F\left(n, \theta_f{}^{(2)}\right)\right]$$

(Air, Oromiehie, et al. 2023) (3.3.1.1.17)

The normalized profile for section BC was calculated in MATLAB and is shown in figure 9. The MATLAB code can be found in Appendix C.

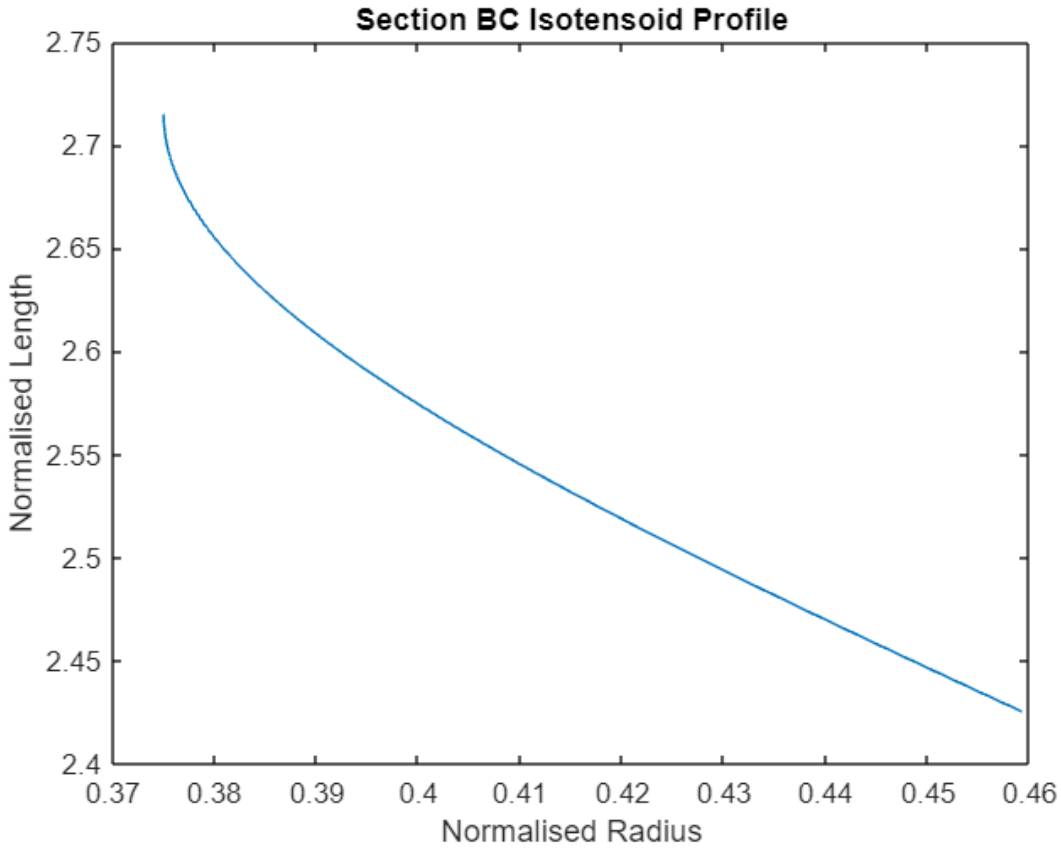

Figure 9 - Section BC Isotensoid Normalised Profile

3.3 Model Generation

The generation of a theoretical model and simulation followed the following steps as outlined below.

3.3.1 CAD Model

The isotensoid profile data generated from the MATLAB script was exported to a Microsoft Excel Worksheet XLSX file. An additional column, representing the z axis position, was generated and populated with '0'. The worksheet was exported as a CSV file and imported into Fusion 360 via the Import Spline CSV script add-in. Figure 10 shows the profile of the pressure vessel made up from the isotensoid spline mirrored over a 1200 mm straight section. The profile was then revolved 360^{o} over the neutral axis to generate the pressure vessel surface model of negligible thickness.

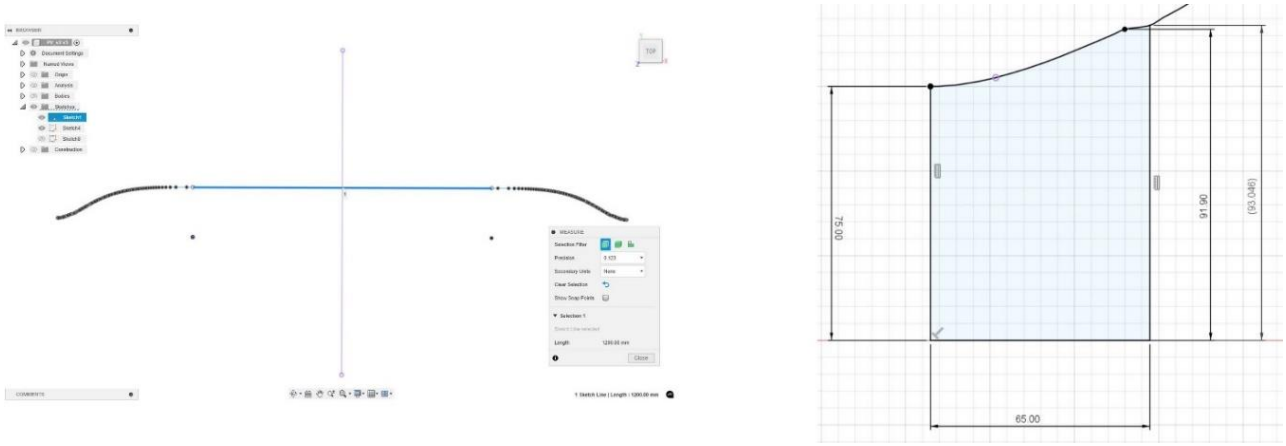

Figure 10 - Pressure Vessel CAD Revolute Profile (left) and Polar Boss Profile (right)

The polar bosses were added as additional bodies to the model by revolving a profile sketch over the neutral axis, in the same manner as the surface model. Two vertical lines were taken from the x-axis and intercepted the isotensoid profile at positions as per section 3.2.1. This additional overlap of approximately 1 mm provides a greater surface area for adhesion and distribution of internal forces. The polar boss was mirrored to the other side. Practically, this will allow additional and better packaging of components to be fitted to the pressure vessel such as pressure relief values, temperature and pressure sensors as well as charge and discharge ports. Figure 11 shows the revolved surface model and a cross-sectional view of the complete pressure vessel with a trivial thickness.

The CAD model was then split into the surface model and the polar boss models and exported as a STEP file. This allowed each component to be imported separately into various stages in ANSYS Workbench for further analysis.

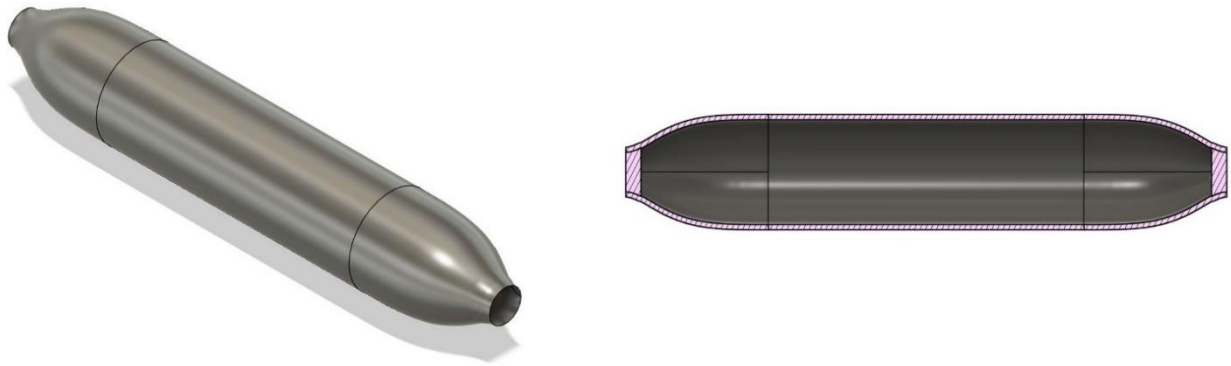

Figure 11 - Pressure Vessel Surface Model (left) and Cross Sectional View (Right)

3.3.2 ANSYS Workbench

The ANSYS Workbench software was used to develop a finite element model of the Type-V CFRP pressure vessel for analysis under a series of loading conditions. Figure 12 shows the project schematic. The following section refers to each individual component (labelled A through G) as a module, and each element (labelled numerically) as a tab.

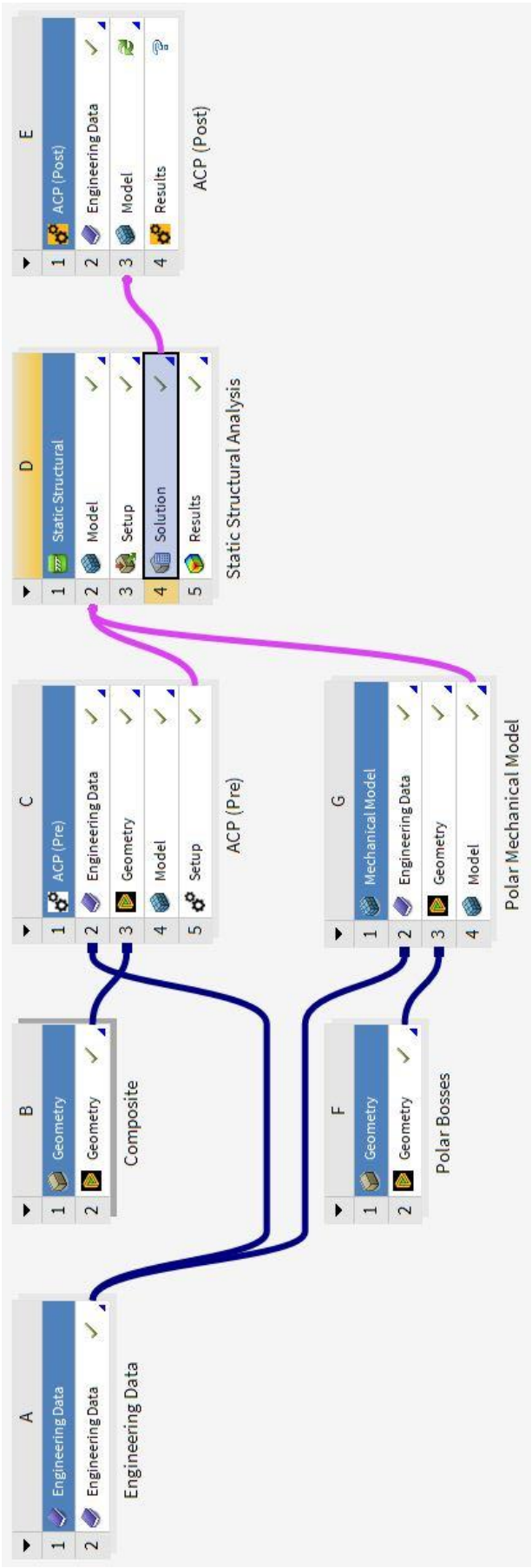

Figure 12 - ANSYS Workbench Project Schematic

3.3.2.1 ACP Pre

The ANSYS Composite PrePost (ACP) add-in module was utilized to define the composite lay-up and fibre orientations in order to accurately model and simulate the stresses undergone within the pressure vessel. Once the pre-defined Engineering Data (section 3.1.4) and Geometry (section 3.3.1) are referenced to the ACP Pre module, the model can be generated. During this stage, the composite surface model geometry is divided into named sections for simplification of the lay-up procedure. The model was then meshed in accordance to section 3.3.3 Mesh Convergence Study.

Under the setup tab a fabric was defined using the material preset from the Engineering Data module and a ply thickness given as 0.2 mm as per Xing et al. (2022). Next, a stackup was defined by selecting a fabric and fibre orientation angle. For the hoop layers on the cylindrical region, a single ply of UD Prepreg with an orientation of 0° was generated. While for the helical layers, two layers of UD Prepreg with angles 22.02° and -22.02° respectively were added. This is shown in figure 13.

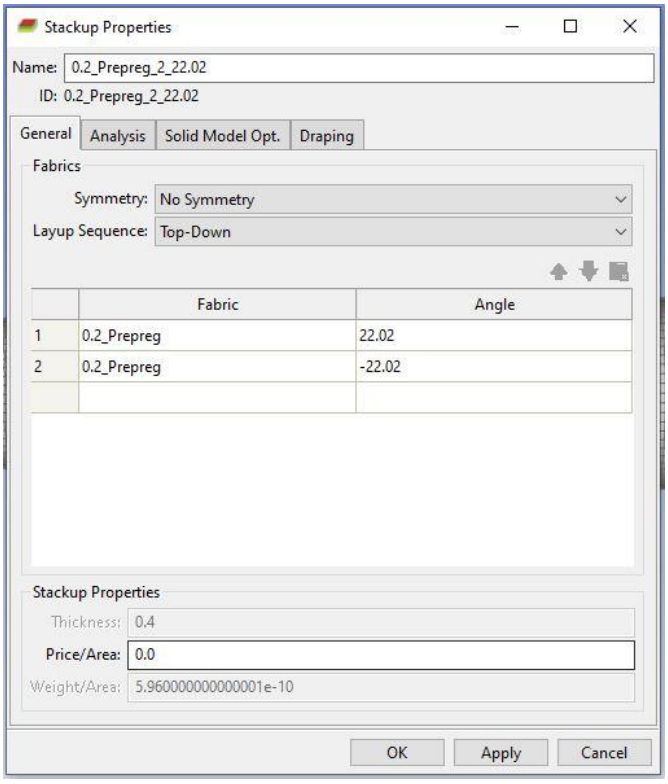

Figure 13 - Helical Layer Stackup Properties

Figure 14 below shows the common layer configurations. The angles are taken from the horizontal neutral axis.

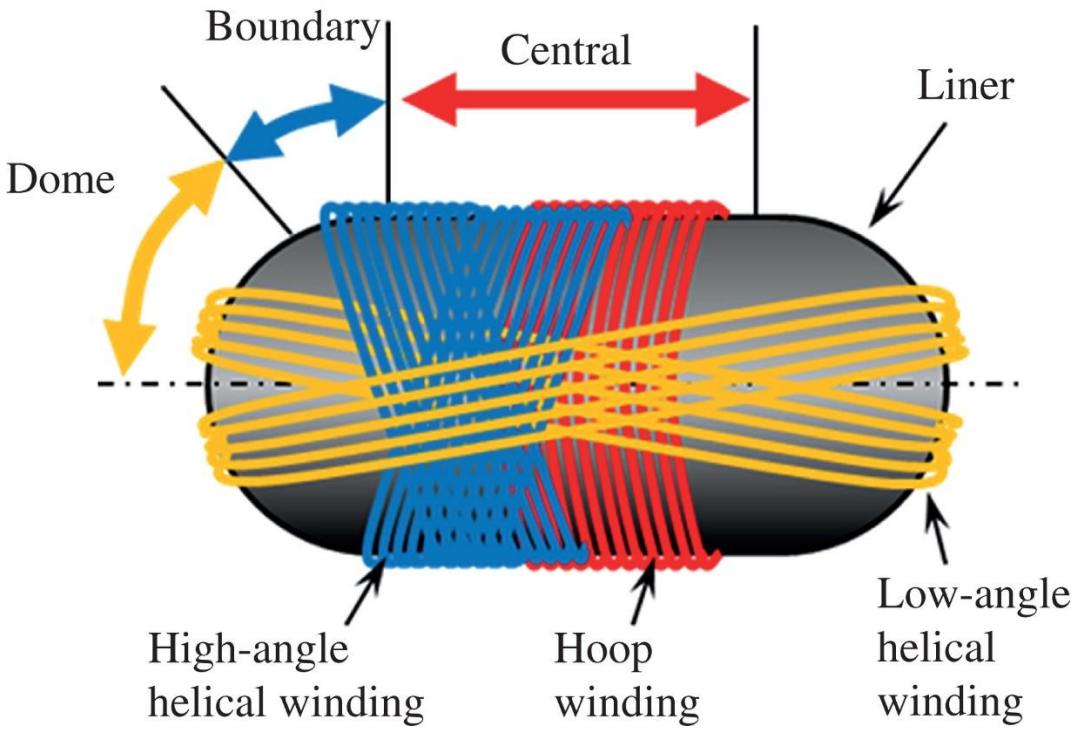

Figure 14 - Pressure Vessel Layer Configurations (Nonobe 2016)

Rosettes were used to define local coordinate systems. A cylindrical rosette was chosen for the cylindrical section with the primary (x) axis orientated radially and the secondary (y); longitudinal. A surface rosette was used to define the coordinates as per the global coordinate system with the x axis along the length of the pressure vessel.

Next, orientated selection sets were used to combine named geometry selections with a rosette and direction of ply build up. This ensures the plies are modelled on the outside of the surface model and do not interfere with the internal capacity of the PV.

Finally, a modelling group was generated combining an orientated selection set and stackup definition. An inner and outer layer was generated over the cylindrical region with the hoop layer

orientation and single ply thickness. Between these layers a series of helical layers were applied across the full surface model, with each layer made up of a 22.02° and -22.02° orientation to achieve symmetry. A total thickness of 20 mm was achieved over the cylindrical region and 19.6 mm over the dome regions. Figure 15 shows the thickness distribution.

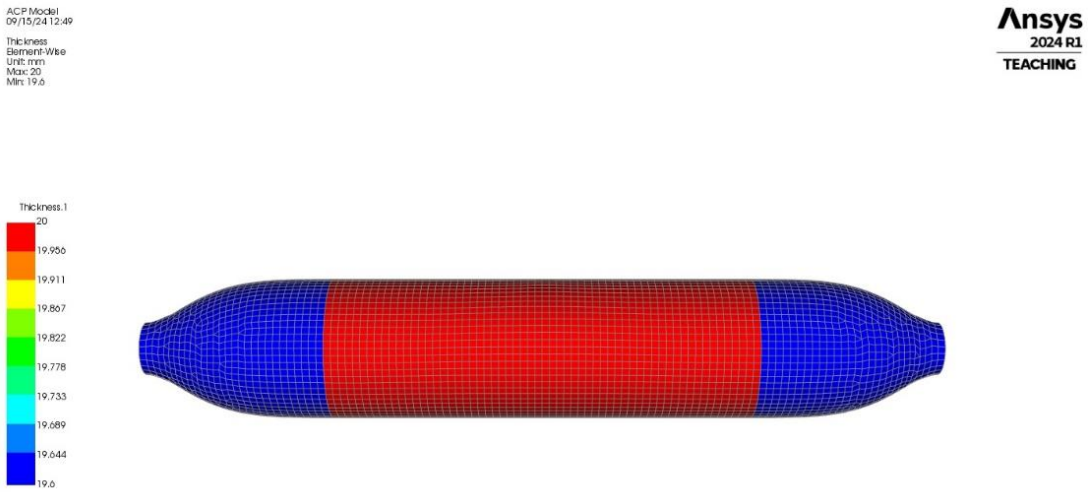

Figure 15 - Composite Lay-up Thickness

3.3.2.2 Mechanical Model

The polar boss solid model was imported from Fusion 360 as a STEP file and assigned the Aluminium Alloy material specifications as outlined in section 3.1.4. Named selections were made to separate the left and right polar bosses for easier identification and the model was meshed as per the mesh convergence study (section 3.3.3).

3.3.2.3 Static Structural

Both geometry tabs from the ACP Pre and Mechanical Model modules were referenced to the Static Strucutral module. Since both models were created within the same global coordinate system in Fusion, the sperate components are automatically aligned in the correct positions.

The use of an epoxy adhesive to secure the polar boss to the composite shell was added to the model utilizing a cohesive zone (CZM). The CZM was based on fracture energies and the properties were taken from literature that used the same ANSYS material properties to allow for comparison (Air, Oromiehie, et al. 2023).

The CZM was modelled using the bonded connection feature. The contact regions are shown below, figure 16, in red for the outer face of the polar bosses and blue for the internal face of the composite. With a loading condition of 70 MPa internal pressure and constraints on the outer faces of both polar bosses, the contact region was reported to be sticking and not experience any debonding.

The results of the CZM are shown below in figure 17. This signifies that the critical zone defined by the BC isotensoid profile provided a sufficiently large enough area for adhesion.

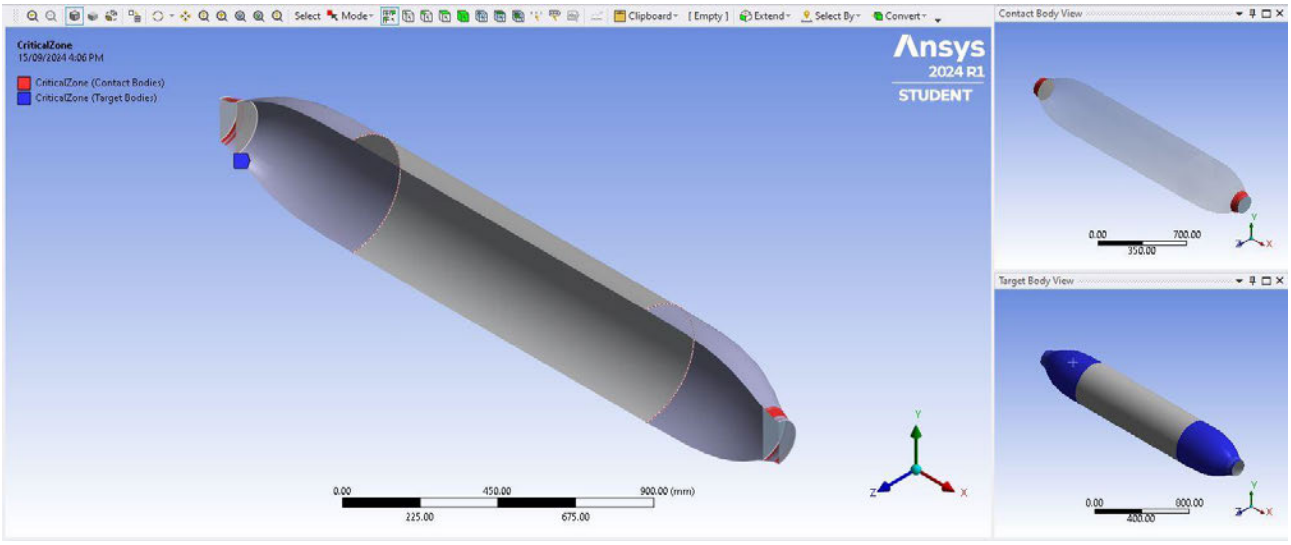

Figure 16 - Bonded Connection at Critical Zone

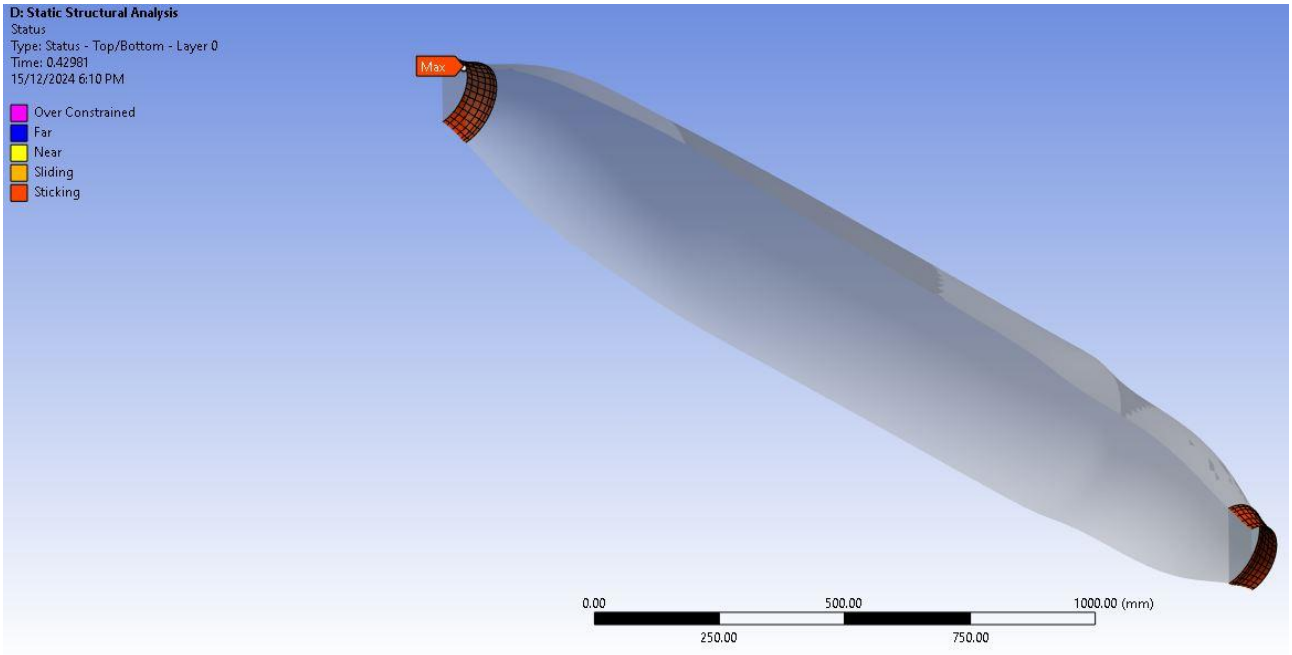

Figure 17 - Cohesive Zone Model Result

3.3.3 Mesh Convergence Study

A mesh convergence study was completed on the model utilizing a simple loading case. A series of simulations were completed with varying mesh refinement. The mesh was manually controlled by dictating the element size. A small insignificant load of 10 MPa was applied to the internal surface of the left polar boss whilst the outer surface of the right polar boss was constrained. A stress probe, shown in figure 18, was added to the model to ensure that stress readings were taken at the exact same spot on each iteration to reduce inaccuracies during the convergence study.

The simulation was run, and the stress recorded at each refinement step. The automatically generated meshing had an average element size of 115 mm and a von Mises stress of approximately 1.24 MPa was recorded. The final refinement resulted in an average element size of 20 mm and von Mises stress of approximately 0.1305 MPa. Figures 19 and 20 show the difference in the mesh generation between the default and final refinements.

Tables 11 through 13 below show the key results from the convergence study.

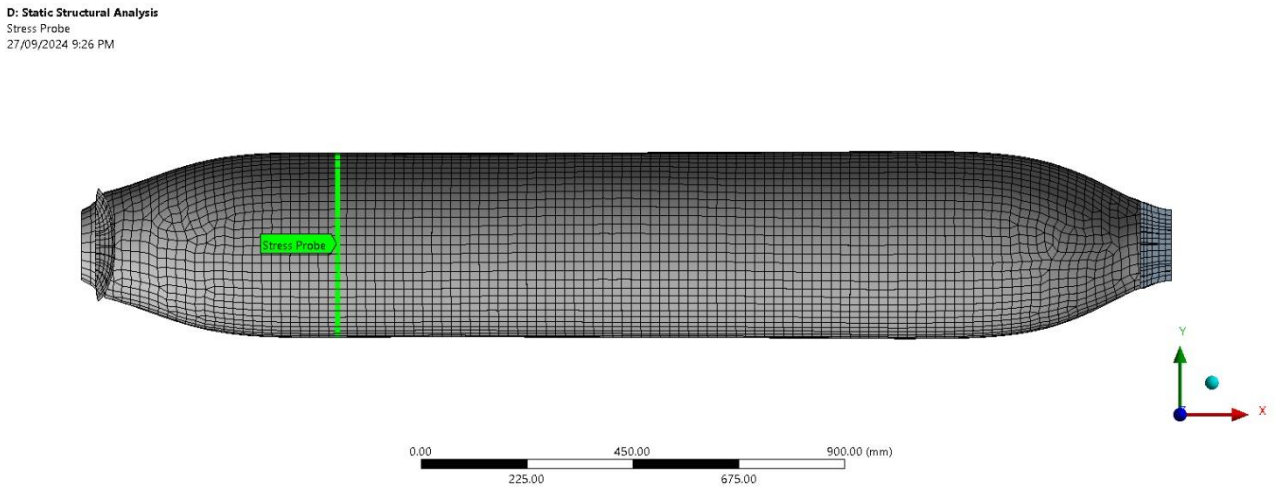

Figure 18 - Convergemce Stress Probe

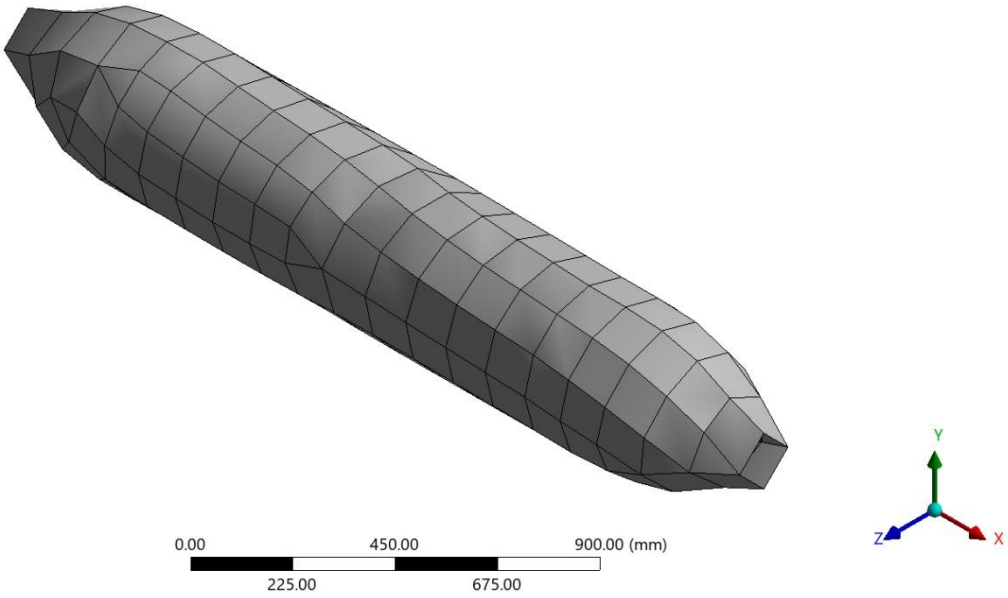

Figure 19 - Default Mesh Generation (115 mm)

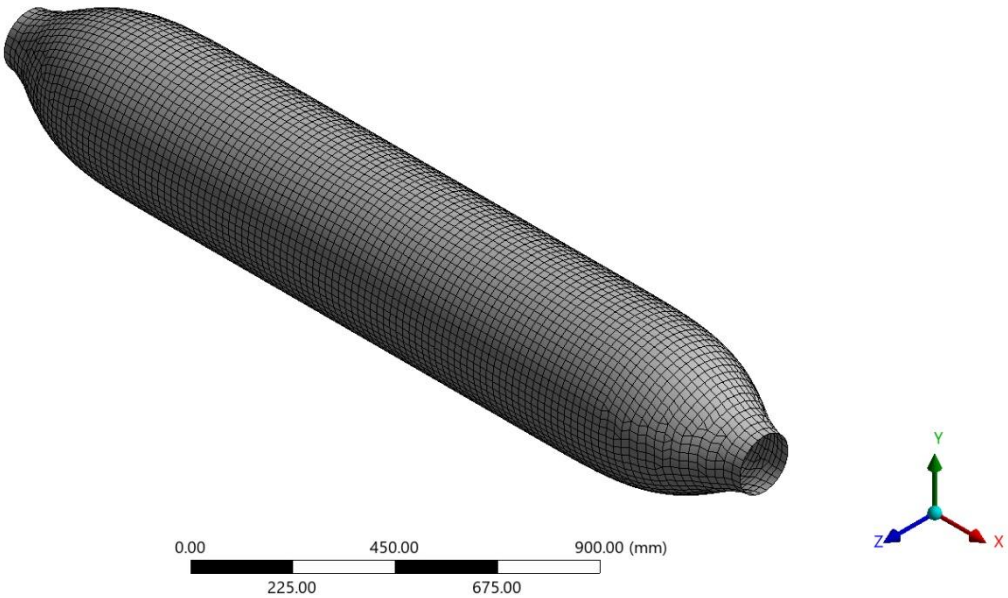

Figure 20 - Final Mesh Generation (20 mm)

Once the mesh converged within 5 to 10 %, as recommended by the ANSYS mesh convergence guidelines (ANSYS 2024), the element size of 20 mm was chosen.

Table 11 - Composite Shell Meshing

Mesh Revision	Element Size (mm)	Nodes	Elements
Default	117.62	218	224
1	80.00	458	468
2	60.00	799	805
3	40.00	1780	1789
4	20.00	6777	6791
5	10.00	27037	27078

Table 12 - Polar Boss Meshing

Mesh Revision	Element Size (mm)	Nodes	Elements
Default	115.02	7923	1626
1	80	8220	1692
2	60	8240	1692
3	40	8679	1794
4	20	12215	2562

Table 13 - Model Convergence Results

Mesh Revision	Element Size (mm)	Von-Mises Stress (MPa)	Convergence (%)
Default	115	1.24290	-
1	80	0.19998	144.561
2	60	0.15812	23.38
3	40	0.13389	16.60
4	20	0.1305	2.56

However, during the simulations, the use of a 20 mm element size resulted in repeated computer crashes. From inspection of the mesh convergence plot, figure 21 below, it could be seen that the model began to converge as the element size dropped below 80 mm. Therefore, it was decided to utilize a 80 mm element size to allow for the simulations to be completed.

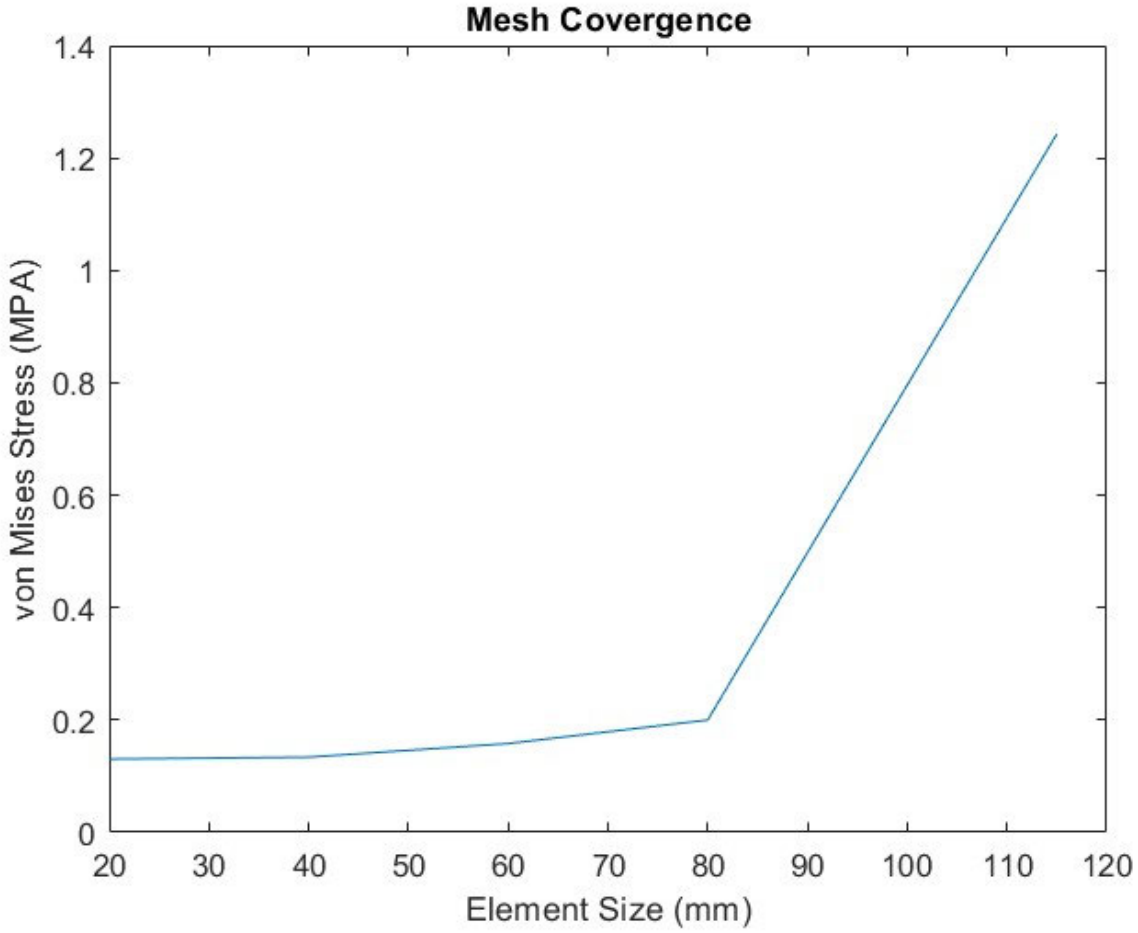

Figure 21 - Mesh Convergence Plot

3.4 Simulations

The key aspects of the simulations are noted below.

3.4.1 Constraints

Since the type V pressure vessels can be utilized in a variety of applications and vehicle types, the mechanisms to secure the vessel to the vehicle are outside the scope of this project. Thus, bracketry to secure the vessel is not included in the model and cannot be used as a constraint. The outer face of both polar bosses was chosen as the geometry to constrain for the FEA simulations. This is the most accurate solution as these sections will be used in the same way for each application. The constraints, highlighted in green, are shown in figure 22 below.

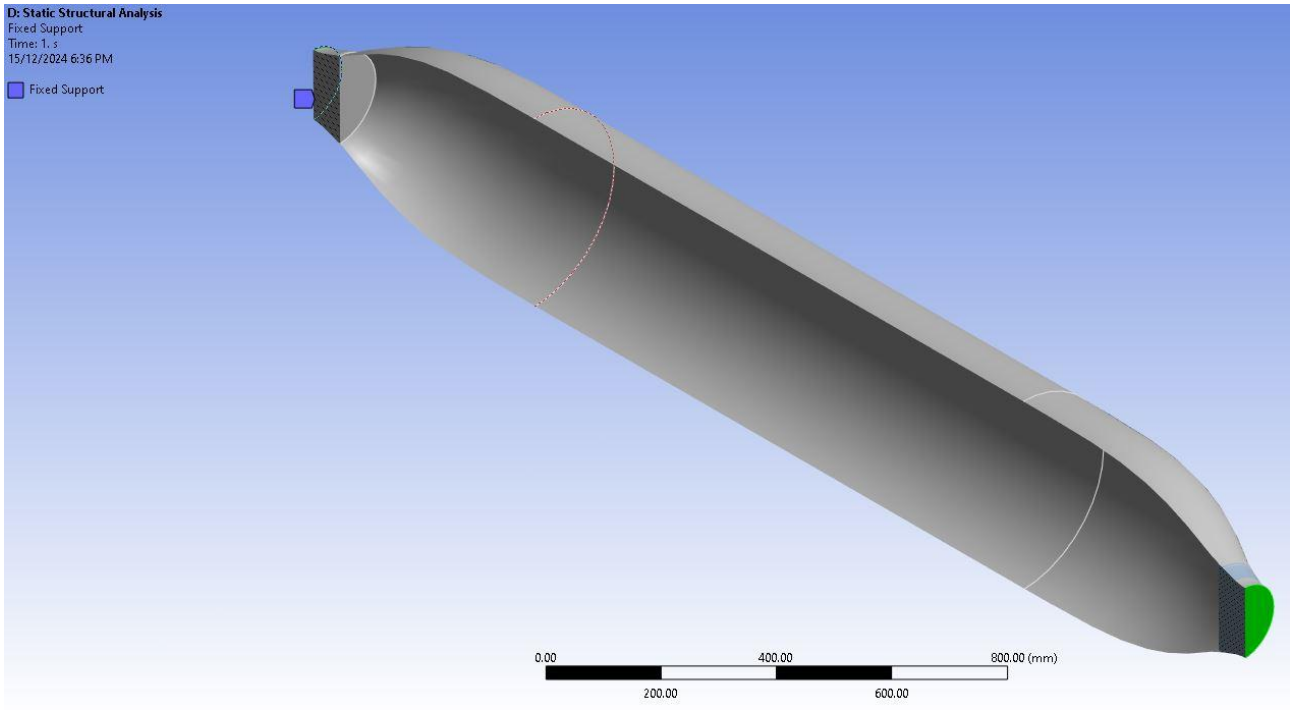

Figure 22 - Model Constraints

3.4.2 Loads

An internal pressure of 70 MPa was applied uniformly to all internal surfaces to simulate the standard working pressure of the vessel. Figure 23 illustrates the load application, highlighted in red.

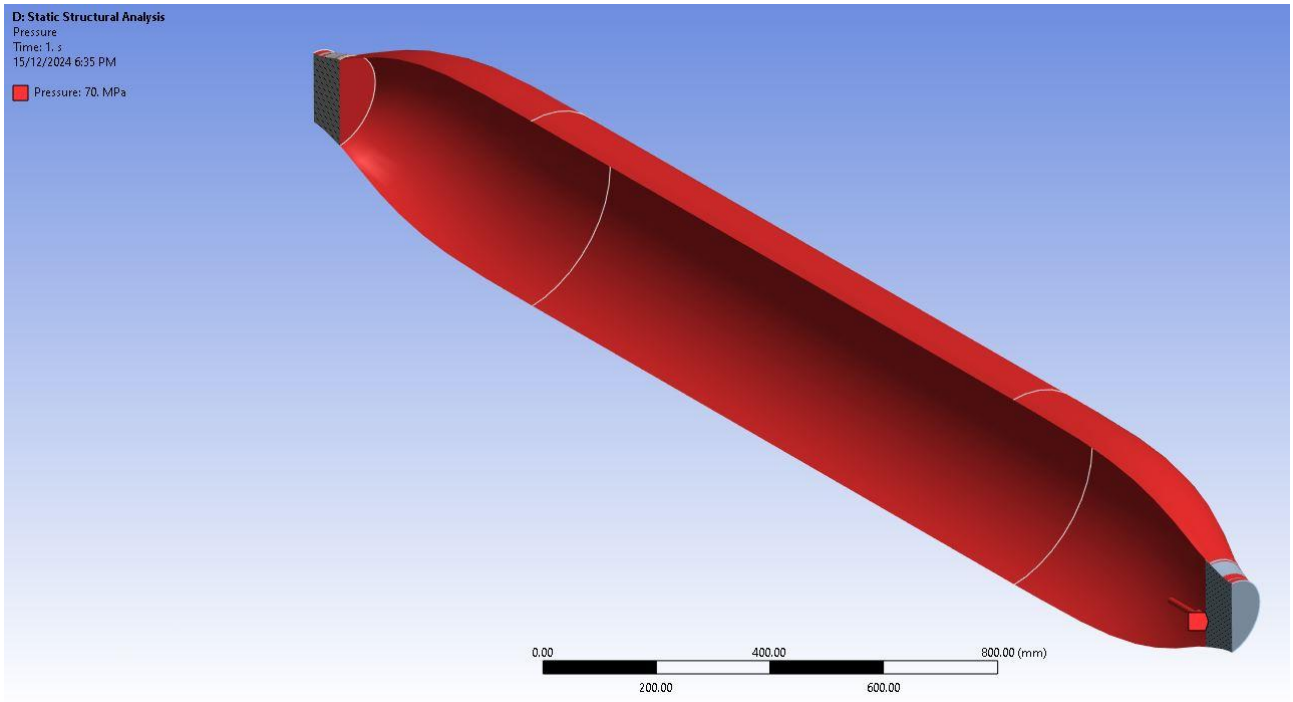

Figure 23 - Model Load Condition

3.4.3 Changes in Geometry

A series of simulations were run to analyze the effect of design considerations on the stress in the critical zone. These are shown below in table 14. These variations in the design were applied to the CAD model generated in Fusion before being applied to the ANSYS workbench. All material properties, meshing, load conditions and constraints were kept constant between the simulations and followed the aforementioned steps.

Initially, the width of the polar boss was reduced to decrease the adhesion surface area, allowing for an evaluation of how the critical zone's surface area influences stress distribution within the vessel. Subsequently, a 0° flange was introduced to expand the adhesion surface area and provide a lip for applying carbon plies. Finally, the flange angle was incrementally increased by 5° to assess the impact of the flange angle on localized stress distribution.

Table 14 - Variations in Design

Simulation	Variable				
Reduction in Polar Boss Width	Percentage (%)				
	0	2.5	5	7.5	10
Addition of 0o Flange	Length (mm)				
	0	2.5	5	7.5	10
Angle of Flange	Degrees (^{o})				
	0	5	10	15	20

CHAPTER 4

SIMULATION RESULTS & DISCUSSION

4.1 Simulation Results

In all cases the CZM reported no cases of failure and the critical zones remained ‘sticking’. These results are consistent with the findings of Air et al. (2023).

Likewise in all cases, the ANSYS composite failure mode tool reported ‘e12’ and ‘s2c’ failures in approximately all mesh elements. This is shown in figure X below. Since these failures occurred for all simulations, the material properties, thickness and orientations do not provide enough strength to support the 70 MPa pressure. This is not unexpected as Air et al. (2023) reported leakage at 0.13 MPa.

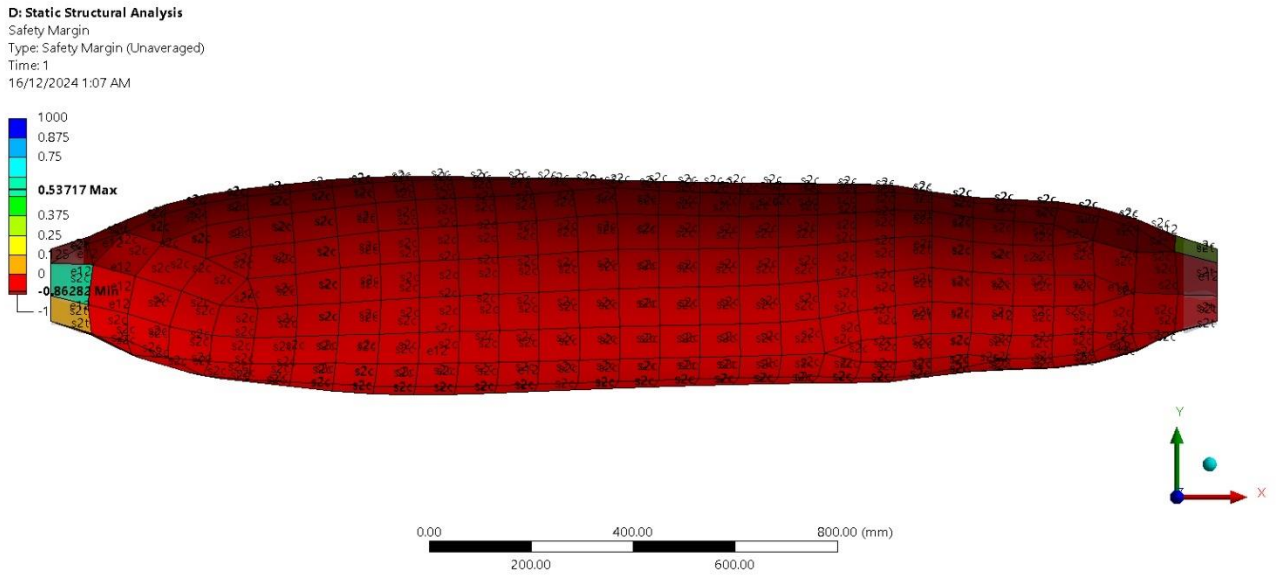

Figure 24 - ANSYS Composite Failure Tool (Safety Margin)

4.1.1 Reduction in Polar Boss Width

The polar boss width was reduced in steps of 2.5 %, from the starting value of 65 mm to 58.5 mm. The von Mises stress (MPa) was measured at each stage and a global maximum, average and local maximum were recorded. A stress concentration factor was calculated as the local maximum divided by the average stress.

Figure 25 shows the results from one of the simulations. The remainder can be found in Appendix D.

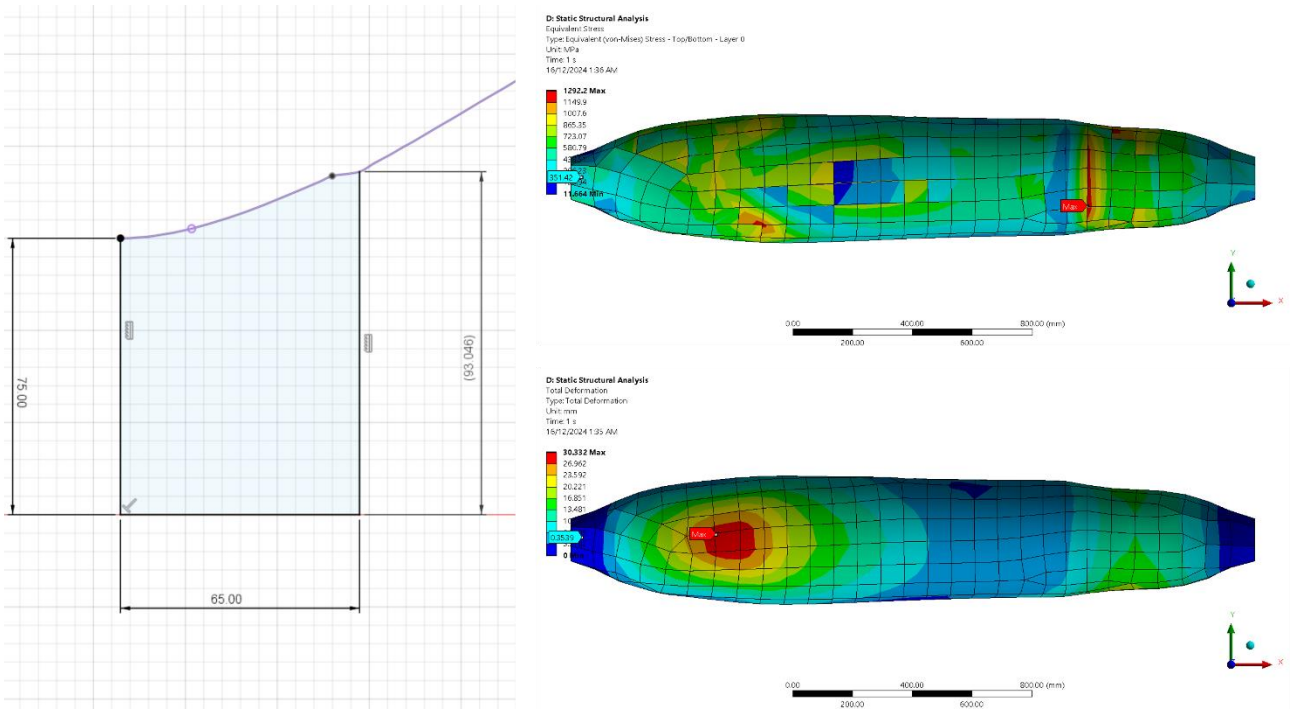

Figure 25 - (i) Polar Boss Geometry (ii) von Mises Stress Distribution (iii) Displacement Distribution

The results obtained are shown below in table 15.

Table 15 - Reduction in Polar Boss Width Results

%	Polar Boss Width	von Mises Stress (MPa)				Displacement (mm)			
		Global Max.	AVG.	Local Max.	Conc. Factor	Global Max.	AVG.	Local Max.	Conc. Factor
0	65	1292.2	310.68	351.42	1.131131711	30.332	0.62884	0.35390	0.562782266
2.5	63.375	1676.1	355.62	368.29	1.035627917	30.339	0.82031	0.39116	0.47684412
5	61.75	1292.3	336.44	358.58	1.065806682	30.338	0.63105	0.30293	0.480041201
7.5	60.125	1292.1	345.84	391.52	1.132084201	30.344	0.84200	0.42199	0.501175772
10	58.5	1409.7	356.49	395.02	1.108081573	30.341	0.86286	0.50103	0.580661985

The localized von Mises stress concentration factor plotted against the polar boss width is shown below in figure 26. Likewise, the change in strain (displacement) is shown in figure 27.

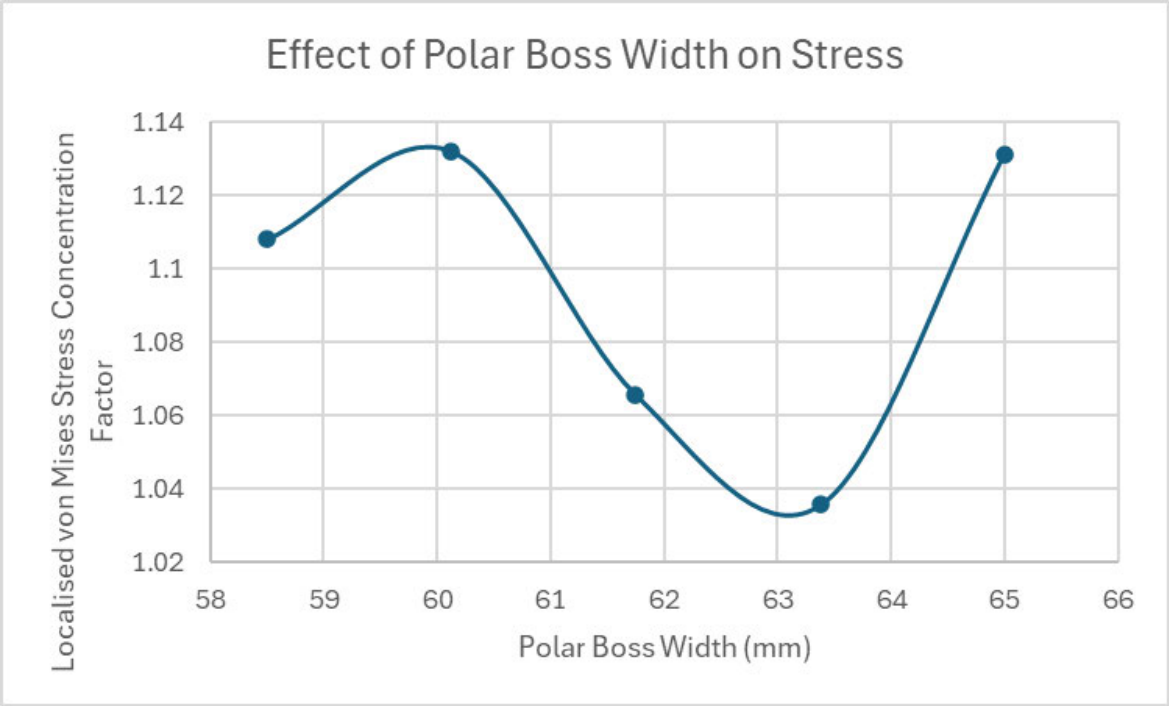

Figure 26 - Effect of Polar Boss Width on Stress

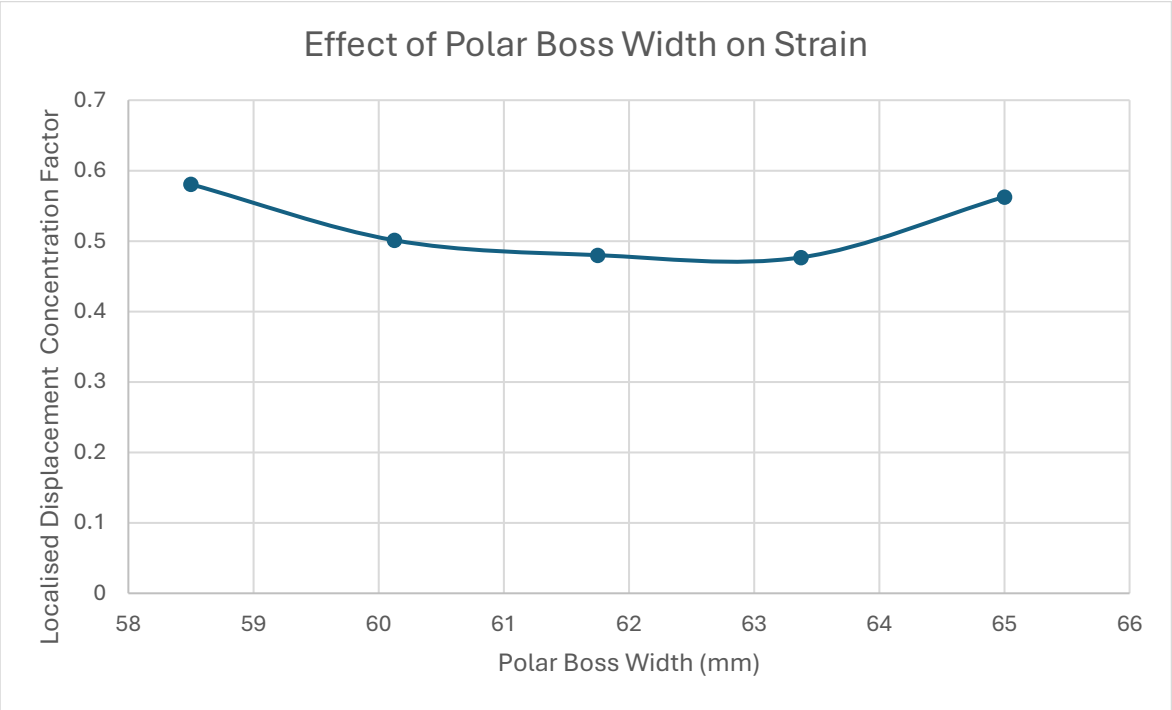

Figure 27 - Effect of Polar Boss Width on Strain

4.1.2 Addition of Variable Length 0º Flange

A flange orientated at 0º was added to the inner face of the polar boss to increase the adhesion surface area, provide a ledge for fibres to placed over and help distribute the stress from the polar boss to the composite layer. The results were recorded in the same fashion as the previous section.

Figure 28 shows the results from one of the simulations. The remainder can be found in Appendix D.

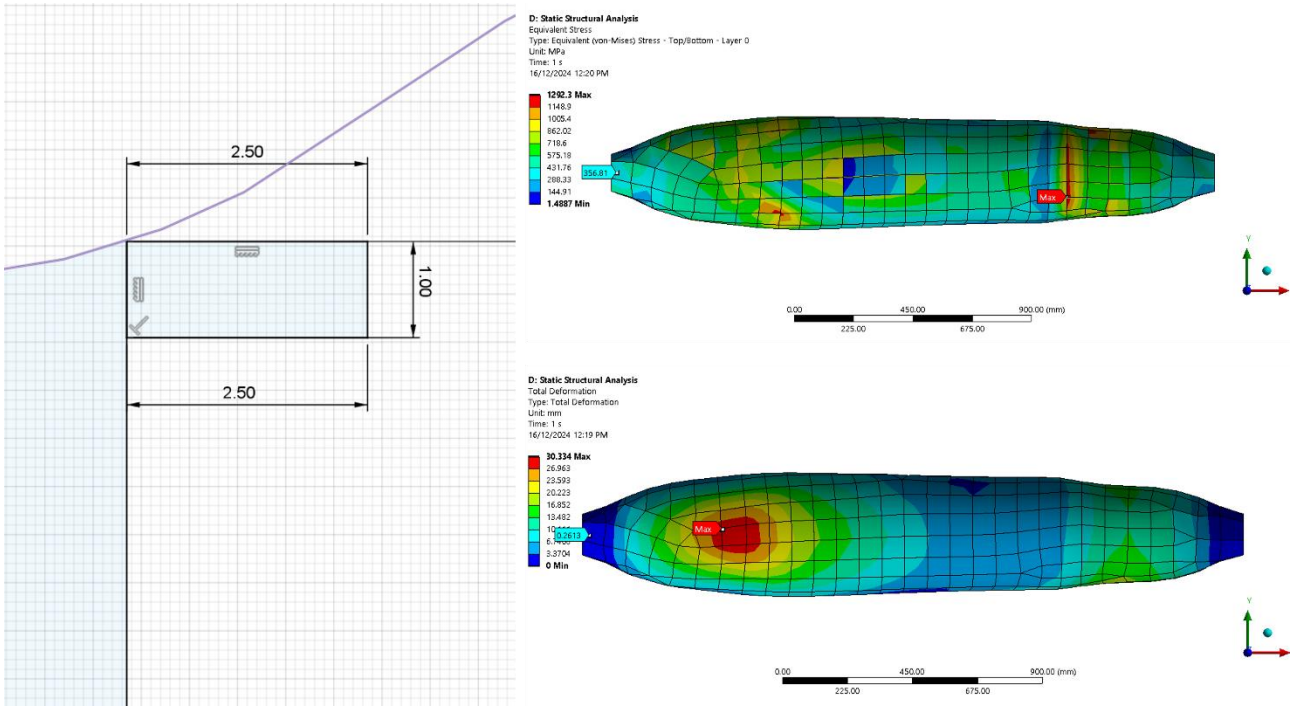

Figure 28 - (i) Polar Boss Geometry (ii) von Mises Stress Distribution (iii) Displacement Distribution

The results obtained are shown below in table 16.

%	Flange Length (mm)	von Mises Stress (MPa)				Displacement (mm)			
		Global Max.	AVG.	Local Max.	Conc. Factor	Global Max.	AVG.	Local Max.	Conc. Factor
0	0	1292.2	310.68	351.42	1.131131711	30.332	0.62884	0.3539	0.562782266
2.5	2.5	1292.3	385.27	356.81	0.926129727	30.334	0.66439	0.2613	0.393293096
5	5	1292.3	378.46	359.67	0.950351424	30.335	0.67956	0.2932	0.431573371
7.5	7.5	1292.3	365.95	360.03	0.983822927	30.334	0.65832	0.2730	0.414752704
10	10	2695.1	408.05	457.5	1.121186129	30.31	0.6099	0.27537	0.451500246

The localized von Mises stress concentration factor plotted against the polar boss width is shown below in figure 29. Likewise, the change in strain (displacement) is shown in figure 30.

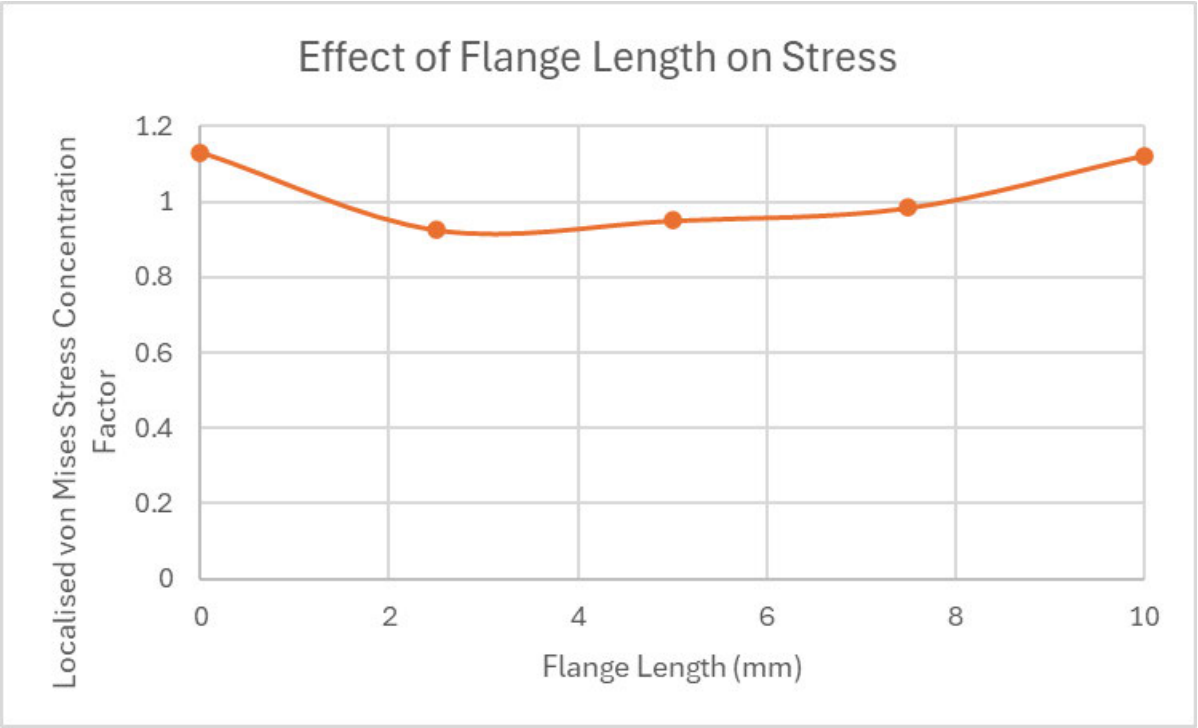

Figure 29 - Effect of Flange Length on Stress

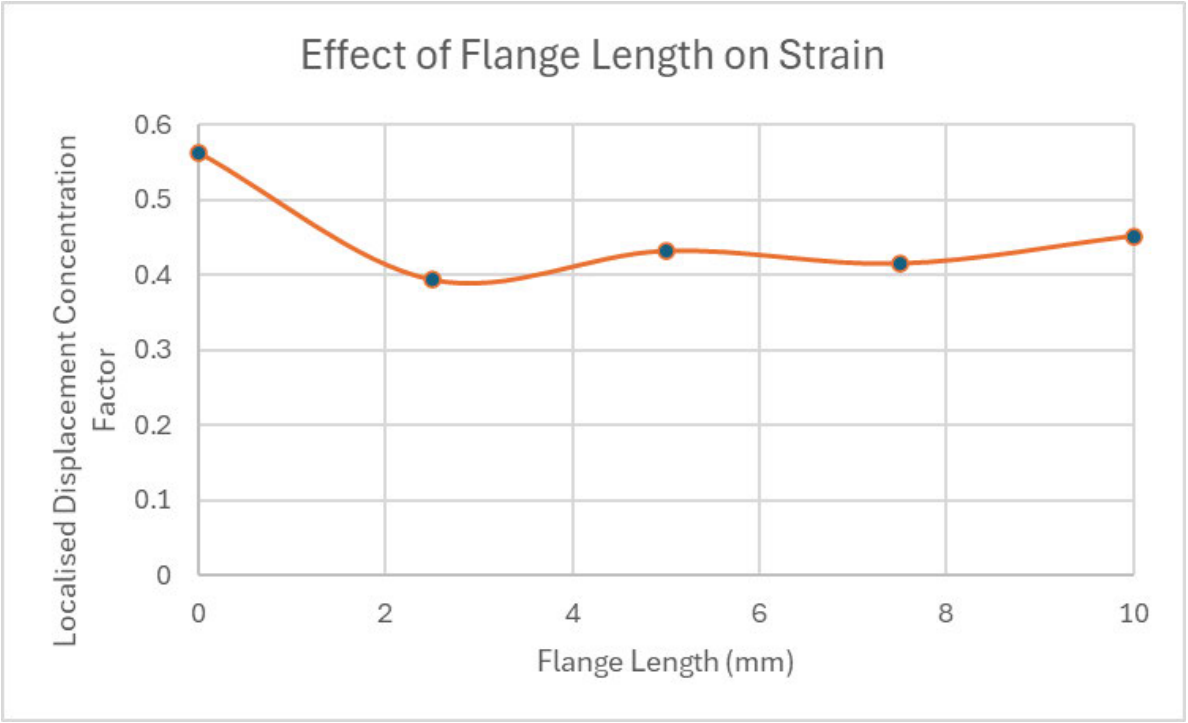

Figure 30 - Effect of Flange Length on Strain

4.1.3 Variation in Flange Angle

The flange orientated was then increased in steps of 2.5° from 0° to 10°. This was done to increase efficiency in stress distribution to reduce localized concentrations around the critical zone. The results were recorded in the same fashion as the previous section.

Figure 31 shows the results from one of the simulations. The remainder can be found in Appendix D.

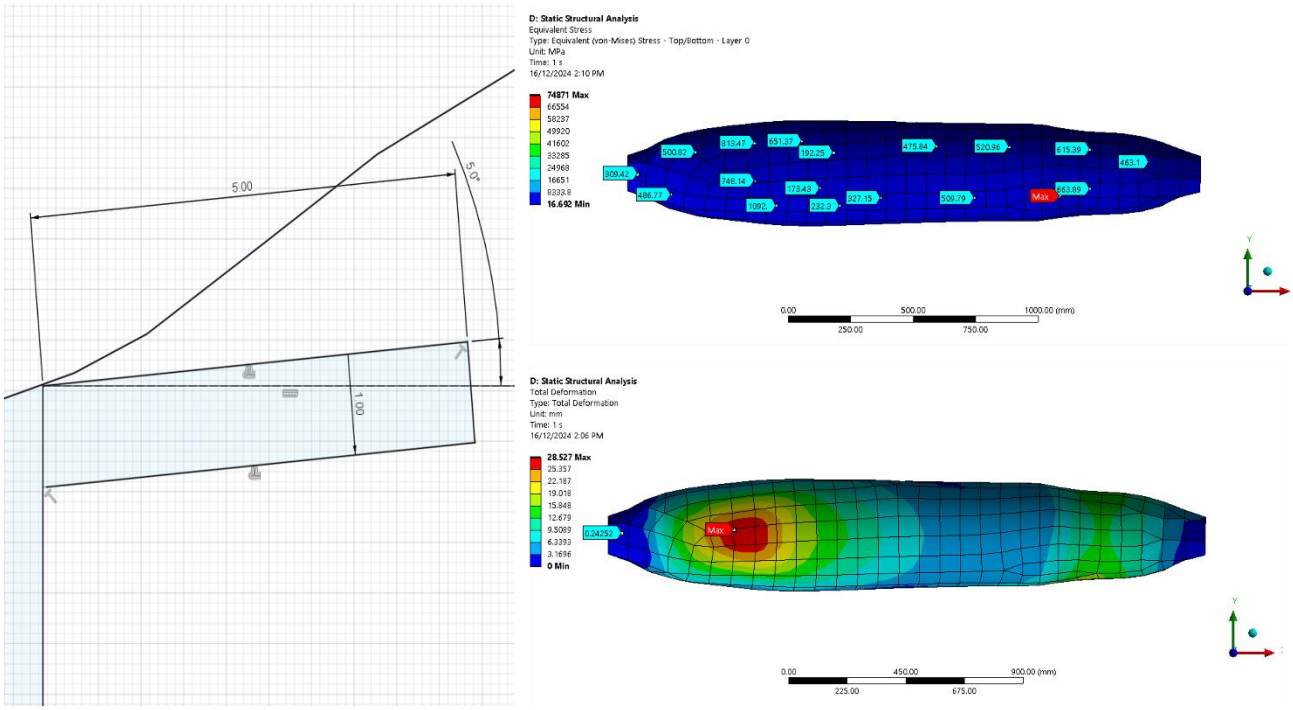

Figure 31 - (i) Polar Boss Geometry (ii) von Mises Stress Distribution (iii) Displacement Distribution

The results obtained are shown below in table 16.

%	Flange Angle (°)	von Mises Stress (MPa)				Displacement (mm)			
		Global Max.	AVG.	Local Max.	Conc. Factor	Global Max.	AVG.	Local Max.	Conc. Factor
0	0	1292.3	378.46	359.67	0.950351424	30.335	0.6795	0.2932	0.431573371
2.5	2.5	1290.8	511.13	316.39	0.619001037	29.515	2.3387	0.5941	0.254038568
5	5	1264.5	529.17	309.42	0.584727025	28.527	1.7289	0.2425	0.140274163
7.5	7.5	1271.9	565.17	210.43	0.372330449	28.273	3.2555	0.1984	0.060970665
10	10	1243.9	507.52	196.51	0.387196564	29.844	3.0698	0.7022	0.228744544

The localized von Mises stress concentration factor plotted against the polar boss width is shown below in figure 32. Likewise, the change in strain (displacement) is shown in figure 33.

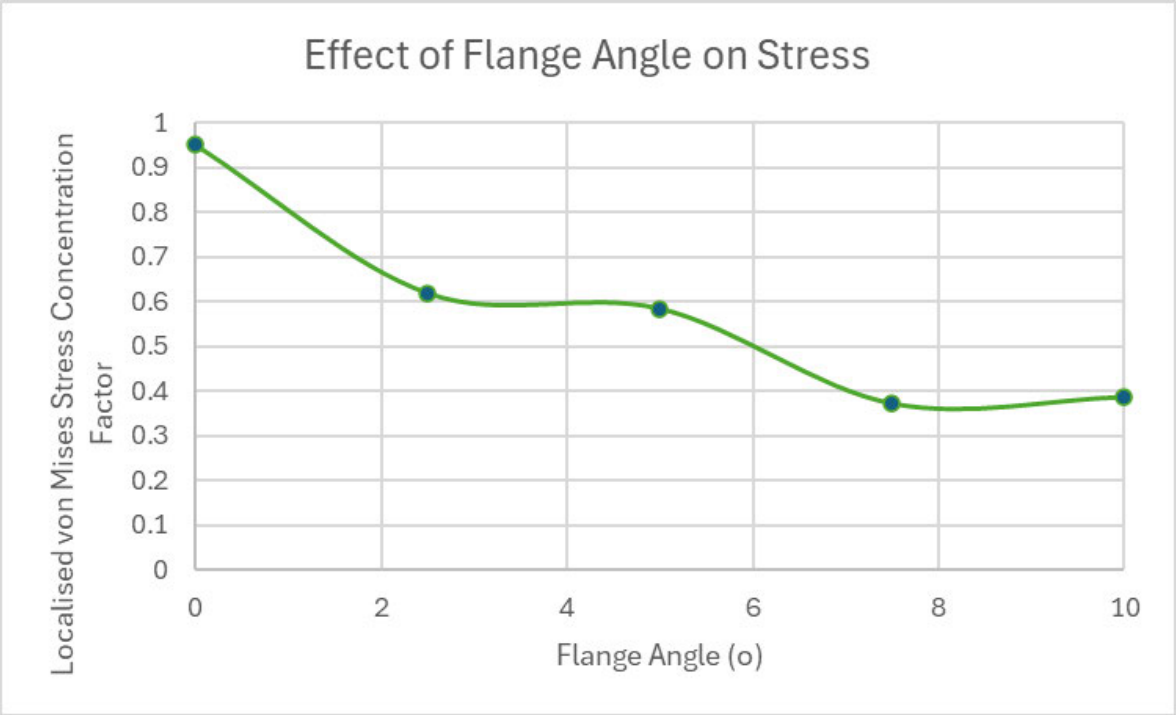

Figure 32 - Effect of Flange Angle on Stress

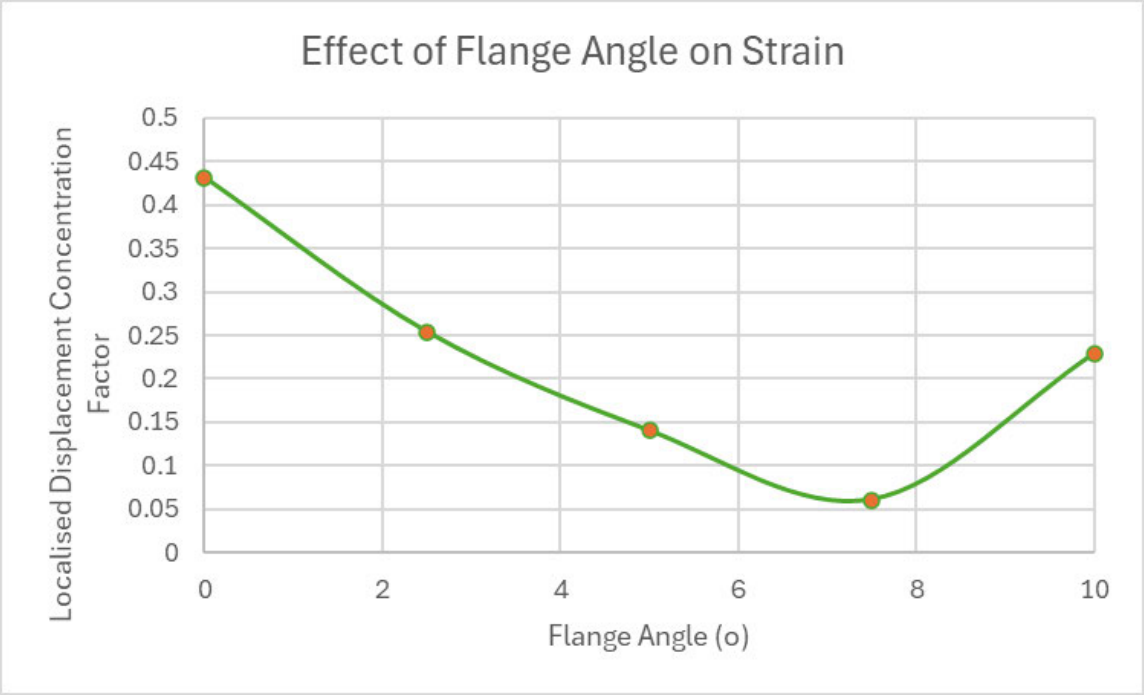

Figure 33 - Effect of Flange Angle on Strain

4.2 Discussion

The effect of reducing the polar boss width had the most variable effect on the stress concentration factor within the vicinity of the critical zone. The concentration factor fluctuates with an almost parabolic curve, with a maximum of approximately 1.13 and minimum of 1.04. The results stay consistently above 1 and thus the stress in the critical zone is greater than the average stress undergone by the vessel body.

Figure 25 (ii) and (iii) shows an area of increased stress and strain within the direct proximity of the critical zone. This follows engineering first principles as concentrations occur when there is a non-uniform distribution of stress due to changes in material properties, geometry, or applied loads. There is an outlier in the global maximum von Mises stress of 1676.1 MPa in the second iteration of the simulation (polar boss width reduced by 2.5 % resulting in a width of 63.375m mm). The source of this outlier is inconclusive as there were no changes to the loading or constraints applied to the model. Whilst the outlier is present, it has little effect on the recorded average and local stresses. The effect

of this is not present in the displacement results and therefore has little implication on the results found. The width of the polar boss is optimized at approximately 63 mm where the stress and strain concentrations are 1.04 and 0.5, respectively.

From analysis of the results, the addition of a 0^{o} flange reduces both the localized stress and strain concentrations. As the flange length increased from 0 mm to 10 mm, the global maximum von Mises stress remained consistent at approximately 1292 MPa up to 7.5 mm but sharply increased to 2695 MPa at 10 mm. The sudden increase at 10 mm is a clear outlier possibly due to stress accumulation or ineffective pathways for stress redistribution across the vessel body. Figures 29 and 30 show the concentrations reducing as the flange length increases and beginning to converge at around the 8 mm mark. The stress concentration reduces from an approximate 1.2 to 1, thus showing the inclusion of a flange allows for almost uniform stress distribution. The strain converges to 0.4 where the localized stress is approximately half that of the average. The outlier at 10 mm significantly impacts the results as in both plots, the concentrations begin to increase. The results highlight the need for optimization, as excessive flange lengths may lead to stress concentrations, undermining the intended benefits of reduced stress and improved adhesion in the critical zone.

The results from the simulations varying the flange angle in increments of 2.5^{o} reveal a significant decrease in stress and strain concentrations as the angle increases. As the flange angle increased the global maximum stress decreased whilst the average increased. This indicates an improvement in stress distribution as it becomes more uniform across the vessel. Furthermore, the local stress decreases and the resultant concentration is reduced to an approximate third of its original value. This demonstrates that the angle of the flange allows for stress to distribute away from the critical zone, increasing the safety in that area. The strain concentration follows the same trajectory with the concentration reaching an approximate 0 by 7.5^{o}. The results show that increasing the flange angle can significantly enhance performance, with 7.5° being a critical point for further investigation.

ANSYS was unable to generate a visualization of the stress distribution in this series of simulations. Approximately 15 areas over the pressure vessel body were chosen at random to be probed. The average of these points was used in place of the ANSYS generated average stress result. The distribution of strain shown in figure 31 follows the same pattern as the results from the previous simulations. Therefore, the results from these simulations were included.

4.2.1 Application of Findings

The findings from this project have several theoretical and practical applications. By optimizing polar boss dimensions and flange configurations, stress concentrations in critical zones can be reduced, improving the structural integrity and lifespan of pressure vessels.

The findings from these simulations will allow for the design of safer pressure vessels. Further expansion on the work completed here will advance the development of type V pressure vessels and increase the chances of widespread adoption into the transportation sector.

4.2.2 Study Limitations

The complexity of composite technologies as well as the significant learning curve required to use the specialist ANSYS software was quite challenging. Hardware and software limitations resulted in a reduction of complexity in the simulations. The converged mesh size of 20 mm resulted in the computer consistently freezing or overheating. Furthermore, the specialization of AFP machines resulted in no accurate way to model the placement of carbon fibre without using the manufactures specific software.

The lack of accuracy in the simulation models and the inclusion of outliers resulted in results that opened the door to further research and exploration. However, the results themselves are not of a quality that can be utilized in other work.

CHAPTER 5

CONCLUSION

In conclusion, a clear lack of research regarding the critical zone of CFRP type V pressure vessels to store hydrogen was found. The findings of recent publications were expanded on to produce a theoretical model suitable for simulation. The reduction of the stress and strain concentration factors within the vicinity of the critical zone was found to be influenced by the reduction of the polar boss width, as well as an increase in flange length and angle. Except for the reduction in polar width, all design considerations that were modelled resulted in the stress and strain concentration factors falling below 1, therefore having a localized value less than the average. This increases the safety of the pressure vessel as the point of failure moves away from the polar bosses and towards the vessel body. However, as found in the literature review, failures are heavily influenced by defects. The optimal design parameters were found to be a polar width of 63 mm with an 8 mm flange orientated 7.5^{o} above the neutral axis. The accuracy of the simulation and results limits the direct use of these findings however they form a strong basis for future work.

5.1 Project Outcomes

The project met five of the size proposed objectives. An extensive review of up-to-date publications was completed. Two publications by Air et al. (2023) were identified as the key leading studies in the development of type V pressure vessels. Key design parameters from the work of Air et al. (2023) as well as current type IV pressure vessels on the market were used to develop a theoretical model. The second objective, identifying and quantifying the critical zone was achieved. The critical zone was defined by a portion of the isotensoid dome profile and a MATLAB script was made to calculate the spline. The third and fourth objectives were met when a FEM was developed utilizing ANSYS and similar CAD programs. Material properties, load conditions and constraints were justified from the literature review. Simulations were completed and the results compiled for analysis. Finally, the

simulation results were analyzed, and design considerations were proposed to optimize the stress distribution over the critical zone. Possible failure modes were researched during the literature review, however due to time constraints and complexities in the theory and implementation in the software no further work was pursued. Thus, objective six was not met.

5.2 Further Work

Whilst this project is limited by the accuracy of the model, it provides a solid foundation for further development. Future work should focus on the pressure vessel body and designing a model capable of withstanding the 70 MPa working pressure as well as the 245 MPa burst pressure required to meet current standards. This will allow for proper examination of failure methods before more work is done on the critical zone and the interaction between the vessel body and the polar bosses. Furthermore, research is required into AFP technologies and the development of a universal way to accurately model the fibre orientation and layering. This will increase the accuracy of future theoretical models.

REFERENCES

Addcomposites 2024a, *AFP Machines and Components*, Addcomposites, viewed 14/12/2024, <https://www.addcomposites.com/post/afp-machines-and-components>.

Addcomposites 2024b, *What is Filament Winding Process?*, Addcomposites, viewed 14/12/2024, <https://www.addcomposites.com/post/filament-winding#:~:text=Filament%20winding%20can%20be%20defined,a%20structural%20solid%20of%20revolution.>.

Ahmad Sobri, S, Heinemann, R & Whitehead, D 2020, 'Carbon Fibre Reinforced Polymer (CFRP) Composites: Machining Aspects and Opportunities for Manufacturing Industries', in pp. 35-65.

Air, A, Shamsuddoha, M & Gangadhara Prusty, B 2023, 'A review of Type V composite pressure vessels and automated fibre placement based manufacturing', *Composites Part B: Engineering*, vol. 253, p. 110573.

Air, A, Oromiehie, E & Prusty, BG 2023, 'Design and manufacture of a Type V composite pressure vessel using automated fibre placement', *Composites Part B: Engineering*, vol. 266, p. 111027.

Air, A, Oromiehie, E & Prusty, BG 2024, 'Optimisation of a composite pressure vessel dome using non-geodesic tow paths and automated fibre placement manufacturing', *Composites Part B: Engineering*, vol. 288, p. 111906.

Alam, S, Yandek, GR, Lee, RC & Mabry, JM 2020, 'Design and development of a filament wound composite overwrapped pressure vessel', *Composites Part C: Open Access*, vol. 2, p. 100045.

Alves, MP, Gul, W, Cimini Junior, CA & Ha, SK 2022, 'A Review on Industrial Perspectives and Challenges on Material, Manufacturing, Design and Development of Compressed Hydrogen Storage Tanks for the Transportation Sector', *Energies*, vol. 15, no. 14, p. 5152.

ANSYS 2024, *Are there guideline about the mesh convergence for Structural Analysis?* , ANSYS, viewed 09/09/2024, <https://innovationspace.ansys.com/courses/wp-content/uploads/sites/5/2024/01/1_Tips-and-Tricks-for-Meshing.pdf>.

Azeem, M, Ya, HH, Alam, MA, Kumar, M, Stabla, P, Smolnicki, M, Gemi, L, Khan, R, Ahmed, T, Ma, Q, Sadique, MR, Mokhtar, AA & Mustapha, M 2022, 'Application of Filament Winding Technology in Composite Pressure Vessels and Challenges: A Review', *Journal of Energy Storage*, vol. 49, p. 103468.

Berro Ramirez, JP, Halm, D, Grandidier, J-C, Villalonga, S & Nony, F 2015, '700 bar type IV high pressure hydrogen storage vessel burst – Simulation and experimental validation', *International Journal of Hydrogen Energy*, vol. 40, no. 38, pp. 13183-92.

Bertin, M, Halm, D, Magneville, B, Renard, J, Saffré, P & Villalonga, S 2012, 'One year OSIRHYS IV project synthesis: mechanical behaviour of 700 bar type iv high pressure vessel code qualification', *15th European conference on composite materials*, p. 8 p.

Bouhala, L, Koutsawa, Y, Karatrantos, A & Bayreuther, C 2024, 'Design of Type-IV Composite Pressure Vessel Based on Comparative Analysis of Numerical Methods for Modeling Type-III Vessels', *Journal of Composites Science*, vol. 8, no. 2, p. 40.

Brádaigh, CO, Grogan, DM, Murray, B & Leen, SB 2016, 'Lightweight thermoplastic composite fuel tanks for space applications', *3rd International Conference and Exhibition on Thermoplastic Composites-ITHEC 2016*.

Car Expert 2023, *2023 Honda CR-V e:HEV RS (2WD) 5 SEATS Price and Spec*, Car Expert, viewed 07/10/2024, <https://www.carexpert.com.au/honda/cr-v/2023-ehev-rs-2wd-5-seats-ea25a1d7>.

Cho, S-M, Kim, K-S, Lee, S-K, Jung, G-S, Lee, S-K & Lyu, S-K 2018, 'Effect of Dome Curvature on Failure Mode of Type4 Composite Pressure Vessel', *International Journal of Precision Engineering and Manufacturing*, vol. 19, no. 3, pp. 405-10.

Composites, H 2019, *POLAR BOSSES FOR COMPOSITE PRESSURE VESSELS; A PRIMER ON DESIGN AND ANAYSIS*, Hanso Composites, viewed 04/10/2023, <https://www.hanshocomp.com/single-post/2019/02/15/polar-bosses-for-composite-pressure-vessels-a-primer-on-design-and-anaysis>.

Deeraj, BDS, Mathew, MS, Parameswaranpillai, J & Joseph, K 2020, 'Chapter 6 - EMI shielding materials based on thermosetting polymers', in K Joseph, et al. (eds), *Materials for Potential EMI Shielding Applications*, Elsevier, pp. 101-10.

EERE 2015, *Hydrogen Storage*, Office of Energy Efficiency & Renewable Energy, viewed 04/10/2023, <https://www.energy.gov/eere/fuelcells/hydrogen-storage#:~:text=Hydrogen%20can%20be%20stored%20physically,pressure%20is%20%E2%88%92252.8%C2%B0C.>.

Fibreglast 2023, *What are Unidirectional Carbon Fiber Fabrics?*, Fibreglast, viewed 04/10/2023, <.
Funck, R & Fuchs, H-P 2001, 'Development of all-composite compressed natural gas (CNG) pressure vessel for vehicle use', *International Conference on Composite Materials*, pp. 1-8.

Gardiner, G 2024, *Honda begins production of 2025 CR-V e:FCEV with Type 4 hydrogen tanks in U.S.*, Composites World, viewed 07/10/2024, <https://www.compositesworld.com/news/honda-begins-production-of-2025-cr-v-efcev-with-type-4-hydrogen-tanks-in-us>.

GenH2 2022, *Hydrogen A to Z Series: D For Density*, GenH2, Titusville, Florida, viewed 25/08/2024, <https://genh2hydrogen.com/blog/defining-hydrogen-from-a-to-z-3/>.

Gentilleau, B, Touchard, F & Grandidier, JC 2014, 'Numerical study of influence of temperature and matrix cracking on type IV hydrogen high pressure storage vessel behavior', *Composite Structures*, vol. 111, pp. 98-110.

Harada, S, Arai, Y, Araki, W, Iijima, T, Kurosawa, A, Ohbuchi, T & Sasaki, N 2018, 'A simplified method for predicting burst pressure of type III filament-wound CFRP composite vessels considering the inhomogeneity of fiber packing', *Composite Structures*, vol. 190, pp. 79-90.

Hua, TQ, Roh, H-S & Ahluwalia, RK 2017, 'Performance assessment of 700-bar compressed hydrogen storage for light duty fuel cell vehicles', *International Journal of Hydrogen Energy*, vol. 42, no. 40, pp. 25121-9.

Hübner, F, Brückner, A, Dickhut, T, Altstädt, V, Rios de Anda, A & Ruckdäschel, H 2021, 'Low temperature fatigue crack propagation in toughened epoxy resins aimed for filament winding of type V composite pressure vessels', *Polymer Testing*, vol. 102, p. 107323.

Hwang, HT & Varma, A 2014, 'Hydrogen storage for fuel cell vehicles', *Current Opinion in Chemical Engineering*, vol. 5, pp. 42-8.

Hyundai 2021, *NEXO: Hyundai's hydrogen fuel-cell first.*, Hyundai, viewed 07/10/2024, <https://www.hyundai.com/au/en/news/vehicles/nexo-hyundai-hydrogen-fuel-cell-first>.

Ibrahim, A, Ryu, Y & Saidpour, M 2015, 'Stress Analysis of Thin-Walled Pressure Vessels', *Modern Mechanical Engineering*, vol. Vol.05No.01, p. 9.

IEA 2019, *The Future of Hydrogen*, Paris, viewed 04/10/2023, <https://www.iea.org/reports/the-future-of-hydrogen,>.

Jaber, M, Yahya, A, Arif, AF, Jaber, H & Alkhedher, M 2024, 'Burst pressure performance comparison of type V hydrogen tanks: Evaluating various shapes and materials', *International Journal of Hydrogen Energy*, vol. 81, pp. 906-17.

Johnson, K, Veenstra, MJ, Gotthold, D, Simmons, K, Alvine, K, Hobein, B, Houston, D, Newhouse, N, Yeggy, B, Vaipan, A, Steinhausler, T & Rau, A 2017, 'Advancements and Opportunities for On-Board 700 Bar Compressed Hydrogen Tanks in the Progression Towards the Commercialization of Fuel Cell Vehicles', *SAE International Journal of Alternative Powertrains*, vol. 6, no. 2, pp. 201-18.

Jois, KC, Welsh, M, Gries, T & Sackmann, J 2021, 'Numerical Analysis of Filament Wound Cylindrical Composite Pressure Vessels Accounting for Variable Dome Contour', *Journal of Composites Science*, vol. 5, no. 2, p. 56.

Katsiropoulos, CV, Chamos, AN, Tserpes, KI & Pantelakis, SG 2012, 'Fracture toughness and shear behavior of composite bonded joints based on a novel aerospace adhesive', *Composites Part B: Engineering*, vol. 43, no. 2, pp. 240-8.

Leavitt, M & Lam, P 2014, *Development of advanced manufacturing technologies for low cost hydrogen storage vessels*, Quantum Fuel Systems Technologies Worldwide, Inc., Irvine, CA (United States).

Leh, D, Saffré, P, Francescato, P, Arrieux, R & Villalonga, S 2015, 'A progressive failure analysis of a 700-bar type IV hydrogen composite pressure vessel', *International Journal of Hydrogen Energy*, vol. 40, no. 38, pp. 13206-14.

Leh, D, Magneville, B, Saffré, P, Francescato, P, Arrieux, R & Villalonga, S 2015, 'Optimisation of 700 bar type IV hydrogen pressure vessel considering composite damage and dome multi-sequencing', *International Journal of Hydrogen Energy*, vol. 40, no. 38, pp. 13215-30.

Liu, PF, Chu, JK, Hou, SJ, Xu, P & Zheng, JY 2012, 'Numerical simulation and optimal design for composite high-pressure hydrogen storage vessel: A review', *Renewable and Sustainable Energy Reviews*, vol. 16, no. 4, pp. 1817-27.

Magneville, B, Gentilleau, B, Villalonga, S, Nony, F & Galiano, H 2015, 'Modeling, parameters identification and experimental validation of composite materials behavior law used in 700 bar type IV hydrogen high pressure storage vessel', *International Journal of Hydrogen Energy*, vol. 40, no. 38, pp. 13193-205.

Mawire, NN 2019, 'Novel, low-cost, CFRP pressure vessel design for hydrogen fuel cell applications'.

Munzke, D, Duffner, E, Eisermann, R, Schukar, M, Schoppa, A, Szczepaniak, M, Strohhäcker, J & Mair, G 2021, 'Monitoring of type IV composite pressure vessels with multilayer fully integrated optical fiber based distributed strain sensing', *Materials Today: Proceedings*, vol. 34, pp. 217-23.

Nebe, M, Johman, A, Braun, C & van Campen, JMJF 2022, 'The effect of stacking sequence and circumferential ply drop locations on the mechanical response of type IV composite pressure vessels subjected to internal pressure: A numerical and experimental study', *Composite Structures*, vol. 294, p. 115585.

Nebe, M, Maraite, D, Braun, C, Hülsbusch, D & Walther, F 2019, 'Experimental Characterization of the Structural Deformation of Type IV Pressure Vessels Subjected to Internal Pressure', *Key Engineering Materials*, vol. 809, pp. 47-52.

Nonobe, Y 2016, 'Development of the fuel cell vehicle mirai', *IEEJ Transactions on Electrical and Electronic Engineering*, vol. 12, no. 1, pp. 5-9.

Park, G, Jang, H & Kim, C 2021, 'Design of composite layer and liner for structure safety of hydrogen pressure vessel (type 4)', *Journal of Mechanical Science and Technology*, vol. 35, no. 8, pp. 3507-17.

Rafiee, R & Torabi, MA 2018, 'Stochastic prediction of burst pressure in composite pressure vessels', *Composite Structures*, vol. 185, pp. 573-83.

Rafiee, R & Salehi, A 2022, 'Estimating the burst pressure of a filament wound composite pressure vessel using two-scale and multi-scale analyses', *Mechanics of Advanced Materials and Structures*, vol. 30, no. 13, pp. 2668-83.

Red River 2023, *Typical Safety Factor for Pressure Vessels*, Red River, viewed 24/04/2024, <https://www.redriver.team/typical-safety-factor-for-pressure-vessels/#:~:text=The%20typical%20safety%20factor%20for%20pressure%20vessels%20is%20often%20referred,value%20used%20in%20design%20calculations.&text=So%2C%20the%20typical%20safety%20factor%20in%20this%20context%20is%203.5.>.

Roh, HS, Hua, TQ & Ahluwalia, RK 2013, 'Optimization of carbon fiber usage in Type 4 hydrogen storage tanks for fuel cell automobiles', *International Journal of Hydrogen Energy*, vol. 38, no. 29, pp. 12795-802.
Sapre, S, Pareek, K & Vyas, M 2020, 'Investigation of structural stability of type IV compressed hydrogen storage tank during refueling of fuel cell vehicle', *Energy Storage*, vol. 2, no. 4.

Schäkel, M, Janssen, H & Brecher, C 2021, 'Process analysis of manufacturing thermoplastic type-IV composite pressure vessels with helical winding pattern', *Society for the Advancement of Material and Process Engineering (SAMPE International Conference)*, pp. 955-67.

Shao, Y, Betti, A, Carvelli, V, Fujii, T, Okubo, K, Shibata, O & Fujita, Y 2016, 'High pressure strength of carbon fibre reinforced vinylester and epoxy vessels', *Composite Structures*, vol. 140, pp. 147-56.

Sloan, J 2023, *Composites end markets: Pressure vessels (2023)*, Composites World, viewed 04/10/2023, <https://www.compositesworld.com/articles/composites-end-markets-pressure-vessels-2023>.

Souza, G & Tarpani, J 2020, 'Using OBR for pressure monitoring and BVID detection in type IV composite overwrapped pressure vessels', *Journal of Composite Materials*, vol. 55, no. 3, pp. 423-36.

Standards Australia 2010, *Pressure Vessels*, SAI Global, viewed 24/04/2024, <.

Su, Y, Lv, H, Zhou, W & Zhang, C 2021, 'Review of the Hydrogen Permeability of the Liner Material of Type IV On-Board Hydrogen Storage Tank', *World Electric Vehicle Journal*, vol. 12, no. 3, p. 130.
Toyota 2024, *2024 Mirai Full Specs*, Toyota, viewed 07/10/2024, <https://www.toyota.com/mirai/features/mpg_other_price/3002/3003>.

Vasiliev, VV & Jones, RM 2009, *Composite Pressure Vessels: Design, Analysis, and Manufacturing*, Bull Ridge Pub.

Villalonga, S, Nony, F, Magnier, C, Yvernes, J, Thomas, C, Delmas, B & Mazabraud, P 2009, 'Composite 700 bar-vessel for on-board compressed gaseous hydrogen storage', *Proc. of 17th International Conference on Composite Materials, Edinburgh, UK*.

Villalonga, S, Thomas, C, Nony, C, Thiebaud, F, Geli, M, Lucas, A, Knobloch, K & Maugy, C 2011, 'Applications of full thermoplastic composite for type IV 70 MPa high pressure vessels', *International Conference on Composite Materials*.

Wang, X, Tian, M, Chen, X, Xie, P, Yang, J, Chen, J & Yang, W 2022, 'Advances on materials design and manufacture technology of plastic liner of type IV hydrogen storage vessel', *International Journal of Hydrogen Energy*, vol. 47, no. 13, pp. 8382-408.

Wu, QG, Chen, XD, Fan, ZC & Nie, DF 2015, 'Stress and Damage Analyses of Composite Overwrapped Pressure Vessel', *Procedia Engineering*, vol. 130, pp. 32-40.

Xing, Y, Xu, W & Buratti, V 2022, 'Using the Kriging Response Surface Method for the Estimation of Failure Values of Carbon-Fibre-Epoxy Subsea Composite Flowlines under the Influence of Stochastic Processes', *Designs*, vol. 6, no. 1, p. 1.

Yamashita, A, Kondo, M, Goto, S & Ogami, N 2015, *Development of High-Pressure Hydrogen Storage System for the Toyota "Mirai"*.

Yan, Y, Zhang, J, Li, G, Zhou, W & Ni, Z 2024, 'Review on linerless type V cryo-compressed hydrogen storage vessels: Resin toughening and hydrogen-barrier properties control', *Renewable and Sustainable Energy Reviews*, vol. 189, p. 114009.

Zhang, J, Lin, G, Vaidya, U & Wang, H 2023, 'Past, present and future prospective of global carbon fibre composite developments and applications', *Composites Part B: Engineering*, vol. 250, p. 110463.

Zhang, J, Lei, L, Zhou, W, Li, G, Yan, Y & Ni, Z 2023, 'Cryogenic mechanical and hydrogen-barrier properties of carbon fiber composites for type V cryo-compressed hydrogen storage vessels', *Composites Communications*, vol. 43, p. 101733.

Zhang, M, Lv, H, Kang, H, Zhou, W & Zhang, C 2019, 'A literature review of failure prediction and analysis methods for composite high-pressure hydrogen storage tanks', *International Journal of Hydrogen Energy*, vol. 44, no. 47, pp. 25777-99.

Zhang, Q, Xu, H, Jia, X, Zu, L, Cheng, S & Wang, H 2020, 'Design of a 70 MPa type IV hydrogen storage vessel using accurate modeling techniques for dome thickness prediction', *Composite Structures*, vol. 236, p. 111915.

Zhou, W, Wang, J, Pan, Z-b, Liu, J, Ma, L-h, Zhou, J-y & Su, Y-f 2022, 'Review on optimization design, failure analysis and non-destructive testing of composite hydrogen storage vessel', *International Journal of Hydrogen Energy*, vol. 47, no. 91, pp. 38862-83.

Zu, L, Koussios, S, Beukers, A & Zhang, D 2014, 'Development of Filament Wound Composite Isotensoidal Pressure Vessels', *Polymers and Polymer Composites*, vol. 22, no. 3, pp. 227-32.

APPENDIX
A
Project Specifications

Specification and Work Plan 19/02/2024

Title: Investigation on the Critical Zone of CFRP Type-V Pressure Vessels for H^2 Storage in the Transportation Sector.

Name : Ryan Richards

Student ID : [redacted]

Supervisor: Belal Yousif

Introduction and Background:

Given the escalating global demand for cleaner, sustainable energy solutions, Hydrogen (H2) has reemerged as a promising alternative to conventional fossil fuels and their byproducts. Its utilization as an energy source traces back over two centuries, propelling the first internal combustion engine (IEA, 2019). Yet, for Hydrogen to significantly contribute to a lasting shift toward clean energy, widespread integration across sectors where current usage remains minimal such as transportation, construction, and power generation is imperative.

However, the adoption of H2 as a sustainable energy source faces notable limitations, particularly concerning its storage, given current technological constraints. While boasting the highest energy per mass among all fuels, Hydrogen's challenge lies in its low ambient temperature density, resulting in comparatively low energy per unit volume (EERE). Thus, advanced storage techniques are essential to accommodate a usable quantity of H2. Gas form storage necessitates high-pressure tanks or vessels with internal pressures ranging from 5 000 to 10 000 psi. Conversely, liquid storage demands cryogenic temperatures due to its -252.8°C boiling point at one atmospheric pressure (EERE), each presenting unique difficulties and limitations.

Carbon fibre reinforced polymer (CFRP) stands as an engineered epoxy polymer matrix reinforced with carbon fibres, having found utility for over half a century in diverse engineering domains, notably aerospace and automotive. This is owing to its favourable mechanical characteristics. Exhibiting up to ten times greater specific strength compared to steel and aluminium, CFRP proves optimal where weight reduction is paramount whilst remaining resilient against repeated and elevated forces is necessary (Jin Zhang et al., 2023). Its advantageous properties encompass high mechanical strength and stiffness, minimal weight and thermal expansion, and superior chemical resistance (Deeraj et al., 2020).

The utilization of CFRP in constructing a pressure vessel engineered to withstand the pressures necessary for storing H2 presents a distinct set of challenges. While CFRP exhibits promising mechanical properties, its inherent structural composition poses significant hurdles. CFRP has a nonhomogeneous structure and thus variations in the density distribution of fibre strands within the matrix diminish the material's ultimate strength. Carbon fibre attains its maximum strength along the length of the strand, necessitating the parallel arrangement of fibres (Fibreglast, 2023). However, the internal pressure within the pressure vessel is isotropic, exerting equal force in all directions. Consequently, utilising CFRP involves the incorporation of multiple layers with differing orientations.

Type V pressure vessels eliminate the need for an internal gas barrier and enabling a single-material construction. This innovative vessel relies exclusively on CFRP for both structural integrity and gas containment (Air et al., 2023). As the type V pressure vessel lacks an integrated liner, a polar boss serves as the connection point for external components. This feature facilitates the attachment of fittings for filling or emptying the vessel and accommodating various sensors (Air et al., 2023; Composites, 2019). However, this design presents two potential areas of failure: the CFRP body and the connection of the polar boss to the vessel body, termed the critical zone. Failures in either area may lead to loss of structural integrity or H2 containment (e.g., burst failure or leaks), with potential causes including permeation and delamination of CFRP layers (Harada et al., 2018; Jiaqiao Zhang et al., 2023).

Research by Takemoto & Yoshikawa (2022) highlights a notable absence of reliable methods for predicting the burst pressure of CFRP pressure vessels without resorting to destructive testing. Unlike vessels made from homogeneous metals and alloys, a design methodology based on stress criteria has yet to be certified, necessitating extensive rounds of destructive testing in current designs. Existing models for CFRP pressure vessels struggle to accurately capture fracture phenomena stemming from localised stress/strain concentrations inherent in the mesostructure of CFRP composites (Takemoto & Yoshikawa, 2022).

Objectives and Aims:

Richards (2023) proposes six objectives, they are as follows.

Objective 1 : Research
Provide an up-to-date extensive review of current known literature on the proposed project with specific emphasis on the mechanical behaviour and failure modes of CFRP based type V pressure vessels, challenges specific to H2 storage in pressure vessels, design considerations and challenges associated with constructing a reliable bond between the CFRP pressure vessel and the external attachments. Identify relevant leading studies on the critical zone of attachments to the CFRP pressure vessel to form a basis for a theoretical model.

Objective 2 : Critical Zone Identification
Utilise the information found in the literature review to identify and quantify the critical zone of attachment where metal components interface with the CFRP pressure vessel. Comprehend the stresses, methods of load transfer, and possible failure modes that arise within this area. Time permitting, evaluate additional factors that affect the system including adhesive joint geometry, stress concentrations, surface preparation, and material compatibility.

Objective 3 : Generate a Finite Element Model
Generate a finite element model of the critical zone using ANSYS or similar software. Define and justify model geometry, material properties and boundary conditions from literature review.

Objective 4 : Modelled Mechanical Behaviour Analysis
Analyse the model under the appropriate loading conditions to assess the stress

distribution, material deformation, and potential failure modes. Form an insight into the mechanical behaviour of the critical zone to increase accuracy of future predictions.

Objective 5 : Modelled Failure Modes Analysis
Examine the simulation results for potential failure modes occurring in the critical zone. Explore factors that may be involved such as adhesive debonding, interfacial delamination, adhesive and cohesive failure. Evaluate the model finding against predetermined failure criteria and comment on the reliability of the attachment under the proposed loading condition.

Objective 6 : Optimization & Proposed Design Improvements
Propose possible future design modifications to optimize the critical zone. Recommend changes in design or manufacturing processes to mitigate stress concentrations, improve bonding techniques, optimize joint designs, or introduce protective coatings.

Richards (2023) proposes the outcomes of this project are:

- Identification and quantification of factors responsible failure modes occurring at the critical zone of metal component attachments to the CFRP structure.
- Theoretical model of the critical zone and simulation analysis.
- Refined metrics that can be applied to evaluate and model behaviour of new designs prior to destructive testing.

Richards (2023) proposes the benefits of these outcomes are:

- Increased safety and reliability in CFRP pressure vessel and attachment design.
- Increased use of CFRP pressure vessels.
- Reduce cost and complexity of H2 storage to promote greater adoption rates in replacing fossil fuels.

Work Plan & Timeline:

Month	**1-2**	**January - February**
Develop a detailed research proposal, specification, and work plan once a topic has been selected. Begin high level research to facilitate basic background information. **Deliverable Due**: Specification & Work Plan 19/02/2024		
Months	**3-4**	**March - April**
Generate a comprehensive literature review using access to Science Direct via UniSQ credentials to gather the most recent journal articles. EndNote 20 software will be utilized for citation management, and the literature review will be assembled and integrated into the dissertation report via the Microsoft Office suite. **Objectives:** 1-2 **Deliverable Due**: Literature Review 02/04/2024		
Months	**5-8**	**May - August**
Develop a series of CAD, FEA, CFM models from the specifications found in the literature review. Apply a variety of loading conditions that simulate real world conditions. Examine the models to identify and develop failure modes. Use this new found information to		

draw conclusions and recommendations for future work. **Objectives:** 3-6 **Deliverable Due**: Methodology 20/05/2024		
Month	**9**	**September**
Analyse preliminary results in order to compile findings and produce a first draft of the dissertation report. **Objectives**: 7 **Deliverable Due**: Draft Dissertation with Preliminary Results 09/09/2024		
Months	**10-11**	**October - November**
Finalise the dissertation report taking on feedback provided during the drafting process. Prepare a presentation summarizing the outcomes, key findings, recommendations, and benefits of the research conducted. **Deliverable Due**: Dissertation 04/11/2024		

Resources Required:

Resource	Quantity	Source	Cost	Comment
Computer high appropriate specifications	1	Student	Nil	Already owned by student
Fusion 360 CAD Software with FEA software extension	1	Student	Nil	Already paid subscription by student
Creo CAD Software with FEA software extension	1	USQ	Nil	Available for students
ANSYS simulation software	1	USQ / Student	Nil	Believed to be available to students from USQ ANSYS offers free subscription for students
Abaqus CAE simulation software	1	USQ	Nil	Mentioned by advisor, to be followed up upon

(Richards, 2023)

References:

Air, A., Shamsuddoha, M., & Gangadhara Prusty, B. (2023). A review of Type V composite pressure vessels and automated fibre placement based manufacturing. *Composites Part B: Engineering*, *253*, 110573. https://doi.org/https://doi.org/10.1016/j.compositesb.2023.110573

Composites, H. (2019). *POLAR BOSSES FOR COMPOSITE PRESSURE VESSELS; A PRIMER ON DESIGN AND ANAYSIS*. Hanso Composites. Retrieved 04/10/2023 from https://www.hanshocomp.com/single-post/2019/02/15/polar-bosses-for-composite-pressure-vessels-a-primer-on-design-and-anaysis

Deeraj, B. D. S., Mathew, M. S., Parameswaranpillai, J., & Joseph, K. (2020). Chapter 6 - EMI shielding materials based on thermosetting polymers. In K. Joseph, R. Wilson, & G. George (Eds.), *Materials for Potential EMI Shielding Applications* (pp. 101-110). Elsevier. https://doi.org/https://doi.org/10.1016/B978-0-12-817590-3.00006-3

EERE. *Hydrogen Storage*. Office of Energy Efficiency & Renewable Energy. Retrieved 04/10/2023 from https://www.energy.gov/eere/fuelcells/hydrogen-storage#:~:text=Hydrogen%20can%20be%20stored%20physically,pressure%20is%20%E2%88%92252.8%C2%B0C.

Fibreglast. (2023). *What are Unidirectional Carbon Fiber Fabrics?* Fibreglast. Retrieved 04/10/2023

Harada, S., Arai, Y., Araki, W., Iijima, T., Kurosawa, A., Ohbuchi, T., & Sasaki, N. (2018). A simplified method for predicting burst pressure of type III filament-wound CFRP composite vessels considering the inhomogeneity of fiber packing. *Composite Structures*, *190*, 79-90. https://doi.org/https://doi.org/10.1016/j.compstruct.2018.02.011

IEA. (2019). *The Future of Hydrogen*. IEA. https://www.iea.org/reports/the-future-of-hydrogen,

Richards, R. (2023). *Research Proposal*. U. o. S. Queensland.

Takemoto, S., & Yoshikawa, N. (2022). Strength evaluation of CFRP structure of high pressure hydrogen tank based on mesoscale analysis. *Materials Today Communications*, *32*, 103966. https://doi.org/https://doi.org/10.1016/j.mtcomm.2022.103966

Zhang, J., Lei, L., Zhou, W., Li, G., Yan, Y., & Ni, Z. (2023). Cryogenic mechanical and hydrogen-barrier properties of carbon fiber composites for type V cryo-compressed hydrogen storage vessels. *Composites Communications*, *43*, 101733. https://doi.org/https://doi.org/10.1016/j.coco.2023.101733

Zhang, J., Lin, G., Vaidya, U., & Wang, H. (2023). Past, present and future prospective of global carbon fibre composite developments and applications. *Composites Part B: Engineering*, *250*, 110463. https://doi.org/https://doi.org/10.1016/j.compositesb.2022.110463

APPENDIX

B

Risk Assessment

University of Southern Queensland **Offline Version**

USQ Safety Risk Management System

Note: This is the offline version of the Safety Risk Management System (SRMS) Risk Management Plan (RMP) and is only to be used for planning and drafting sessions, and when working in remote areas or on field activities. It must be transferred to the online SRMS at the first opportunity.

Safety Risk Management Plan – Offline Version			
Assessment Title:	Investigation on the Critical Zone of Metal Component Attachments on H2 Pressure Vessels Made of Carbon Fiber-Reinforced Epoxy using modelling software	Assessment Date:	11/10/2023
Workplace (Division/Faculty/Section):	School of Engineering	Review Date:(5 Years Max)	1/02/2027

Context			
Description:			
What is the task/event/purchase/project/procedure?	Research and theoretical modelling using computer software		
Why is it being conducted?	Dissertation		
Where is it being conducted?	Offcampus		
Course code (if applicable)	ENP4111	Chemical name (if applicable)	
What other nominal conditions?			
Personnel involved	Ryan Richards		
Equipment	Standard office space (desk, chair), laptop etc.		
Environment	Offcampus office space		
Other			
Briefly explain the procedure/process	Literature Review, Develop 3D Model, Run Simulations, Analyse Results & Draw Conclusions		
Assessment Team - who is conducting the assessment?			
Assessor(s)	Dr. B.F. Yousif		
Others consulted:			

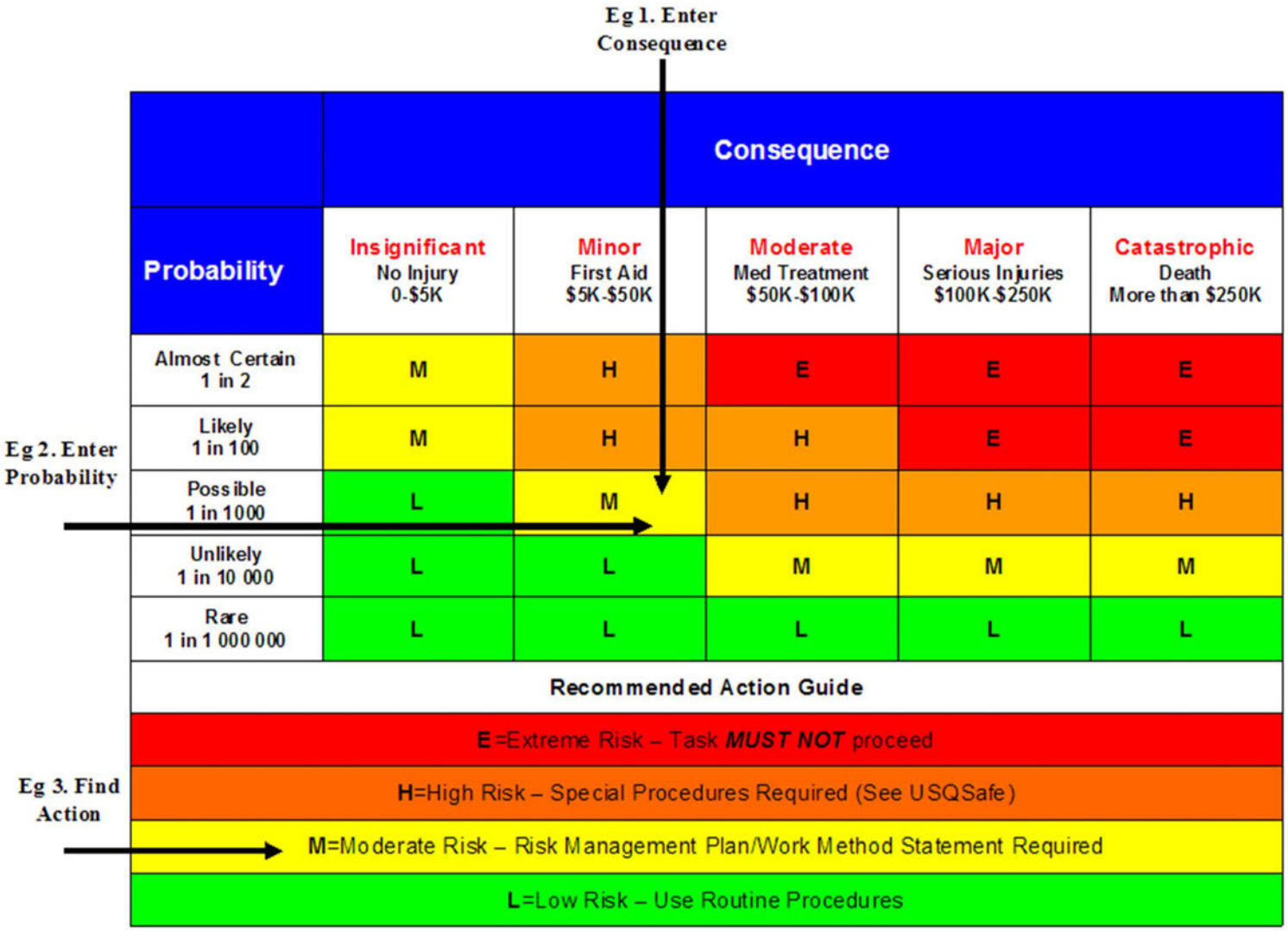
Eg 1. Enter Consequence
Eg 2. Enter Probability
Eg 3. Find Action
Consequence
Probability
Insignificant
No Injury
0-$5K
Minor
First Aid
$5K-$50K
Moderate
Med Treatment
$50K-$100K
Major
Serious Injuries
$100K-$250K
Catastrophic
Death
More than $250K
Almost Certain
1 in 2
M H E E E
Likely
1 in 100
M H H E E
Possible
1 in 1000
L M H H H
Unlikely
1 in 10 000
L L M M M
Rare
1 in 1 000 000
L L L L L
Recommended Action Guide
E=Extreme Risk – Task MUST NOT proceed
H=High Risk – Special Procedures Required (See USQSafe)
M=Moderate Risk – Risk Management Plan/Work Method Statement Required
L=Low Risk – Use Routine Procedures

Step 1 (cont)	Step 2	Step 2a	Step 2b	Step 3			Step 4				
Hazards: From step 1 or more if identified	*The Risk:* What can happen if exposed to the hazard without existing controls in place?	*Consequence:* What is the harm that can be caused by the hazard without existing controls in place?	*Existing Controls:* What are the existing controls that are already in place?	*Risk Assessment:* Consequence x Probability = Risk Level			*Additional controls:* Enter additional controls if required to reduce the risk level	*Risk assessment with additional controls:*			
				Probability	Risk Level	ALARP? Yes/no		Consequence	Probability	Risk Level	ALARP? Yes/no
Example											
Working in temperatures over 35^0 C	Heat stress/heat stroke/exhaustion leading to serious personal injury/death	catastrophic	Regular breaks, chilled water available, loose clothing, fatigue management policy.	possible	high	No	temporary shade shelters, essential tasks only, close supervision, buddy system	catastrophic	unlikely	mod	Yes
Long study periods	Muscle & Eye Strain, Headaches	Minor	Mandated regular study breaks	Possible	Moderate	No	If muscle strain occurs, invest in a sit/stand desk arrangement and high quality desk chair. If Eye strain and headaches occur, invest in a yellow ambient overhead light over the computer monitor.	Minor	Unlikely	Low	Yes
File management	Loss of unsaved files, images, tables, references etc	Insignificant	Single folder to hold all related documents to the project, backed up regularly	Unlikely	Low	Yes		Select a consequence	Select a probability	Select a Risk Level	Yes or No
Data corruption	Loss of data, most recent report, model, simulation etc	Moderate	Folder storing all work for this project backed up both on computer local drive, external harddrive and cloud storage	Unlikely	Moderate	Yes	Mandate daily and/or weekley routine backups across all medians (local, external and cloud storage)	Moderate	Rare	Low	Yes
Unscheduled computer or software updates	Downtime, possible loss of unsaved work	Minor	Schedule computer updates to oustide of study hours. Routinely check for software updates and calender when they are due to occur if unable to schedule (automatic system wide updates)	Rare	Low	Yes		Select a consequence	Select a probability	Select a Risk Level	Yes or No
Corporate espionage	Work stolen by competitors, information leaked online etc	Major	Do not publish work online. Keep antivirus software on computer up to date	Rare	Low	Yes		Select a consequence	Select a probability	Select a Risk Level	Yes or No
		Select a consequence		Select a probability	Select a Risk Level	Yes or No		Select a consequence	Select a probability	Select a Risk Level	Yes or No
		Select a consequence		Select a probability	Select a Risk Level	Yes or No		Select a consequence	Select a probability	Select a Risk Level	Yes or No
		Select a consequence		Select a probability	Select a Risk Level	Yes or No		Select a consequence	Select a probability	Select a Risk Level	Yes or No

Step 1 (cont)	Step 2	Step 2a	Step 2b	Step 3			Step 4				
Hazards: From step 1 or more if identified	***The Risk:*** What can happen if exposed to the hazard without existing controls in place?	***Consequence:*** What is the harm that can be caused by the hazard without existing controls in place?	***Existing Controls:*** What are the existing controls that are already in place?	***Risk Assessment:*** Consequence x Probability = Risk Level			***Additional controls:*** Enter additional controls if required to reduce the risk level	***Risk assessment with additional controls:***			
				Probability	**Risk Level**	**ALARP? Yes/no**		**Consequence**	**Probability**	**Risk Level**	**ALARP? Yes/no**
Example											
Working in temperatures over 35^{0} C	Heat stress/heat stroke/exhaustion leading to serious personal injury/death	catastrophic	Regular breaks, chilled water available, loose clothing, fatigue management policy.	possible	high	No	temporary shade shelters, essential tasks only, close supervision, buddy system	catastrophic	unlikely	mod	Yes
		Select a consequence		Select a probability	Select a Risk Level	Yes or No		Select a consequence	Select a probability	Select a Risk Level	Yes or No
		Select a consequence		Select a probability	Select a Risk Level	Yes or No		Select a consequence	Select a probability	Select a Risk Level	Yes or No
		Select a consequence		Select a probability	Select a Risk Level	Yes or No		Select a consequence	Select a probability	Select a Risk Level	Yes or No
		Select a consequence		Select a probability	Select a Risk Level	Yes or No		Select a consequence	Select a probability	Select a Risk Level	Yes or No
		Select a consequence		Select a probability	Select a Risk Level	Yes or No		Select a consequence	Select a probability	Select a Risk Level	Yes or No
				Select a probability	Select a Risk Level	Yes or No		Select a consequence	Select a probability	Select a Risk Level	Yes or No
				Select a probability	Select a Risk Level	Yes or No		Select a consequence	Select a probability	Select a Risk Level	Yes or No
				Select a probability	Select a Risk Level	Yes or No		Select a consequence	Select a probability	Select a Risk Level	Yes or No
				Select a probability	Select a Risk Level	Yes or No		Select a consequence	Select a probability	Select a Risk Level	Yes or No
				Select a probability	Select a Risk Level	Yes or No		Select a consequence	Select a probability	Select a Risk Level	Yes or No

Step 5 - Action Plan (for controls not already in place)			
Additional controls:	*Resources:*	*Persons responsible:*	*Proposed implementation date:*
			Click here to enter a date.
			Click here to enter a date.
			Click here to enter a date.
			Click here to enter a date.
			Click here to enter a date.
			Click here to enter a date.
			Click here to enter a date.
			Click here to enter a date.
			Click here to enter a date.
			Click here to enter a date.
			Click here to enter a date.
			Click here to enter a date.

Step 6 - Approval					
Drafter's name:				Draft date:	Click here to enter a date.
Drafter's comments:					
Approver's name:	Dr. B.F. Yousif		Approver's title/position:	Associate Professor (Mechanical Engineering)	
Approver's comments:					
I am satisfied that the risks are as low as reasonably practicable and that the resources required will be provided.					
Approver's signature:				Approval date:	Click here to enter a date.

APPENDIX

C

MATLAB Code

```
% Isotensoid Profile Calculator

% Purpose of Program/Function
% Generates an isotensoid profile for CFRP TYPE-V PV Domes

% Description of Inputs/Outputs
% Inputs Required:
% R = cylindrical radius (m)
% r0 = polar boss radius (m)

% Outputs:
% Isotensoid profile plot and values (m)

% Ryan Richards [redacted]
% ENP4111 2024
% 29/08/2024

% Log of Testing
% Tested 29/08/2024 - No Logged Errors

% Log of Modifications

%% Housekeeping
clear
clc
```

The profile is split into two sections; AB which ranges from the cylindrical region to the start of the polar boss and BC which covers from the start of the polar boss to the polar boss opening. Section BC is also the adhesion zone between the polar boss and the CFRP body.

The isotensoid profile is given by a series of coordinates of form: (z,r).

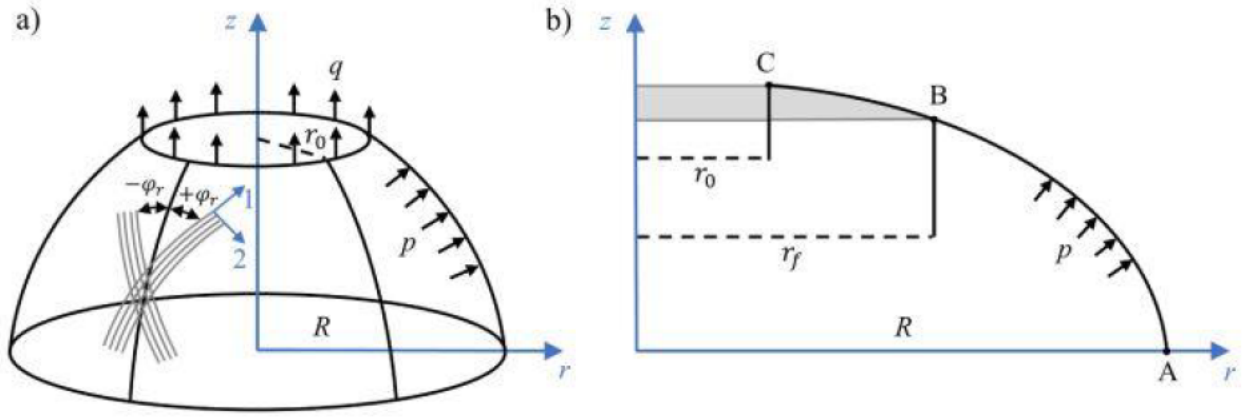


```
% Inputs

R = 0.200;                          % cylindrical radius (m)
```

```
r0 = 0.075;                          % polar boss radius (m)
```

Section AB

Normalised z value:

$$\bar{z}_{AB} = \sqrt{1+\bar{r}_2^{\,2}} \times E\left(k,\theta^{(1)}\right) - \frac{\bar{r}_2^{\,2}}{\sqrt{1+\bar{r}_2^{\,2}}} \times F\left(k,\theta^{(1)}\right)$$

```
%zbar_AB = (sqrt(1 + r2bar_2) .* ellipticE(k,theta_1)) - ((r2bar_2/sqrt(1 +
r2bar_2)) .* ellipticF(k,theta_1));
```

Normalised r value:

$$\bar{r}_{AB} = \sqrt{1-\left(1-\bar{r}_1^{\,2}\right) \times \sin\left(\theta^{(1)}\right)^2}$$

```
%rbar_AB = sqrt(1 - (1 - r1bar_2) .* (sind(theta_1)).^2);
```

Where;

```
% r0 Values
r0bar = r0/R;
r0bar_2 = r0bar ^2;
% rf Values
rfbar = sqrt(3/2) * r0bar;
rfbar_2 = rfbar ^2;
```

$$\bar{r}_1^{\,2} = \frac{1}{2}\left(\sqrt{\frac{1+3\bar{r}_0^{\,2}}{1-\bar{r}_0^{\,2}}} - 1\right) \qquad \bar{r}_2^{\,2} = \frac{1}{2}\left(\sqrt{\frac{1+3\bar{r}_0^{\,2}}{1-\bar{r}_0^{\,2}}} + 1\right)$$

```
% r1 & r2 Values
r1bar_2 = 0.5 * (sqrt((1+3*r0bar_2)/(1-r0bar_2))-1);
r2bar_2 = 0.5 * (sqrt((1+3*r0bar_2)/(1-r0bar_2))+1);
```

$$k = \sqrt{\frac{1-\bar{r}_1^{\,2}}{1+\bar{r}_2^{\,2}}}$$

```
% k Value
k = sqrt((1-r1bar_2)/(1+r2bar_2));
```

$$0 \le \theta^{(1)} \le \theta_f{}^{(1)} \qquad \theta_f{}^{(1)} = \sin^{-1}\sqrt{\frac{1-\bar{r}_f{}^2}{1-\bar{r}_1{}^2}}$$

```
% Theta Range
thetaf_1 = asind(sqrt((1-rfbar_2)/(1-r1bar_2)));
theta_1 = 0:0.1:thetaf_1;
```

rbar_AB Calculation

```
rbar_AB = sqrt(1 - (1 - r1bar_2) .* (sind(theta_1)).^2);
```

zbar_AB Calculation

```
zbar_AB = (sqrt(1 + r2bar_2) .* ellipticE(k,theta_1)) - ((r2bar_2/sqrt(1 +
r2bar_2)) .* ellipticF(k,theta_1));
```

Plot Normalised AB Profile

```
figure
plot(rbar_AB,imag(zbar_AB));
xlabel('Normalised Radius');
ylabel('Normalised Length');
title('Section AB Isotensoid Profile');
```

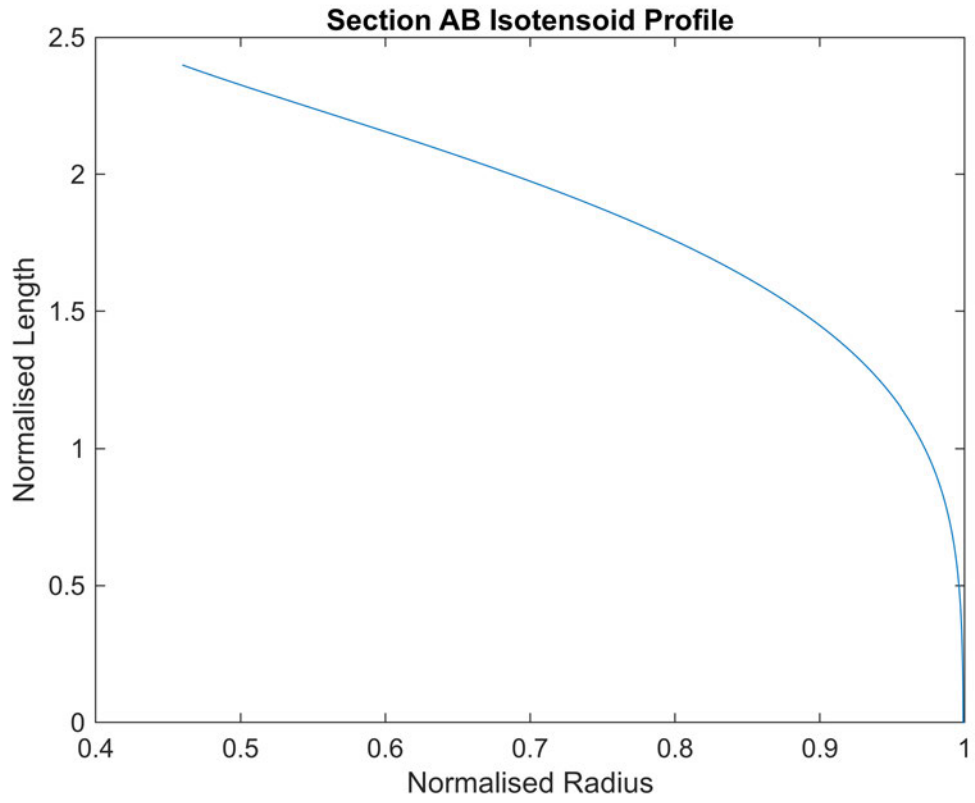

Section BC

Normalised z value:

$$\bar{z}_{BC} = \sqrt{n_1 + n_2} \times [E(n, \theta^{(2)}) - (1 - n^2) F(n, \theta^{(2)})] + c_2$$

```
%zbar_BC = (sqrt(n1 + n2) .* ellipticE(n,theta_2)) - ((1 - (n^2))) .*
ellipticF(n,theta_2)) + c2;
```

Normalised r value:

$$\bar{r}_{BC} = \sqrt{\bar{r}_0^{\,2} + n_1 \times \cos(\theta^{(2)})^2}$$

```
%rbar_BC = sqrt(r0bar_2 + (n1 .* (cosd(theta_2) .^2)));
```

Where;

$$n = \sqrt{\frac{n_1}{n_1 + n_2}} \qquad n_1 = \frac{1}{2}\sqrt{\bar{r}_0^{\,4} + \frac{4\left(\bar{r}_f^{\,2} - \bar{r}_0^{\,2}\right)^2}{\bar{r}_f^{\,4}\left(1 - \bar{r}_0^{\,2}\right)}} - \bar{r}_0^{\,2} \qquad n_2 = \frac{1}{2}\sqrt{\bar{r}_0^{\,4} + \frac{4\left(\bar{r}_f^{\,2} - \bar{r}_0^{\,2}\right)^2}{\bar{r}_f^{\,4}\left(1 - \bar{r}_0^{\,2}\right)}} + \bar{r}_0^{\,2}$$

```
% n Values
n1 = 0.5 * (sqrt(r0bar_2 ^2 + ((4 * ((rfbar_2 - r0bar_2)^2))/(rfbar_2 ^2 * (1 -
r0bar_2))) - r0bar_2));
n2 = 0.5 * (sqrt(r0bar_2 ^2 + ((4 * ((rfbar_2 - r0bar_2)^2))/(rfbar_2 ^2 * (1 -
r0bar_2))) + r0bar_2));
n = sqrt(n1/(n1+n2));
```

$$\theta_f^{(2)} \le \theta^{(2)} \le \frac{\pi}{2} \qquad \theta_f^{(2)} = \cos^{-1}\sqrt{\frac{\bar{r}_f^{\,2} - \bar{r}_0^{\,2}}{n_1}}$$

```
% Theta Range
thetaf_2 = acosd(sqrt((rfbar_2-r0bar_2)/n1));
theta_2 = thetaf_2:0.1:90;
```

$$c_2 = \sqrt{1 + \bar{r}_2^{\,2}} \times E\left(k, \theta_f^{(1)}\right) - \frac{\bar{r}_2^{\,2}}{\sqrt{1 + \bar{r}_2^{\,2}}} \times F\left(k, \theta_f^{(1)}\right) - \sqrt{n_1 + n_2} \times \left[E\left(n, \theta_f^{(2)}\right) - (1 - n^2) F\left(n, \theta_f^{(2)}\right)\right]$$

```
% c2 Value
c2 = (sqrt(1+r2bar_2)) .* (ellipticE(k,thetaf_1)) - ((r2bar_2/sqrt(1+r2bar_2)) .*
(ellipticF(k,thetaf_1))) - (sqrt(n1 + n2) .* (ellipticE(n,thetaf_2) - ((1-(n^2)) .*
ellipticF(n,thetaf_2))));
```

rbar_BC Calculation

```
rbar_BC = sqrt(r0bar_2 + (n1 .* (cosd(theta_2) .^2)));
```

zbar_BC Calculation

```
zbar_BC = (sqrt(n1 + n2) .* ellipticE(n,theta_2)) - ((1 - (n^2)) .*
ellipticF(n,theta_2)) + c2;
```

Plot Normalised BC Profile

```
figure
plot(rbar_BC,imag(zbar_BC));
xlabel('Normalised Radius');
ylabel('Normalised Length');
title('Section BC Isotensoid Profile');
```

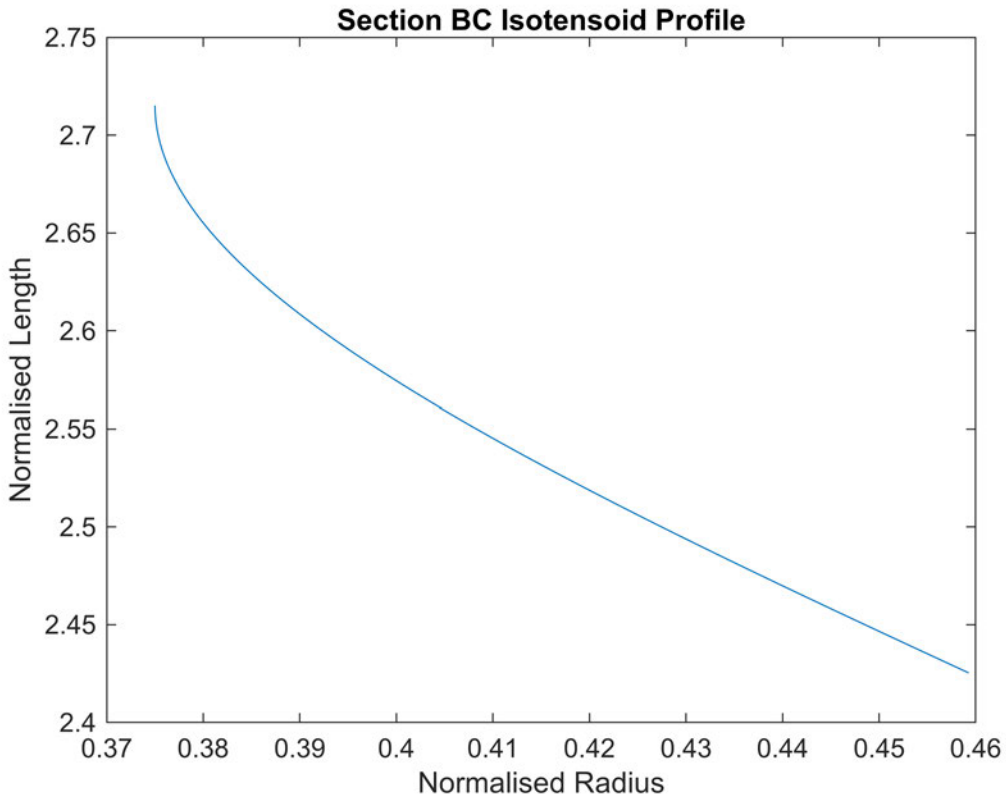

Complete Isotensoid Profile

```
r_AB = rbar_AB * R;
z_AB = imag(zbar_AB);

r_BC = rbar_BC * R;
z_BC = imag(zbar_BC);
```

Plot Profile

```
figure
plot(r_AB,z_AB,r_BC,z_BC);
xlabel('Radius (m)');
ylabel('Normalised Length');
title('Isotensoid Profile');
```

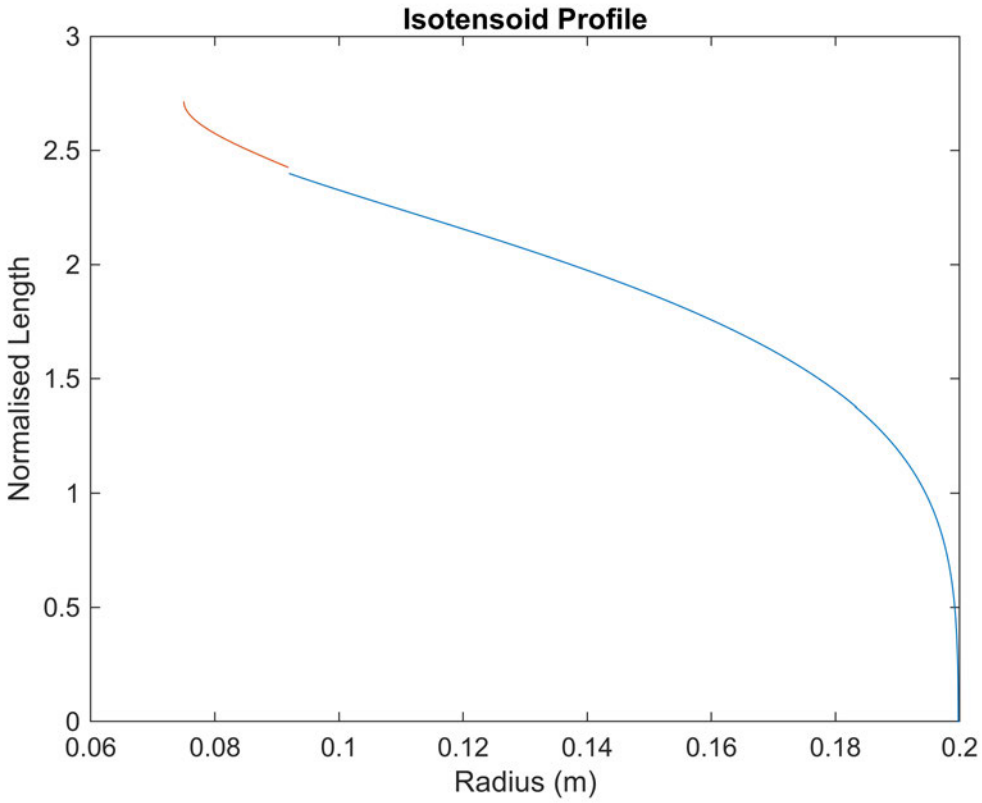

Coordinate Matrix and XLSX Export

```
r_combined = [r_AB, r_BC];
z_combined = [z_AB, z_BC];

coordinates = [transpose(z_combined), transpose(r_combined)];

xlswrite('Isotensoid_Coordinates.xlsx', coordinates);
```

APPENDIX

D

Results

	Identifier	Variable	Polar Boss Width	von Mises Stress (MPa)				Displacement (mm)				Failure Criteria	CZM Failure
				Global Max.	AVG.	Local Max.	Concentration	Global Max.	AVG.	Local Max.	Concentration		
Reduction in Polar Boss Width (%)	1	0	65	1292.2	310.68	351.42	1.131131711	30.332	0.62884	0.3539	0.562782266	e12, s2c	N
	2	2.5	63.375	1676.1	355.62	368.29	1.035627917	30.339	0.82031	0.39116	0.47684412	e12, s2c	N
	3	5	61.75	1292.3	336.44	358.58	1.065806682	30.338	0.63105	0.30293	0.480041201	e12, s2c	N
	4	7.5	60.125	1292.1	345.84	391.52	1.132084201	30.344	0.842	0.42199	0.501175772	e12, s2c	N
	5	10	58.5	1409.7	356.49	395.02	1.108081573	30.341	0.86286	0.50103	0.580661985	e12, s2c	N
		Variable	Flange Length										
Addition of Flange (mm)	6	0	0	1292.2	310.68	351.42	1.131131711	30.332	0.62884	0.3539	0.562782266	e12, s2c	N
	7	2.5	2.5	1292.3	385.27	356.81	0.926129727	30.334	0.66439	0.2613	0.393293096	e12, s2c	N
	8	5	5	1292.3	378.46	359.67	0.950351424	30.335	0.67956	0.29328	0.431573371	e12, s2c	N
	9	7.5	7.5	1292.3	365.95	360.03	0.983822927	30.334	0.65832	0.27304	0.414752704	e12, s2c	N
	10	10	10	2695.1	408.05	457.5	1.121186129	30.31	0.6099	0.27537	0.451500246	e12, s2c	N
		Variable	Flange Angle										
Reduction in Polar Boss Width (%)	11	0	0	1292.3	378.46	359.67	0.950351424	30.335	0.67956	0.29328	0.431573371	e12, s2c	N
	12	2.5	2.5	1290.8	511.13	316.39	0.619001037	29.515	2.3387	0.59412	0.254038568	e12, s2c	N
	13	5	5	1264.5	529.17	309.42	0.584727025	28.527	1.7289	0.24252	0.140274163	e12, s2c	N
	14	7.5	7.5	1271.9	565.17	210.43	0.372330449	28.273	3.2555	0.19849	0.060970665	e12, s2c	N
	15	10	10	1243.9	507.52	196.51	0.387196564	29.844	3.0698	0.7022	0.228744544	e12, s2c	N

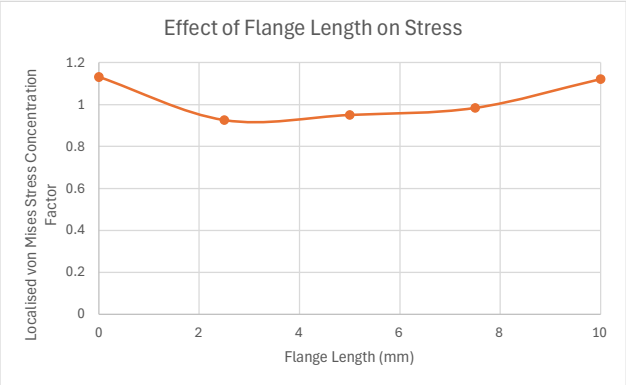
Effect of Flange Length on Stress
Localised von Mises Stress Concentration Factor
1.2
1
0.8
0.6
0.4
0.2
0
0
2
4
6
8
10
Flange Length (mm)

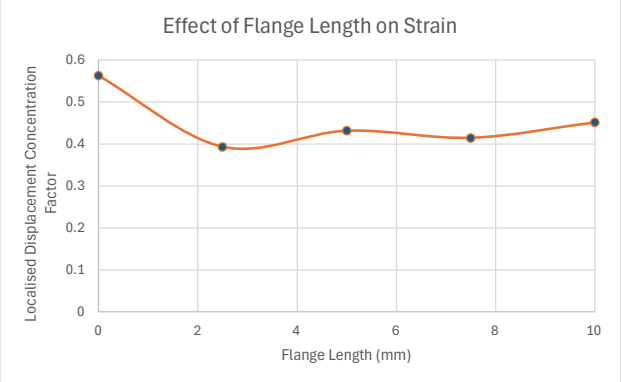
Effect of Flange Length on Strain
Localised Displacement Concentration Factor
0.6
0.5
0.4
0.3
0.2
0.1
0
0
2
4
6
8
10
Flange Length (mm)

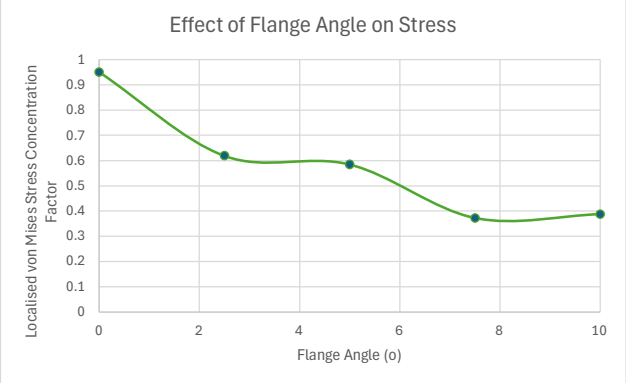
Effect of Flange Angle on Stress
Localised von Mises Stress Concentration Factor
1
0.9
0.8
0.7
0.6
0.5
0.4
0.3
0.2
0.1
0
0
2
4
6
8
10
Flange Angle (o)

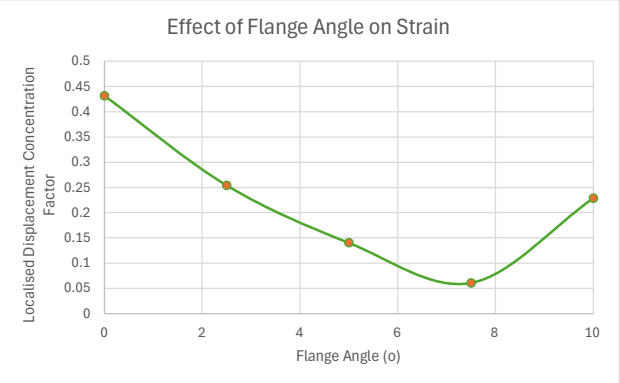
Effect of Flange Angle on Strain
Localised Displacement Concentration Factor
0.5
0.45
0.4
0.35
0.3
0.25
0.2
0.15
0.1
0.05
0
0
2
4
6
8
10
Flange Angle (o)

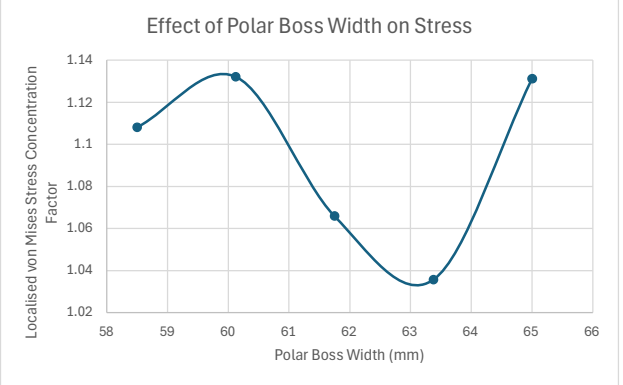
Effect of Polar Boss Width on Stress
Localised von Mises Stress Concentration Factor
1.14
1.12
1.1
1.08
1.06
1.04
1.02
58
59
60
61
62
63
64
65
66
Polar Boss Width (mm)

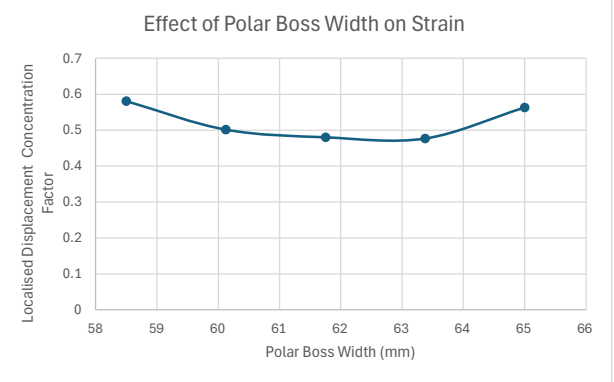
Effect of Polar Boss Width on Strain
Localised Displacement Concentration Factor
0.7
0.6
0.5
0.4
0.3
0.2
0.1
0
58
59
60
61
62
63
64
65
66
Polar Boss Width (mm)

Simulation 1

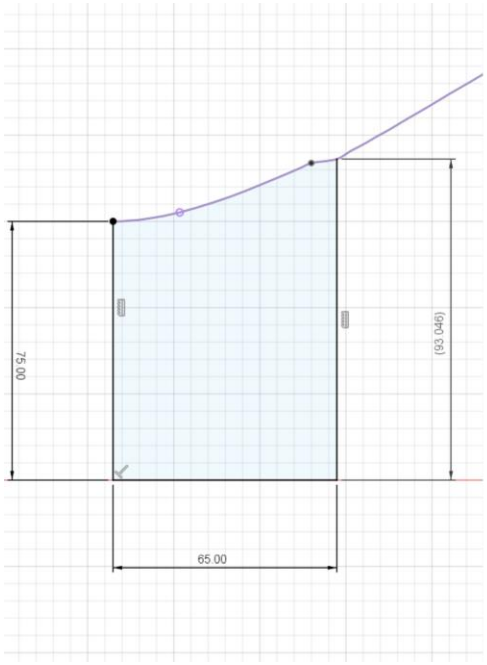

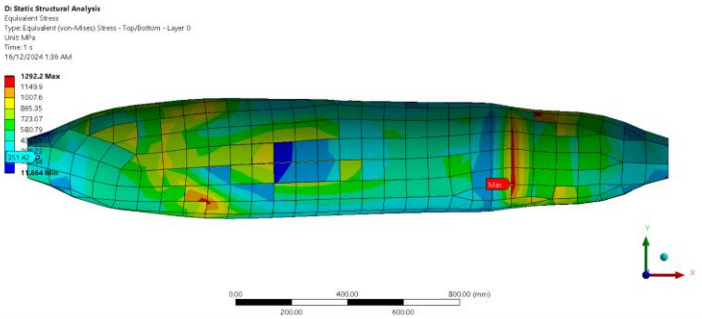

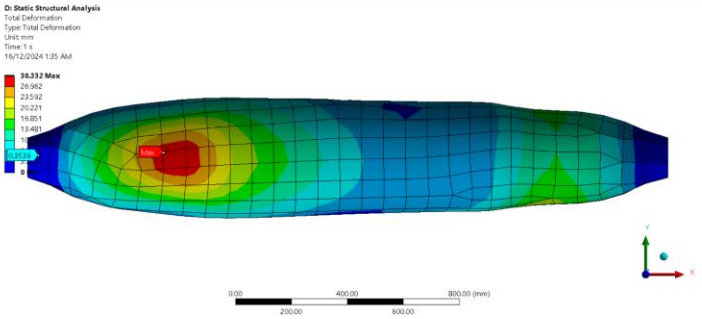

Simulation 2

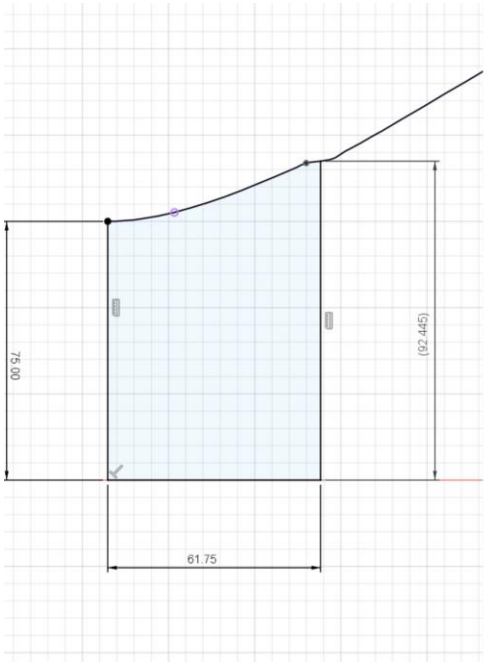

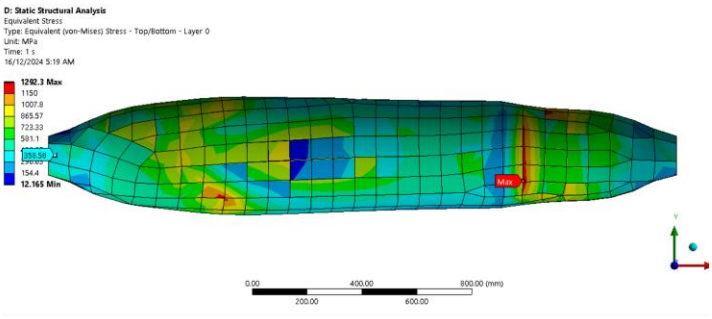

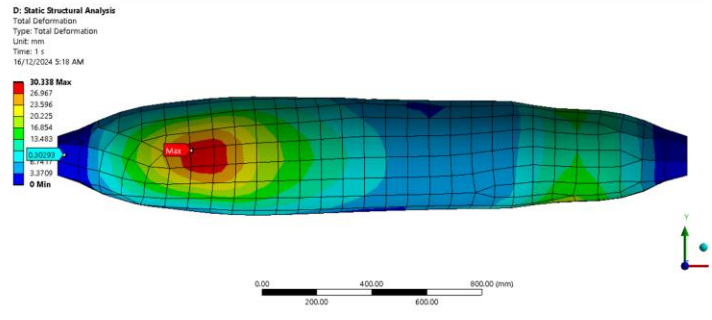

Simulation 3

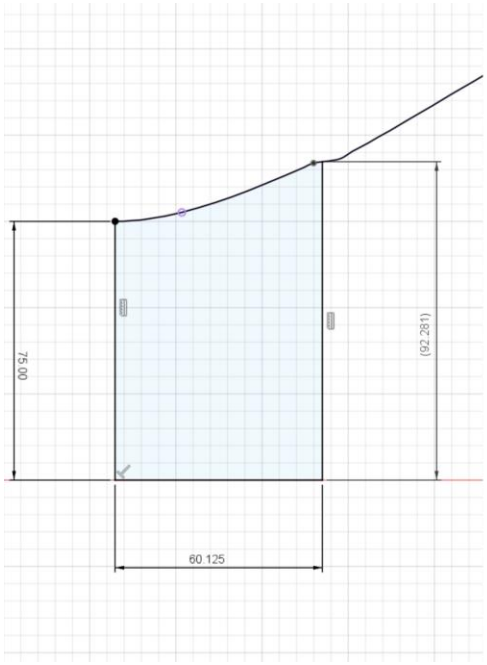

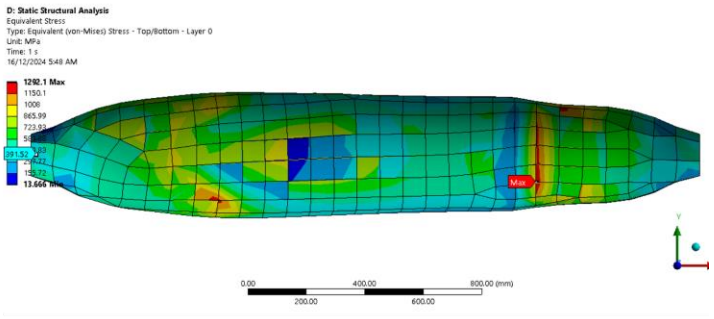

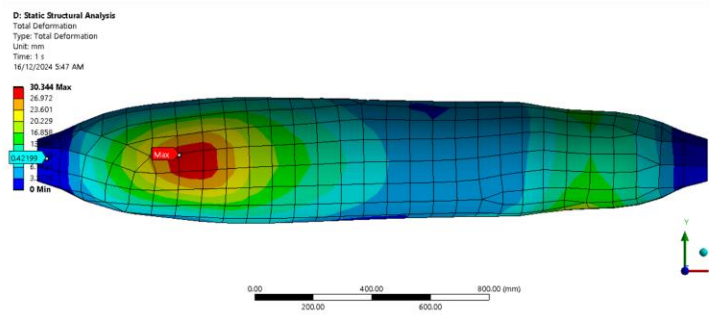

Simulation 4

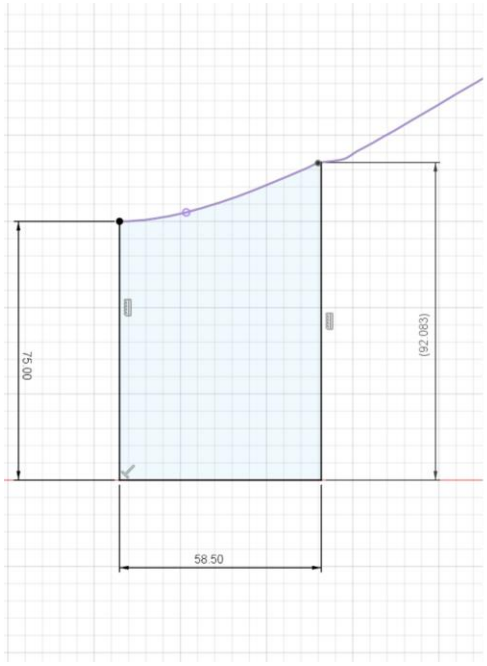

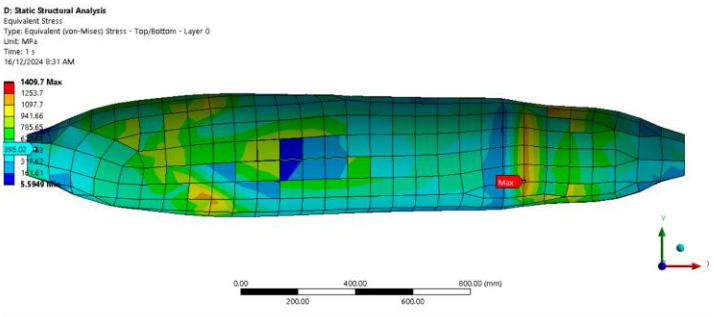

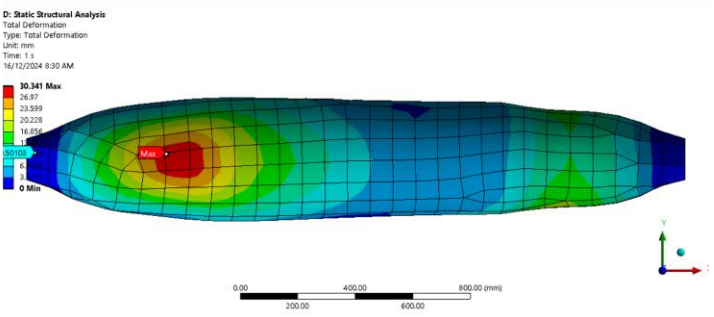

Simulation 5

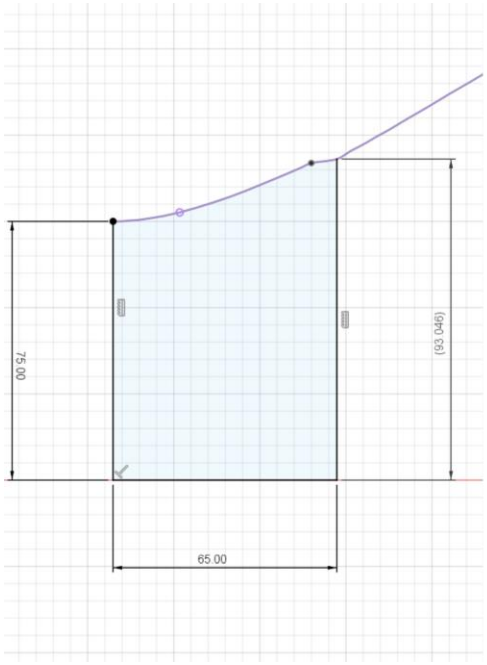

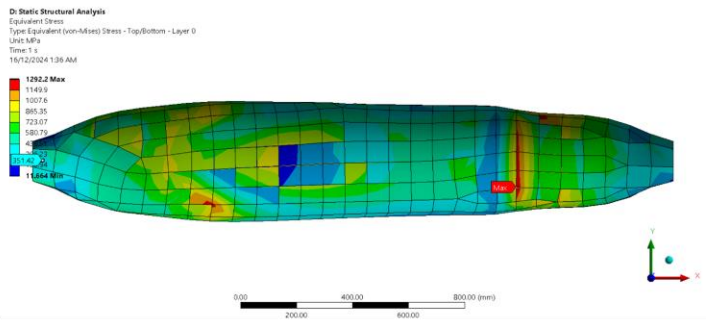

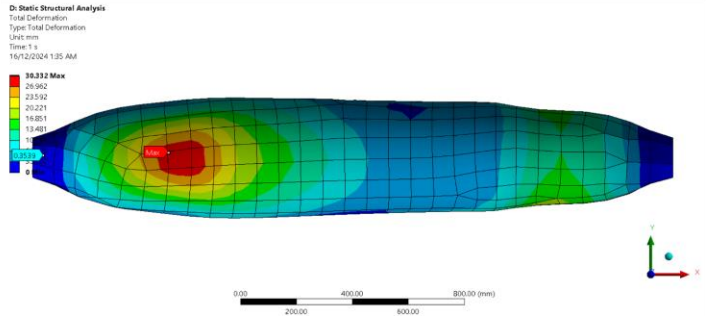

Simulation 6

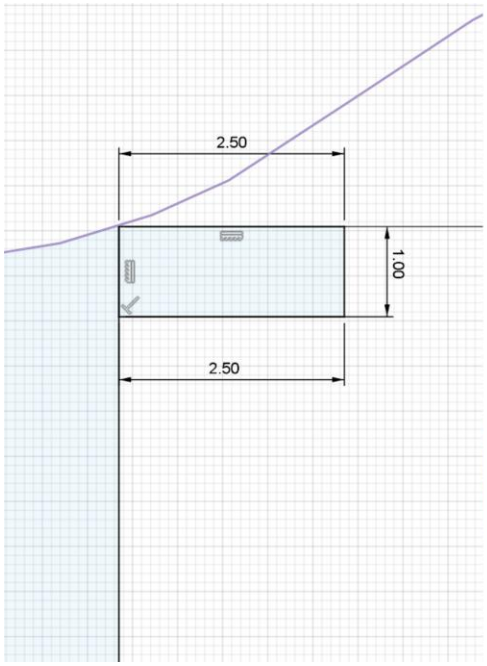

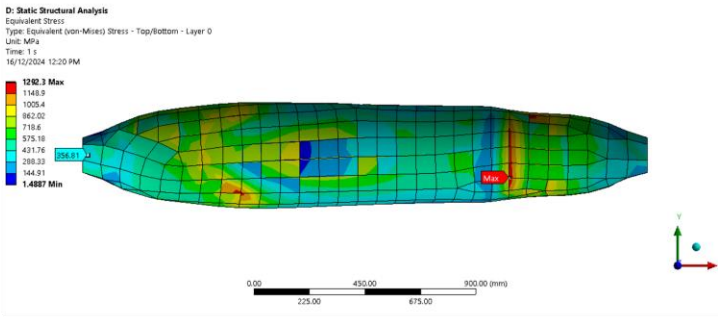

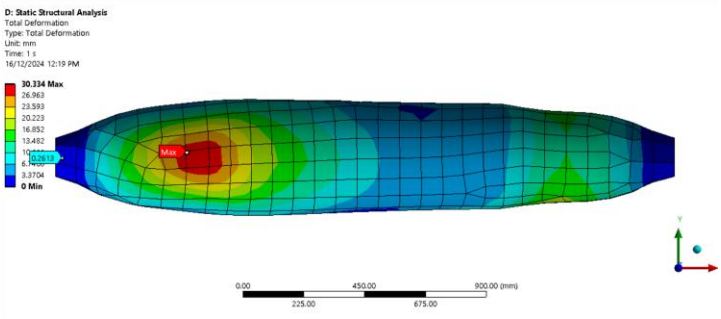

Simulation 7

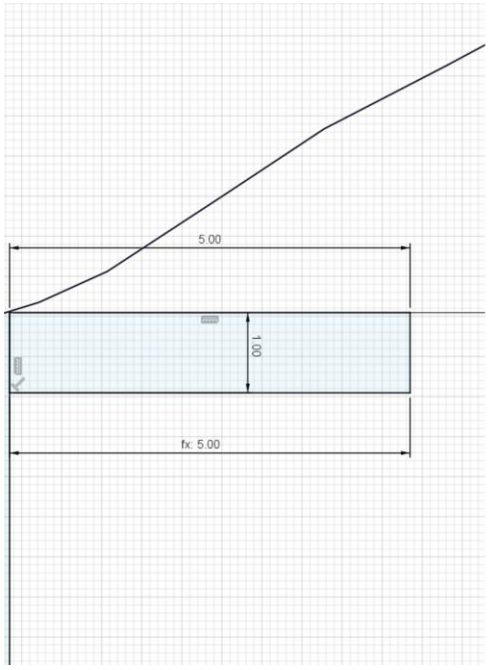

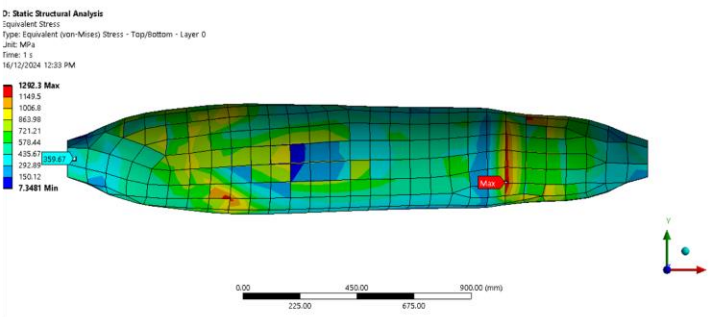

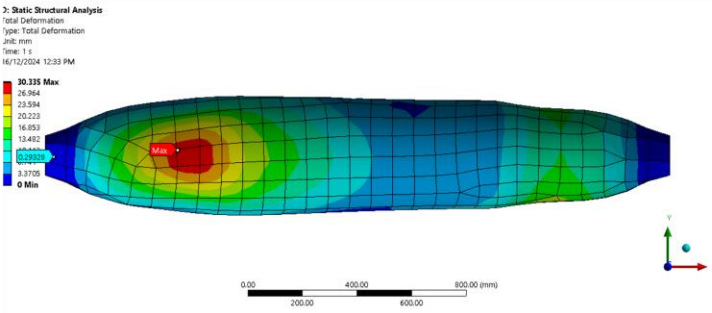

Simulation 8

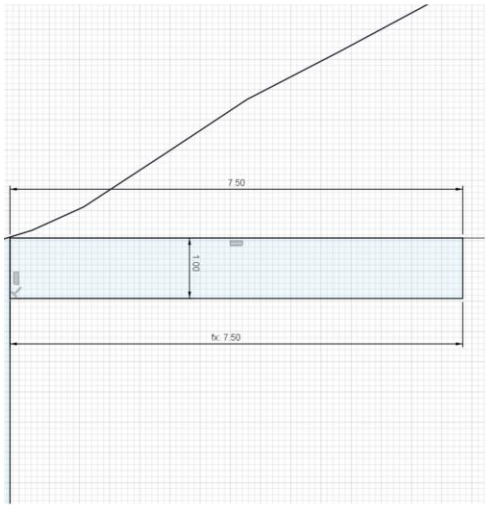

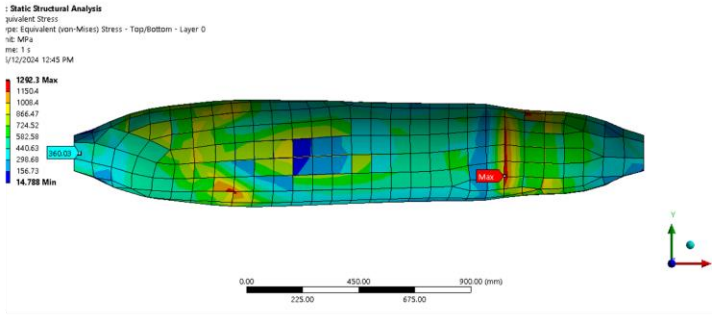

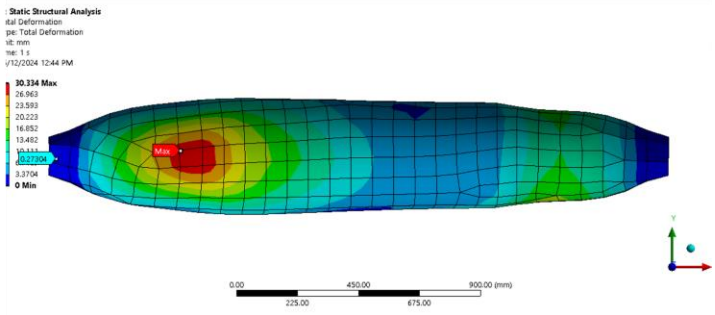

Simulation 9

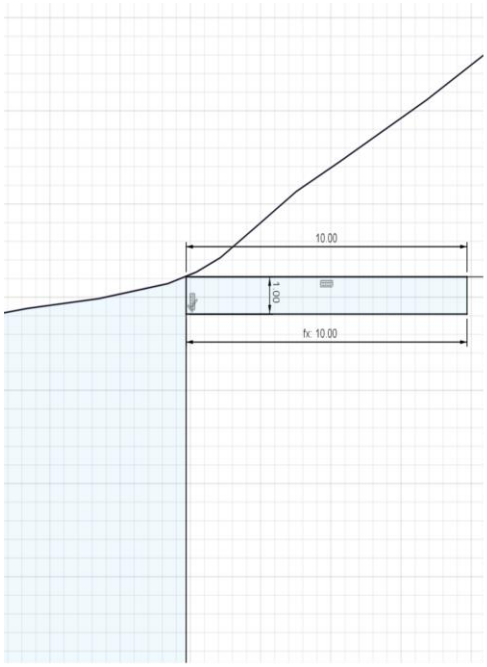

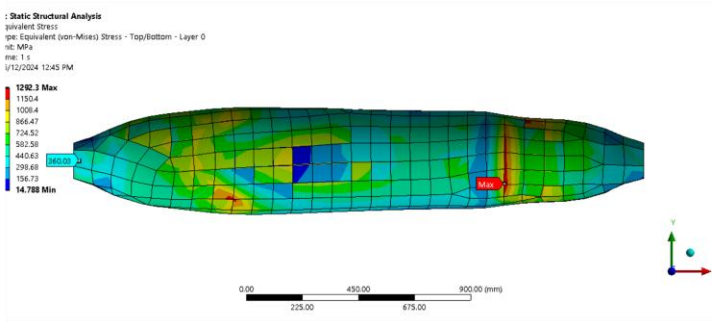

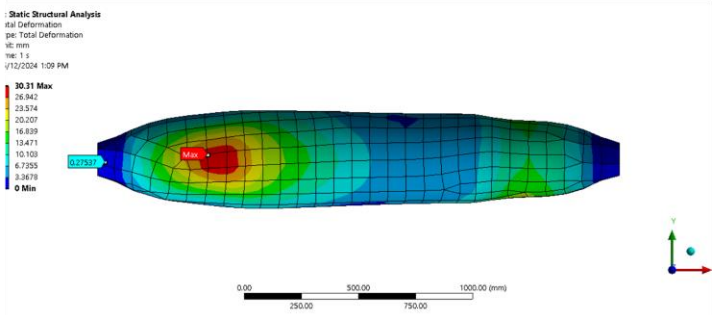

Simulation 10

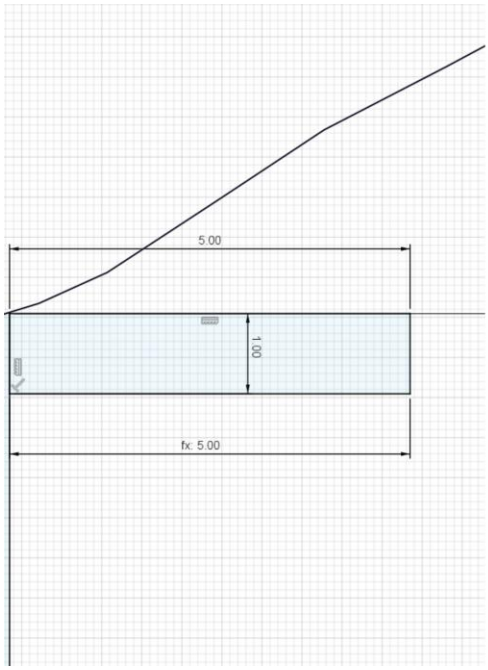

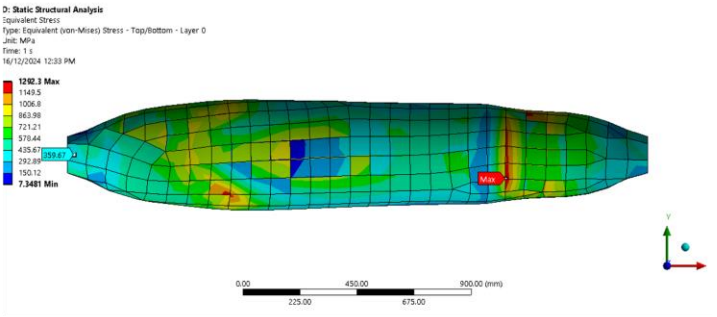

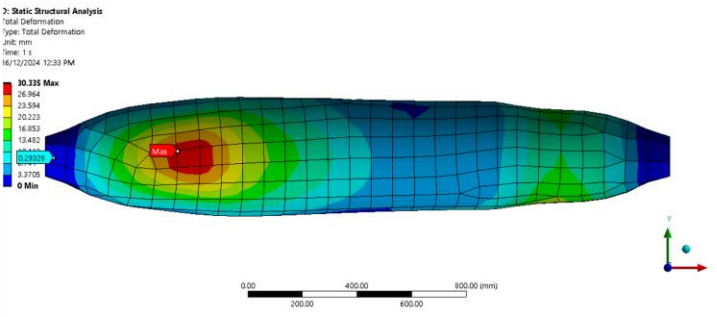

Simulation 11

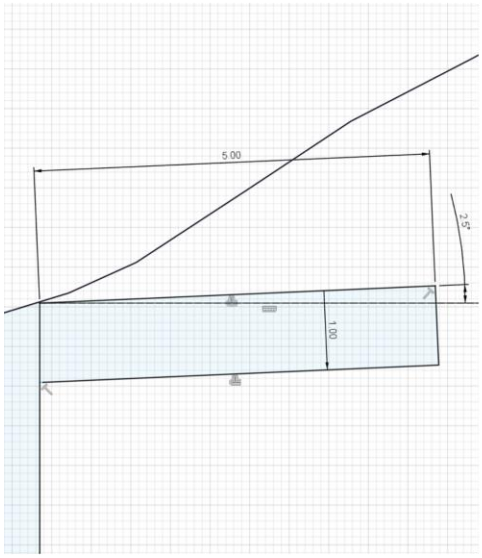

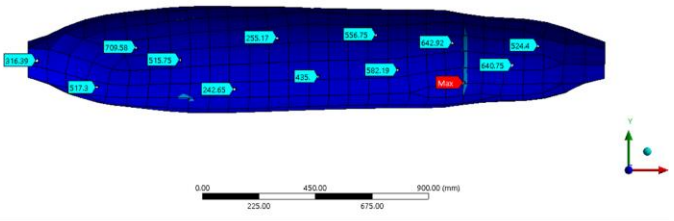

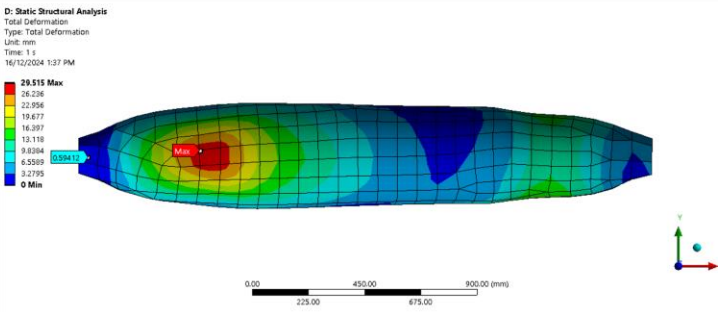

Simulation 12

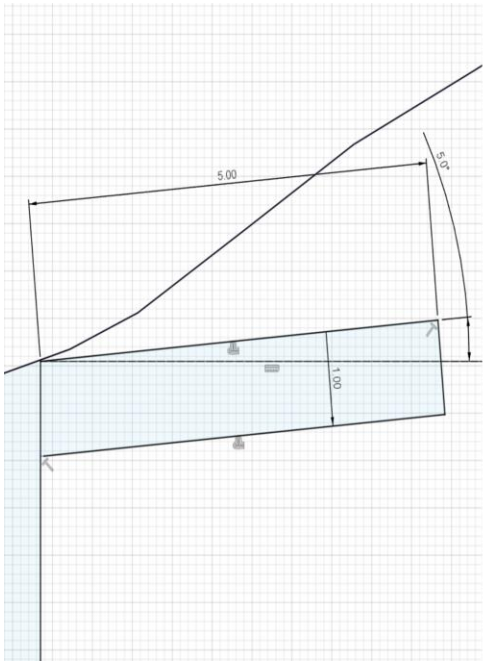

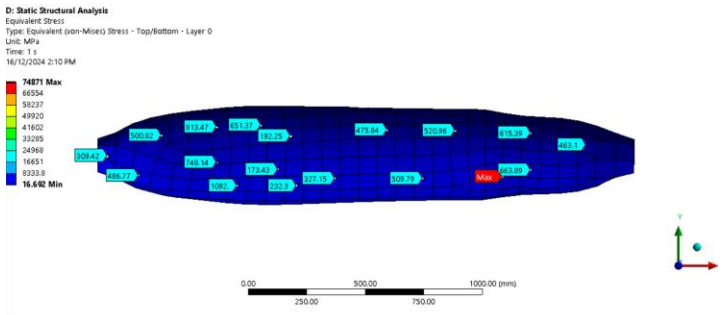

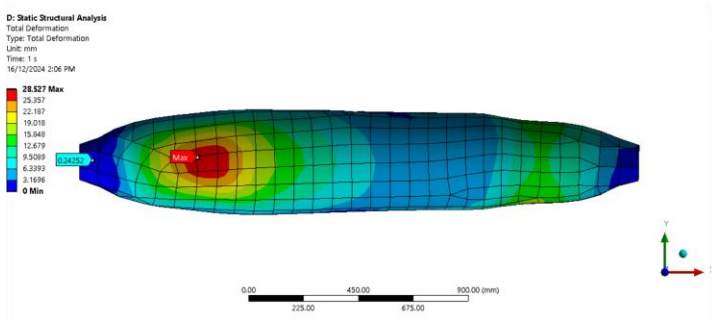

Simulation 13

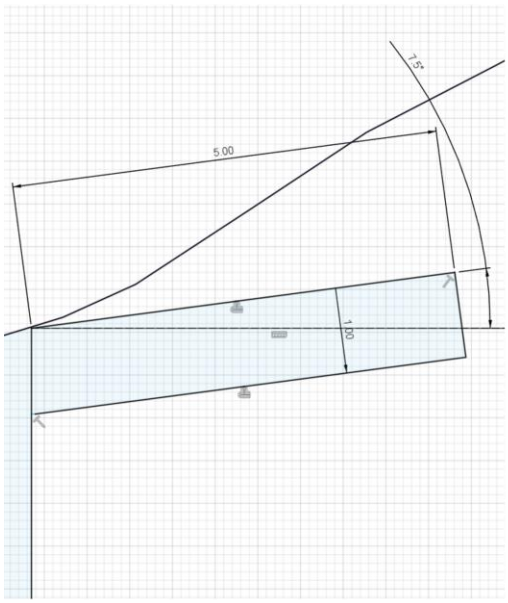

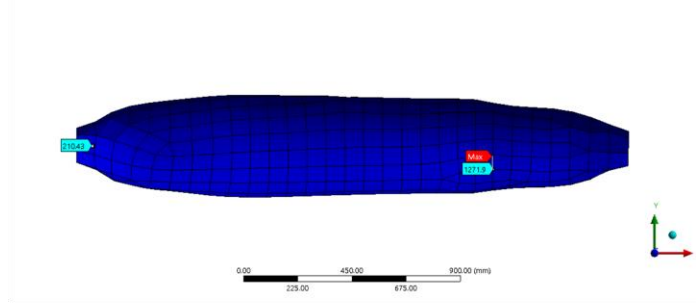

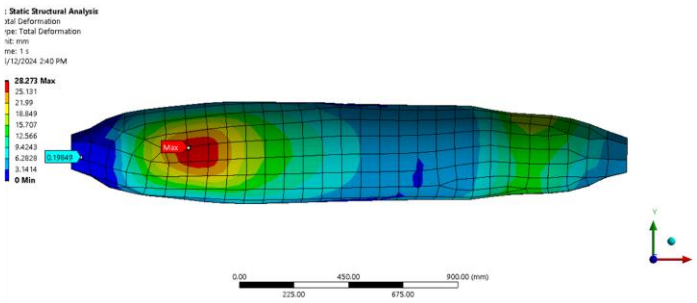

Simulation 14